REGULATION OF CELL POLARITY IN STOMATAL ASYMMETRIC CELL DIVISION IN *ARABIDOPSIS*

BY

WANCHEN SHAO

A dissertation submitted to the

School of Graduate Studies

Rutgers, The State University of New Jersey

In Partial fulfillment of the requirements

For the degree of

Doctor of Philosophy

Graduate Program in Plant Biology

Written under the direction of

Juan Dong

And approved by

_____

_____

_____

_____

New Brunswick, New Jersey

October 2017

ABSTRACT OF THE DISSERTATION

Regulation of Cell Polarity in Stomatal Asymmetric Cell Division

in *Arabidopsis*

By WANCHEN SHAO

Dissertation Director

Dr. Juan Dong

Cell polarization, manifested by the asymmetric distribution of intracellular molecules, structures and functions within a cell, is an essential feature and plays critical roles in developmental and environmental responses for almost all cellular organisms. Polarly localized proteins at the cell cortex are keys to asymmetric cell division (ACD), a fundamental process underlying the precise control of self-renewal and differentiation of stem cells in both animals and plants.

The BREAKING OF ASYMMETRY IN THE STOMATAL LINEAGE (BASL) protein was one of the first polarity factors identified in *Arabidopsis* that controls stomatal ACD. Remarkably, the localization and function of this plant-specific polarity protein resemble that of the conserved PAR protein complexes in animal ACD. However, how BASL protein is polarized to the cell cortex and how its polarity is precisely maintained at the plasma membrane have been major questions in the field.

Presented in this dissertation are my genetic, molecular and cell biological studies that implicate novel mechanisms for polarity establishment, maintenance and attenuation in stomatal lineage cells. Chapter 1 is a review of current knowledge about the molecular mechanisms for protein polarization in plants (modified from a review article published by Shao and Dong, 2016 Dev. Biol.). Chapter 2 describes a positive genetic interaction between BASL and the MAPKK kinase YODA (YDA). My collaboration with Dr. Ying Zhang (the Dong Lab) and Dr. Pengcheng Wang (the Zhu Lab at Purdue U.) demonstrated that a canonical MAPK signaling pathway is integrated into the BASL polarization process during stomatal ACD (Zhang et al., 2015). My results show that YDA physically interacts and co-polarizes with BASL in stomatal ACD cells, providing a molecular basis for the forward feedback loop between BASL protein and the MAPK signaling pathway for establishing cell polarity. The identification of this positive feedback loop and the differential expression of polarity complex in two daughter cells also provided new insights into the mechanism for differential daughter cell fate determination in plants (Zhang et al., 2016b).

In Chapter 3, to understand how this self-amplifying, positive feedback signaling system is maintained and attenuated in plant cells, I characterized the subcellular distribution and dynamic trafficking of BASL and YDA. My cell biological data demonstrated that the plasma membrane-associated BASL and YDA proteins are internalized into the endomembrane system and delivered to multi-vesicular body and vacuole for degradation in stomatal lineage cells. It is therefore hypothesized that the plasma membrane-associated BASL and YDA proteins are subject to an elegant

regulation by endomembrane trafficking so that the amount of active molecules and the distribution pattern can be controlled dynamically and precisely in cell development.

In Chapter 4, I studied a newly identified polarity regulator, ICR1, which promotes the vacuolar degradation of internalized BASL and YDA, thus alleviating the positive feedback signaling at the plasma membrane. More interestingly, ICR1 is a plant-specific, Microtubule (MT)-binding protein. This reveals a new role of MT cytoskeleton in the regulation of vacuolar trafficking in plant cells. In addition, my collaboration with Dongmeng Li (the graduate student in the Dong Lab) links ICR1 function with FAB1/PIKfyve (Phosphatidylinositol 3-phosphate 5-kinase), an important player in promoting endosome maturation, vacuolar targeting and degradation of BASL-YDA. Thus, a working model that integrates the MT-scaffold function of ICR1 into endosomal regulation in the process of vacuolar targeting is proposed.

Overall, my work contributes to the formulation of the BASL-centered polarization machinery that was promoted by a positive feedback regulation with a MAPK signaling pathway and downregulated by a MT-based ICR1 vacuolar targeting system to achieve dynamic and precise spatiotemporal signaling at the polarity site.

PREFACE

Role of the author

CHAPTER 1

A literature review modified from Shao and Dong (2016, Dev. Biol.) that was co-written by Dr. Juan Dong and myself.

CHAPTER 2

The positive feedback regulation between BASL and the YDA MAPK signaling pathway was a collaborative effort that is published at Zhang et al. (2015, Dev. Cell). I contributed to the genetic understanding of BASL and YDA in polarization.

CHAPTER 3

The endomembrane trafficking of BASL-YDA was part of my major project. Dr. Kezhen Yang performed the BFA treatment on *BASLpro::*GFP-BASL. I performed the other experiments and analyses.

CHAPTER 4

Functional characterization of ICR1 in the vacuolar degradation of BASL-YDA was part of my major project. Dr. Xiaoyu Guo performed *in vitro* pull-down and kinase assay for ICR1's physical interaction with YDA and its regulation on the MAPK signaling, respectively. Dongmeng Li initiated the FAB1 project and discovered the overexpression *FAB1B* phenotype in stomatal development. I performed the other experiments and analyses.

ACKNOWLEDGEMENTS

At the end of my graduate life, I would like to thank the people who have helped, supported and encouraged me in the past few years. First of all, I would like to thank my advisor, Dr. Juan Dong. This work would not have been possible without her careful guidance and support. She guided me tirelessly in every aspect, from specific experimental designs to capacity building. On countless cases, Juan helped me succeed solving the difficulties encountered in research. I have benefitted so much from her rigorous attitude of scholarship, open-minded suggestions and enthusiasm for scientific inquiry.

I am very fortunate to have had the opportunity to work with a group of wonderful people in the Dong Lab. Besides numerous engaging discussions and suggestions in research, they also provided me with a pleasant working atmosphere. I will always recall this unforgettable graduate life which is full of warmth. I am particularly thankful for Dr. Ying Zhang, who taught me and helped me in my early graduate years. I have been extremely fortunate to collaborate with Ying, who built the foundation for many findings here and greatly contributed to the success of my first project. I also would like to thank Dr. Xiaoyu Guo, a talented biochemist who engaged and helped on my second project. She is always patient and has given me so many helpful experimental recommendations. Many thanks to Dr. Xueyi Xue, who is so knowledgeable, generous and willing to share his experience with others. I am also grateful to Helen Xia, an undergraduate student who helped me a lot on thesis editing.

My graduate research and personal development also greatly benefited from the guidance of my thesis committee, Drs. Andrea Gallavotti, Pal Maliga and Ruth Steward. It is truly an honor to have them and I will always treasure the guidance and discussions they provided generously.

I am grateful to the Department of Plant Biology at Rutgers for providing administrative, technical, and moral support. I wish to thank the graduate advisor Dr. Bingru Huang and many other professors for their diligence in ensuring that we students have the resources necessary to be successful. I learned a lot from the well-designed core courses offered in our department.

Lastly, I wish to thank my family and friends for their unconditional love and support throughout my graduate school experience. I certainly could not have completed this work without their support, especially my husband Haojun Yin. Thanks to his understanding and intensive care, I lived through down times and frustrations to become a better person. Thanks to my parents, Wei Shao and Jie Zhang, for helping me maintain a balanced life, and for providing me with spiritual comfort.

Table of Contents

ABSTRACT OF THE DISSERTATION ii
PREFACE v
ACKNOWLEDGEMENTS vi

CHAPTER 1. INTRODUCTION 1
Significance of cell polarity and asymmetric cell division 1
Model systems for studying cell polarity in plant development 1
Molecular machinery for the establishment of cell polarity 5
Functions of polarity proteins in asymmetric cell division 13
Other key factors in stomatal development and patterning 17
Ligand-receptor signaling components 17
Research goals 20

CHAPTER 2. The MAPKKK YDA is a polarity partner of BASL in the stomatal lineage cells. 21
ABSTRACT 21
INTRODUCTION 22
RESULTS 25
Promoter activity analysis of MAPKs 25
The MAPKKK YDA is polarly localized 26
BASL recruits YDA to the polarity crescent 28
YDA physically interacts with BASL 30
Compromised MAPK signaling leads to defective polarization of BASL 31
DISCUSSION 33
METHODS 37

CHAPTER 3. Intracellular trafficking of the BASL-YDA polarity complex 41
ABSTRACT 41
INTRODUCTION 42

RESULTS 45
The PM-associated YDA and BASL are regulated by endomembrane trafficking . 45
YDA and BASL are transported through WM-sensitive late endosomes 47
YDA is highly colocalized with FAB1A-decorated late endosomes 48
BASL and YDA are targeted in the vacuole for degradation 51
DISCUSSION 53
METHODS 56

CHAPTER 4. Microtubule-associated ICR1 attenuates the BASL-YODA polarity proteins through vacuolar degradation 59
ABSTRACT 59
INTRODUCTION 60
RESULTS 61
Promoter activity of the ICRs family 61
ICR proteins are associated with the microtubule cytoskeleton 63
Genetic redundancy of the ICR gene family 64
ICR1 overexpressor resembles the loss-of-function basl mutants 67
Analysis of icr1 mutants 70
ICR1 overexpression induces protein degradation of both BASL and YDA 73
PINs are not downregulated by ICR1 75
ICR1 promotes BASL and YDA targeting towards the vacuole. 76
ICR1 associates with the microtubules 79
ICR1 physically interacts with YDA. 81
FAB1 localize to ICR1-decorating MTs 84
FAB1 promotes BASL-YDA degradation. 87
DISCUSSION 89
METHODS 93

CONCLUSION AND PERSPECTIVES 101
REFERENCES 104

List of Figures

Fig. 1.1. Schematic of Arabidopsis stomatal lineage cell. 5
Fig. 1.2. Actin-dependent positive feedback loops for symmetry-breaking polarization in yeast and maize stomatal cells 12
Fig. 1.3. *basl* stomatal phenotypes and BASL polar localization. 14
Fig. 1.4. Established signaling pathways of stomatal development. 20
Fig. 2.1. Promoter activity of MAPKs and MKKs. 26
Fig. 2.2. Polar localization of MAPKKK YDA. 27
..... 29
Fig. 2.3. BASL recruits YDA to the cell cortex. 29
Fig. 2.4. BASL interacts with YDA at the cell cortex. 31
Fig. 2.5. Defective BASL polarity due to compromised MAPK activities. 32
Fig. 2.6. Models for the feedback loop between BASL and the YDA MAPK pathway. 33
Fig. 3.1. Diagram of the subcellular endocytic pathway in plants. 42
Fig. 3.2. The PM-associated YDA and BASL are regulated by endomembrane trafficking. 46
Fig. 3.3. Transport of YDA and BASL is dependent on WM-sensitive late endosomes. 48
Fig. 3.4. Colocalization of YDA with endosome markers in both tobacco cells and *Arabidopsis* stomatal lineage cells. 51
Fig. 3.5. BASL and YDA are targeted in the vacuole. 52
Fig. 4.1. Phylogenetic tree and promoter activity of *ICR* members. 63
Fig. 4.2. Expression of fluorescent protein-tagged ICRs in plant cells. 64
Fig. 4.3. Genetic redundancy of the *ICR* family. 66
Fig. 4.4. Overexpression of ICR1 resembles loss-of-function *basl* mutants. 69
Fig. 4.5. *ICR1* mutant phenotype in leaf epidermis. 72
Fig. 4.6. ICR1 overexpression induces YDA and BASL protein turnover. 74
Fig. 4.7. PINs are not downregulated by ICR1 76
Fig. 4.8. ICR1 promotes BASL and YDA targeting towards the vacuole. 78
Fig. 4.9. Cellular localization of ICR1 reveals direct MT-binding. 81

Fig. 4.10. ICR1 physically interacts with YDA. 83
Fig. 4.11 FAB1 localized to ICR1-decorating MTs. 86
Fig. 4.12. ICR1 physically interacts with YDA. 88
Fig. 4.13. Hypothetical model of downregulation mechanisms of ICR1 on BASL-YDA polarity complex. 89

List of Abbreviations

Organelles and cell types:

MMC	Meristemoid Mother Cell
GMC	Guard Mother Cell
M	Meristemoid
SMC	Subsidiary Mother Cell
SLGC	Stomatal Lineage Ground Cell
GC	Guard Cell
ER	Endoplasmic Reticulum
TGN	Trans-Golgi Network
PM	Plasma Membrane
LE	Late Endosome
PVC	Pre-Vacuolar Compartment
MVB	Multivesicular Body
CME	Clathrin-Mediated Endocytosis
CavME	Caveolae-Mediated Endocytosis
MT	Microtubule
PPB	Preprophase Band

Chemical inhibitors:

PI	Propidium iodide
BFA	Brefeldin A
ConcA	Concanamycin A
WM	Wortmannin

CHAPTER 1. INTRODUCTION

Significance of cell polarity and asymmetric cell division

One of the most intriguing and essential features of cells is their ability to break symmetry, which manifests as cell polarity. Cell polarization is often initiated by an assembly of specialized cell cortical membrane domains in a cell. During this process, proteins, mRNAs, organelles, and cytoskeletal components among other molecules become distributed unevenly. Polarization occurs essentially in all cellular organisms and is required for a variety of fundamental processes in morphogenesis, cell division, as well as cell differentiation (Freisinger et al., 2013; Yang and Lavagi, 2012). Multiple model systems have been employed to investigate the mechanisms of cell polarization, including single-cell systems (e.g. budding yeast, plant pollen tube and root hair) and multicellular systems (e.g. mammalian epithelial cells, plant puzzle-shaped epidermal cells).

During the development of multicellular organisms, cell polarization is also required for another universally fundamental process, asymmetric cell division (ACD). During ACD, precursor cells divide to create daughter cells that differ in size, location, and cellular components. Such division functions to maintain stem cell population, specify various cell fates and provide patterning (Abrash and Bergmann, 2009a; Knoblich, 2008; Munoz-Nortes et al., 2014).

Cell polarization occurs early in an asymmetric cell division, and by providing a spatial cue, is significant for subsequent checkpoints, e.g. mitotic spindle alignment, division

plane positioning and daughter cell fate differentiation (Knoblich, 2008, 2010; Neumuller and Knoblich, 2009).

Model systems for studying cell polarity in plant development

Currently, cell polarity and polar growth have been characterized in 1) ***tip growth***: cells undergo tip extension with sustained unidirectional growth, and 2) ***diffused growth***: multi-directional anisotropic cell expansions that happen at specific regions (Qin and Dong, 2015). Several model systems offer fascinating platforms for elucidating the mechanisms of plant cell polarity control. In *Arabidopsis*, the single-cell pollen tube and root hair have been used as excellent model systems for studying tip growth (Cardenas, 2009). Leaf pavement cells have been established as an ideal system for diffused polar growth (Lin et al., 2015). In recent years, zygotes and stomatal lineage cells have emerged as new systems for investigating cellular polarization for asymmetric cell divisions (Dong and Bergmann, 2010).

Tip polar growth: root hairs and pollen tubes

Root hairs originate from root epidermis and exhibit rapid tip growth at the rate of 10-40 nm/s due to continuously localized vesicle targeting and exocytosis to the growth site (Galway et al., 1997; Hepler et al., 2001). Many essential genes have been identified to regulate tip growth, involving in the calcium-mediated signaling, reactive oxygen species (ROS), and small GTPases pathways (Carol and Dolan, 2006; Guan et al., 2013; Molendijk et al., 2001).

Pollen tubes are generated from pollen grains and extend rapidly (growth speed 1 cm/h) to directionally deliver sperm to the ovule for fertilization. Even when cultured *in vitro*, pollen maintains its developmental status and polarity. So the easy manipulation and haploid genome background facilitate genetic analysis of the essential mechanisms regulating polarity control (Qin and Dong, 2015; Yang, 2008).

Diffused polar growth: pavement cells

Unlike unicellular root hairs and pollen tubes, pavement cells in leaf epidermis expand by diffused growth. With their jigsaw-puzzle appearance, pavement cells provide an excellent platform for investigating the mechanisms of cell-to-cell coordinated polarity and morphogenesis (Smith, 2003). The precisely matched lobes and indentations of adjacent cells suggest critical cell-to-cell communication and spatiotemporal coordination, which is similar to convergent extension of animal planar cells (Klein and Mlodzik, 2005; Yang, 2008). Accumulating evidence has suggested a complex mechanism including reorganization of cortical microtubules and fine actin microfilaments that is precisely regulated by a Rho GTPase family and cytoplasmic auxin signaling (Lin et al., 2012; Settleman, 2005; Xu et al., 2010).

Cell polarity in asymmetric cell division: zygotes and stomatal lineage cells

Asymmetric cell division (ACD) is a fundamental process in the development of cell-type diversity in multicellular organisms. Cell polarization is a typical intrinsic regulatory measure that is required early in an ACD and is essential for subsequent

cellular procedures, e.g. cytoskeleton organization, vesicular trafficking and daughter cell fate differentiation (De Smet and Beeckman, 2011).

Zygote polarization is required for the first asymmetric division to the embryo axis. During early embryogenesis, zygotic symmetry breaking is the first and key step for establishing apical-basal polarity along the axis and determining the following cell fates (Brownlee and Bouget, 1998). After fertilization, a zygote anisotropically expands and undergoes the first ACD, generating precursors of apical and basal cell lineages with distinct cell fates. The apical cell undergoes several rounds of divisions, eventually giving rise to the majority portion of an embryo, whereas the basal cell forms an extra-embryonic suspensor though a series of transverse divisions and connects the embryo with maternal tissue for nutrition (Faure et al., 2002; Pillitteri et al., 2016). The uppermost part of suspensor called the hypophysis will later form the root meristem through ACD, and the root meristem contributes to the organizing center of root apical meristem (Abrash and Bergmann, 2009b).

In the dicotyledon *Arabidopsis*, stomatal cell lineage begins with an epidermal cell named Meristemoid Mother Cell (MMC), which undergoes an asymmetric division to generate a differentiated cell type, meristemoid. After several rounds of ACD, the meristemoid differentiates into a Guard Mother Cell (GMC), which eventually forms a pair of guard cells (Pillitteri and Dong, 2013) (**Fig.1.1**). In the monocotyledonous system *Zea mays*, a GMC first undergoes an ACD and then one symmetric division to form a pair of guard cells, while the neighboring Subsidiary Mother Cells (SMCs)

asymmetrically divide to form subsidiary cells flanking the guard cells (Tena, 2016; Vaten and Bergmann, 2013).

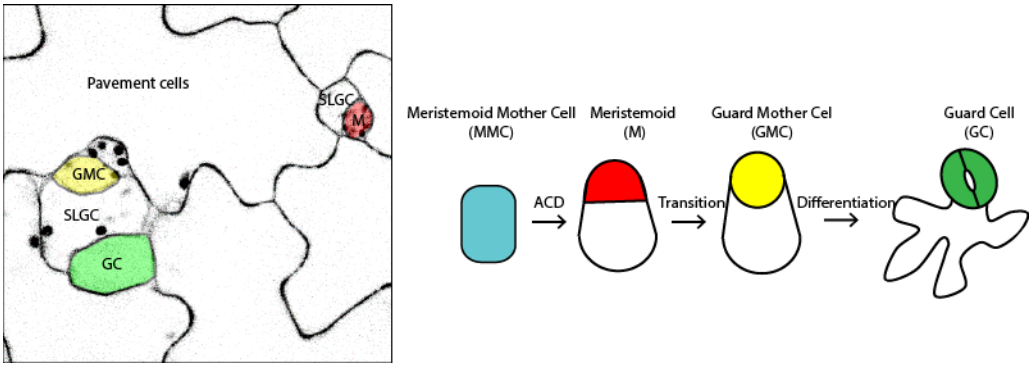

Fig. 1.1. Schematic of Arabidopsis stomatal lineage cell.
Left Panel: Confocal images of 5-dpg adaxial *Arabidopsis* leaf epidermis. Colors highlight the specific cell identities of stomatal lineage cells. Right Panel: Diagram of stages in *Arabidopsis* stomatal development based on Dong and Bergmann (2010). An epidermal cell named meristemoid mother cell (MMC) divides asymmetrically to generate two daughter cells of divergent sizes and identities. The smaller daughter cell, the meristemoid (M), differentiates into a guard mother cell (GMC) after a few rounds of ACD, and ultimately form stomata. The larger daughter cell, the Stomatal Lineage Ground Cell (SLGC) typically expands and differentiates as a pavement cell.

Molecular machinery for the establishment of cell polarity

The molecular mechanisms underpinning cell polarity have been described in model systems, such as the worm *C. elegans* embryo, the fruit fly *Drosophila* nervous systems, and the budding yeast *S. cerevisiae* (Inaba and Yamashita, 2012). Hallmark polarity proteins in animals, e.g. the Cdc42 small GTPase (Chant, 1999; Slaughter et al., 2009b) and conserved Partitioning defective (PAR) proteins (Goldstein and Macara, 2007; Nance and Zallen, 2011), have been investigated intensively for the past several decades. However, many of these highly conserved proteins found in animal cells are missing from the plant systems. Unlike animal cells, plant cells have a rigid cellulosic extracellular matrix, the cell wall, which provides physical support and forms

communication routes. This fundamental difference leads to some unique mechanisms in plants for generating polarity for symmetry breaking. Current progress suggests that common regulatory modes, i.e. protein spontaneous clustering and cytoskeleton reorganization, underlie protein polarization in both animal and plant cells. Despite these commonalities, it is important to note that intrinsic mechanisms in plants are heavily influenced by extrinsic cues. Intrinsic mechanisms refer to those in which cell fate differentiation occurs prior to cytokinesis of the parental cell (Goldstein and Macara, 2007; Knoblich, 2008). Extrinsic factors drive differentiation outcome due to the asymmetric placement of the daughter cells into two distinct microenvironments (Fuller and Spradling, 2007). Although both processes are important in complex organisms, intrinsic processes and extrinsic processes may have more weight over the other under certain conditions. Contrary to the dominant roles of animal polarity proteins being solely intrinsic cues, plant polarity proteins seem to participate in both intrinsic and extrinsic pathways to regulate divisional asymmetries in development. Representative mechanisms are discussed here to illustrate how cell polarity is established in multiple systems.

Protein polarization: Positive-feedback loops

The positive-feedback loop in establishing cell polarity was extensively studied in the single-celled organism yeast *S. cerevisiae,* which continuously produces small daughter cells via polarizing the mother cell to form a bud. The polarization of the mother cell manifests as a patch enriched with cytoskeleton and membrane trafficking components at the polarity site, which promotes the growth of the daughter cell. The polarity

regulator, small Rho GTPase Cdc42, was first identified by Adams et al. (1990) and later established as “the center of cell polarization” ubiquitously from yeast to humans (Etienne-Manneville, 2004; Park and Bi, 2007). Loss of Cdc42 function leads to mother cell polarization failure and causes division problems (Adams et al., 1990). The cycling of Cdc42 between active guanosine triphosphate (GTP)-bound and inactive guanosine diphosphate (GDP)-bound forms is controlled by orchestrated activity of activators (guanine nucleotide exchange factors, GEFs), inhibitors (ATPase-activating proteins, GAPs) and other modulators (Rho GTPase-dissociation inhibitors, GDIs) (Vetter and Wittinghofer, 2001). One of the two major pathways that distribute Cdc42 in highly polarized fashion at the cell cortex is actin-independent and requires a Cdc42-Bem1-Cdc24 centered positive feedback loop. Bem1 is a scaffold protein and Cdc24 is a GEF activator of Cdc42. In the absence of any spatial cues, stochastically activated Cdc42 molecules may spontaneously cluster to initiate a cortical site where Bem1 is recruited, which locally accumulates Cdc24 that further activates Cdc42 to expand the polarity domain (Butty et al., 2002; Smith et al., 2013). More recently, a Cdc42 effector p21-activated kinase (Shpak et al.) was also found as a part of the complex; PAK binds to Cdc24 and contributes to the spontaneous polarization of yeast cells (Kozubowski et al., 2008; Woods et al., 2015). Thus, positive feedback loops provide a base for spontaneous initiation of Cdc42 polarization. However, in plants, how positive feedback loops are involved and regulate cell polarization remains unclear. My collaborative work presented later in Chapter 2 revealed that positive feedback loops and protein spontaneous clustering are also part of the polarization process in plants (Zhang et al.,

2015), which to some extent resembles the self-organizing polarization of Cdc42-Bem1-Cdc24 found in yeast.

Vesicle trafficking in establishing cell polarity

Plasma membrane proteins are synthesized in the cytosol and then sorted into specialized carrier cargoes for delivery to targeted plasma membrane loci, eventually to be released by membrane fusion. Therefore, intrinsic mechanisms that regulate the membrane proteins sorting and directional vesical trafficking are critical for polarity formation (Drubin and Nelson, 1996; Mellman and Nelson, 2008).

Vesicular trafficking through endomembrane network comprised dynamic cargo secretion as the exocytosis pathways (Belanger and Quatrano, 2000) and uptake of extracellular biomolecules to the intracellular destination as endocytosis pathways (Mayor et al., 2014). These two pathways are highly coordinated and interconnected to maintain plasma membrane integrity. Continuous membrane deformation, budding, fission, tethering and fusion are critical to vesicular trafficking process in all eukaryotic systems (Peer, 2011). After synthesis, proteins are translocated to the endoplasmic reticulum (ER) and are subsequently sorted through the Golgi apparatus and trans-Golgi network (TGN). Subsequently, secretory proteins are packed into secretory vesicles to target to the plasma membrane. Some proteins sorted by TGN can be directed to a lytic compartment, e.g. lysosome in mammalian cells and vacuole in plants and yeasts (Geldner, 2004; Peer, 2011).

Polarized exocytosis has been found to be essential in cell polarity formation (Belanger and Quatrano, 2000). A conserved complex, the exocyst, is responsible for the polar docking of vesicles to the PM (Cole and Fowler, 2006). In plants, by delivering membrane and wall material, polarized exocytosis promotes tip growth of root hairs and pollen tubes. Polar localization of ROP1, a plant-specific Rho GTPase, is mediated by ADP-ribosylation factor (ARF) GTPase–regulated vesicular trafficking in pollen tubes (Xu and Scheres, 2005a, b). The dynamic F-actin filaments participate in the positive feedback activation of ROP1 by providing tracks for polarized exocytosis (Molendijk et al., 2001). Similarly, in yeast, active Cdc42-guided, actin-dependent exocytosis enhances the Cdc42 enrichment at the polarization site by a positive feedback loop (Pruyne et al., 2004; Rohatgi et al., 1999).

Endocytosis which retrieves excessive signaling molecules and wall materials from the plasma membrane (PM), is another key mechanism for cell polarity establishment and maintenance (Mayor et al., 2014). The endocytosis pathway has been extensively studied and well characterized in animal and yeast systems. In animal cells, the Clathrin-Mediated Endocytosis (CME) and Caveolae-Mediated Endocytosis (CavME) are the predominant endocytic routes for protein internalization (Elkin et al., 2016; Takei and Haucke, 2001). The major adaptor protein AP2 complex is recruited to the plasma membrane by domain-enriched phosphatidylinositol lipid PI(4,5)P2 and this process recruits clathrin coat rapidly for cargo recognition (Kirchhausen et al., 2014; Traub and Bonifacino, 2013). Mathematic modeling demonstrated that the balance of diffusion, directed transport, and endocytosis was sufficient to maintain polarization of active Cdc42 in yeast (Marco et al., 2007).

In plant cells, CME was also identified to function in establishing and sustaining cell polarity. The primarily studied example for trafficking-based protein polarization is the PIN-FORMED (PIN) auxin transporter. PINs are membrane integral proteins and often occupy distinct plasma membrane domains in *Arabidopsis* plants (Friml, 2003). Polar targeting and maintenance of PINs at the plasma membrane involve rapid and constitutive vesicular recycling between the PM and endosomes (Feraru and Friml, 2008; Grunewald and Friml, 2010). Drug interference with the clathrin-dependent cargo recruitment blocks internalization of PINs and results in polarity defects, which suggests the essential roles of CME in internalization of PM-resident proteins (Dhonukshe et al., 2007).

Cell polarization: cytoskeletal reorganization

In yeast, the second positive feedback loop in Cdc42 polarization involves active Cdc42-guided, actin-dependent exocytosis (Pruyne et al., 2004; Rohatgi et al., 1999). Two forms of actin structure (patches and cables) are positively regulated by Cdc42. Cdc42-GTP promotes the formation of actin cables, which are nucleated by formin-family proteins (Pruyne et al., 2004) and provide tracks for the delivery of exocytotic vesicles carrying Cdc42-GTP (Evangelista et al., 2002; Pruyne et al., 2004). This, in turn, enhances the Cdc42 enrichment at the polarization site (Marco et al., 2007; Wedlich-Soldner et al., 2003; Wedlich-Soldner et al., 2004) (**Fig. 1.2**). Actin patches, a Cdc42-dependent platform for endocytosis and cell wall remodeling, contain a dynamic network of branched actin filaments that are polymerized by the Arp2/3 complex (Moseley and Goode, 2006).

In *Arabidopsis*, the Rho family has diverged into the Rho-like GTPase from Plants (ROP) family that shares the common ancestor of Cdc42 (Gu et al., 2004). Similar to their counterparts in yeast and animals, ROP polarization also involves feedback loops (Hazak et al., 2010; Zhang and McCormick, 2007) that coordinate cytoskeleton organization and vesicular trafficking to establish cell polarity as well as promote polar growth in plants (Fu et al., 2005; Gu et al., 2005). The roles of ROPs in plant asymmetric cell division were demonstrated by their functional connection with PAN leucine-rich repeat receptor-like kinases in maize stomatal development. The polarization of PANs provides a representation of an extrinsic-cue induced process.

In maize (*Zea mays*), each stomatal complex is composed of two guard cells flanked by two subsidiary cells. The production of subsidiary cells requires asymmetric cell division of the precursor subsidiary mother cells (SMC). Prior to SMC ACD, the SMC polarization is demonstrated by the asymmetric accumulation of PAN proteins at the plasma membrane of a SMC abutting the neighboring guard cells, followed by the formation of actin patch at the polarity site (Cartwright et al., 2009). Loss of PAN1 or PAN2 led to failures of SMC premitotic polarization and abnormal SMC division (Cartwright et al., 2009; Zhang et al., 2012). It was hypothesized that PAN proteins are polarized by hypothetical ligand signals derived from contacting guard cells. Recent work disclosed that prior to PAN polarization, the SCAR/WAVE complex (activator of the actin nucleating Arp2/3 complex) polarizes in SMCs independent of PANs and is required for PAN polarization (Facette et al., 2015). The early polarization of SCAR/WAVE was unexpected because PAN proteins physically interact and polarize ROP proteins (Humphries et al., 2011), which activate the SCAR/WAVE complex and

thus the Arp2/3 complex for promoting the formation of actin patches in SMCs (Facette et al., 2015). It remains obscure how the SCAR/WAVE complex becomes polarized and how it determines PAN polarization. PAN proteins are membrane embedded receptors. Many plasma membrane proteins require endosomal recycling, during which actin facilitates many aspects of membrane trafficking in plant cells (Kaksonen et al., 2006; Samaj et al., 2004). It is tantalizing to hypothesize that the actin network is inconspicuously reorganized by locally polarized SCAR/WAVE, which in turn influences membrane trafficking and polarization of PAN proteins in SMCs. However, what serves as the initial cue derived from GCs to polarize SMCs remains a fascinating question in the field.

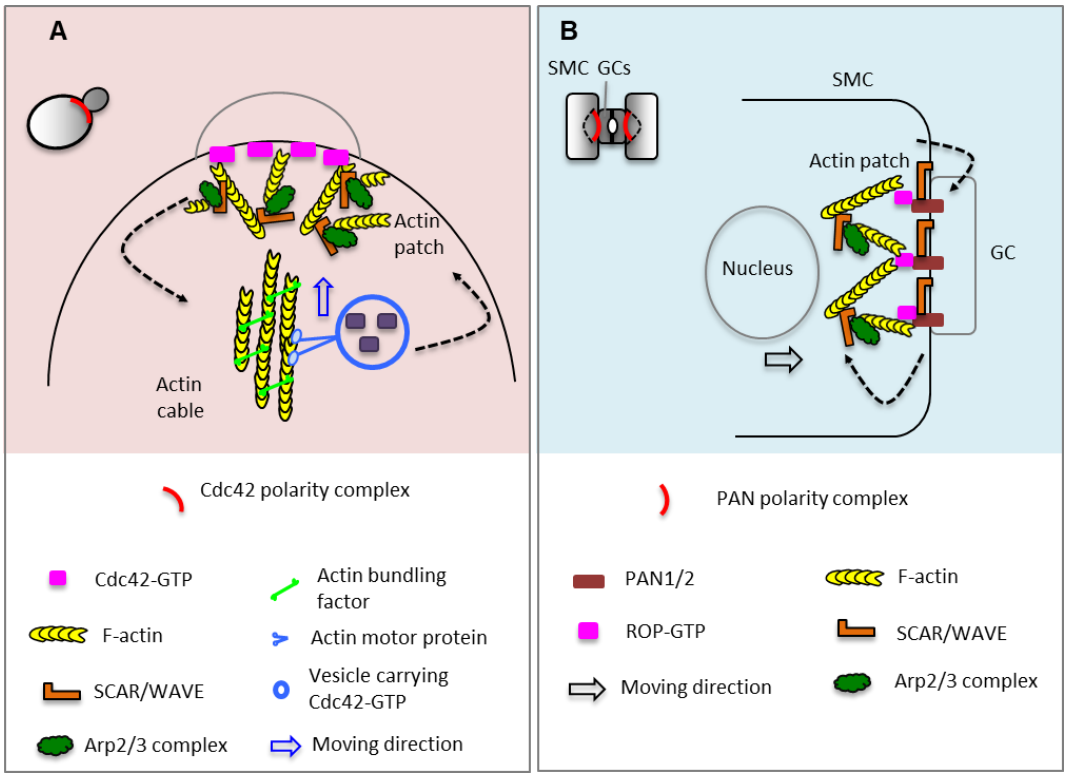

Fig. 1.2. Actin-dependent positive feedback loops for symmetry-breaking polarization in yeast and maize stomatal cells (Modified from Fig. 2 in Shao and Dong (2016, Dev. Biol.)). **(A)** Cytoskeletion-dependent polarization of Cdc42 in yeast. Cortically localized active Cdc42-GTP triggers Formin activity (bundling factor) to form actin cables. Actin cables provide tracks for the delivery of *exo*cytotic vesicles carrying Cdc42-GTP to the polarizing site,

resulting in further nucleation of actin cables, which in turn enhances the Cdc42 polar enrichment (dashed arrows). Blue arrow shows the moving direction of Cdc42-GTP vesicles driven by actin motor proteins. The formation of actin patches is stimulated by Cdc42-GTP activated SCARE/WAVE and Arp2/3, which promote actin nucleation and branching. Actin patches are necessary for dynamic delivery of PM and cell wall materials. **(B)** PAN1/2 polarization in maize Subsidiary Mother Cells (SMCs). In SMC, polarized PAN1/2 physically bind to ROP and lead to ROP activation. Polarized ROP activates the SCAR/WAVE and Arp2/3 activity and thus nucleation of actin to form a dense actin patch at the polarity site. Actin patches may help directional nuclear migration (black arrow) during SMC ACD. Interestingly, the polarization of SCAR/WAVE is also required for PAN1/2 polarization, suggesting an interdependent activation (dashed arrows).

Functions of polarity proteins in asymmetric cell division

In higher plants, the key roles of cell polarization in stem cell ACD have emerged and are manifested by asymmetrically distributed proteins and signaling pathways. Similar to the differentiation mechanism found in animals, plants also utilize intrinsically polarized proteins to regulate asymmetric signaling and cell division. Asymmetric cell divisions that are coordinated with the polarity of the mother cells override the influence of cell shape on the selection of the division plane and cortical polarity proteins contribute heavily to defining PM domains and thus division plane establishment. However, our understanding of the cell polarization mechanisms for ACD remains limited.

Polarized proteins- BASL and POLAR

In *Arabidopsis*, the stomatal lineage cells divide asymmetrically to produce highly specialized guard cells that conduct gas exchange between the plant and the atmosphere (Bergmann and Sack, 2007). The initiation of stomatal precursor cells occurs in young developing leaves and their division orientation appears random relative to the leaf axis (Lau and Bergmann, 2012), suggesting an intrinsic polarization property of the cells.

This is strongly supported by the discovery of the plant-specific BASL gene (Dong et al., 2009). In the absence of *BASL*, stomatal lineage cells lose their full capacity to divide asymmetrically, thus producing an enlarged proliferating population with equal division pattern and disturbed daughter cell fate segregation (Dong et al., 2009) (**Fig. 1.3A, 1.3B**). The localization of BASL protein is mainly featured by its strong polar accumulation at the cell cortex which is indispensable for its function (Dong et al., 2009) (**Fig. 1.3C**). BASL accumulates into the nucleus prior to its cortical polarization, but the nuclear pool seems to be a form of storage. The BASL protein does not contain a transmembrane domain and is not likely attached to the plasma membrane directly but through association with PM-embedded partners.

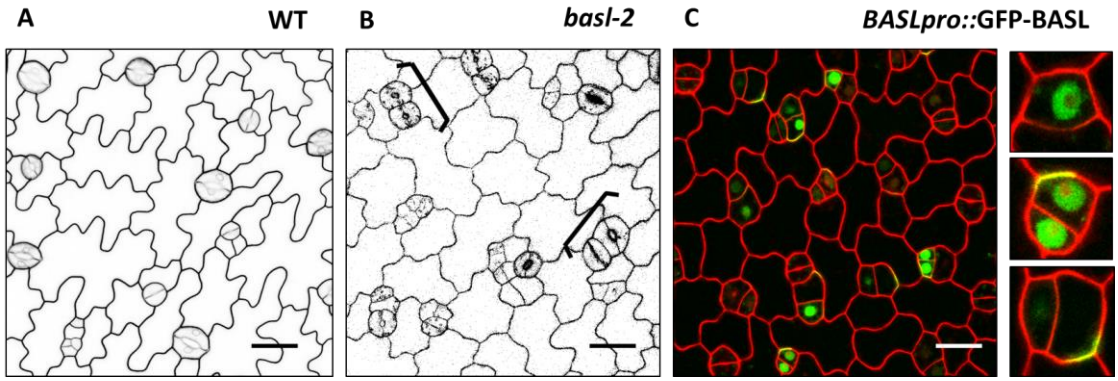

Fig. 1.3. *basl* stomatal phenotypes and BASL polar localization.
(**A**-**B**) Confocal images of 3-dpg adaxial cotyledons stained with propidium iodide (red). **(A)** WT. (**B**) *basl-2* null mutant. Braces indicate clustered small cells and stomata. Scale bars: 25 μm. Others at same scale. (**C**) Dual localization of GFP-BASL driven by its endogenous promoter in stomata lineage cells. Insets showed a close view of BASL localization in different cell types.

POLAR is another polarized protein of unknown function in the *Arabidopsis* stomatal lineage. The cortical polarization pattern of POLAR mirrors that of BASL and is dependent on the presence of BASL (Pillitteri et al., 2011). But how POLAR

contributes to the polarity pathway to regulate stomatal ACD remains unknown because mutations in POLAR did not yield discernible defects.

Division orientation

In animals, the cleavage plane that separates two daughter cells is defined by the contractile actomyosin ring, which uses the mitotic spindle as a positional cue (von Dassow, 2009). Correct spindle positioning is the linchpin to deciding placement of the cytokinesis furrow and ensuring that cell fate determinants are appropriately segregated (Williams and Fuchs, 2013). Conserved Partitioning defective (PAR) polarity proteins play fundamental roles in the regulation of ACD orientation in *C. elegans*, *Drosophila*, and vertebrates (Goldstein and Macara, 2007). In *Drosophila* neuroblast ACD, the PAR complex (PAR3 and PAR6 scaffold proteins and aPKC kinase) is polarized at the apical cortex and accumulates another apical complex (Pins, Gαi, Mud/NuMA) that directs and establishes spindle orientation. Mud/NuMA is a MT-binding protein that localizes to spindle poles and interacts with the dynein motor complex (Siller et al., 2006). The cortical-attached, MT minus-end directed motility of dynein exerts a pulling force to help navigate the mitotic spindle (Kiyomitsu and Cheeseman, 2012). Alternatively, dynein may serve as a cortical anchor of the plus-end depolymerizing microtubules that indirectly allows spindle positioning (Grill et al., 2003; Kozlowski et al., 2007). A number of MT plus-end binding proteins, e.g. CLASP, EB1 and the MCAK MT depolymerase have also been identified to contribute to MT dynamics and spindle orientation (reviewed in (Lu and Johnston, 2013)).

By contrast, the selection of cell division plane in plants is determined prior to the formation of the mitotic spindle. Previous research proposed that plant cells may rely on a specialized MT apparatus, the preprophase band (PPB), to organize cell division plane. The PPB is a cortical array of cytoskeletal filaments that are composed of microtubules (MTs) and filamentous actins (F-actins) and transiently assembled at G2 phase and dissembled at mitosis (Mineyuki, 1999). The cortical demarcation of the PPB loyally predicts where the division plane is placed, although the formation of PPB is not absolutely required across plant species. Recently, this theory was challenged by the discovery of a mutant *trm* which showed abolished PPB formation but normal interphase MTs. Without interfering with other MT arrays, *trm* mutant exhibited impaired PPB only and this defect did not affect the general orientations of the future cell division planes, but rather induced a loss of precision in individual division orientations (Schaefer et al., 2017). Thus, instead of being a causal determinant of the division plane, PPB may serve to limit spindle rotations by providing an equatorial reference for spindle orientation. This function model highly resembled the role of centrioles and astral MTs during mitosis in mammalian cells (Morin and Bellaiche, 2011; Schaefer et al., 2017), suggesting a potentially conserved machinery of division plane specification in the eukaryotes. However, how cell polarization orientates the division planes in plant cells remains unclear.

Asymmetric cell fate determination

In animals, the PAR proteins can asymmetrically segregate cell fate-determining factors. In *Drosophila* neuroblast ACD, the apically polarized PAR complex directs the fate-

determining complex, including Numb (an endocytic protein), Brain tumor (BRAT, a translation inhibitor) and Prospero (a transcription factor) to partition into the basal cell (Knoblich, 2008). After mitosis, the cell fate determinants act together to prevent stem cell self-renewal while promoting differentiation (Berdnik et al., 2002; Knoblich et al., 1995; Sonoda and Wharton, 2001; Spana and Doe, 1995).

In plants, asymmetric cell fate is found to be specified by mobile transcription factors. During root ACD, directional movement of the GRAS transcription factor SHORT ROOT (SHR), from the stele into the endodermal cells, helps to establish the asymmetric identity of the cortex and endodermis in *Arabidopsis* roots (Helariutta et al., 2000; Nakajima et al., 2001). Another example showed that the bHLH transcription factor TARGET OF MONOPTEROS 7 (TMO7) travels from the pro-vasculature of the early embryo into the hypophysis to direct asymmetric division (Schlereth et al., 2010). During stomatal ACD, it is known that the bHLH transcription factor SPEECHLESS (SPCH) initiates stomatal ACD and promotes fate differentiation (Lau et al., 2014a; MacAlister et al., 2007b), but how cell polarization is linked to SPCH expression requires further investigation.

Other key factors in stomatal development and patterning

Ligand-receptor signaling components

During *Arabidopsis* stomatal development, both intrinsic and extrinsic signaling pathways were identified and established as essential regulatory mechanisms. Extrinsic signaling triggered by ligand-receptor interaction (Torii, 2012) is shown to be required

to orient the polarities of spacing ACD and maintain ‘one-cell rule’ in stomata development. Too Many Mouth (TMM) (Nadeau and Sack, 2002b), a leucine-rich repeat (LRR) receptor-like protein, can associate with another LRR-RLKs ERECTA family (ER, ER-like 1 and ER-like 2) (Shpak et al., 2005b) to sense the signaling from a group of small, secreted peptide EPFLs (Hara et al., 2007; Hunt and Gray, 2009; Lee et al., 2012) as guiding cues. EPF1 and EPF2 interact with the TMM, and ERECTA, to activate the downstream MAPK pathway, although direct connections have not been established (Jewaria et al., 2013; Lee et al., 2015; Nadeau and Sack, 2002a; Shpak et al., 2005b).

The YDA MAPK pathway

The canonical MAPK cascade, composed of the MAPKKK YODA, MKK4/5 and MPK3/6, inhibits stomatal formation by phosphorylation of the nuclear bHLH transcription factor SPEECHLESS (SPCH) for degradation (Bergmann et al., 2004; Lampard et al., 2008; Lukowitz et al., 2004; Wang et al., 2007). As a universal regulatory pathway among eukaryotes, MAPK signaling mediates various developmental and environmental stimuli, e.g. stress response, defense and immunity response (Nakagami et al., 2005). Although broadly expressed, these MAPKs have specialized effects on promoting pavement cell differentiation and inhibiting stomata initiation. In the absence of *YDA* or *MKK4/5*, severe stomatal clustering was observed (Wang et al., 2007), whereas constitutively active forms of these proteins produced an epidermis composed of solely pavement cells, which phenocopied *spch* loss-of-function and implicated SPCH as a downstream target that inhibits stomata production. Other

members, MKK7/9 were also identified to promote guard mother cell (GMC) transition, based the observations that expression of constitutively active forms of MKK7/9 created clustering-stomatal phenotype (Lampard et al., 2009).

Downstream of MAPK YDA cascade signaling is a set of basic helix-loop-helix (bHLH) transcription factors that function in regulating the transition and differentiation progress through the lineage development. Expression of SPCH initiates stomatal ACD and promotes fate differentiation (Lau et al., 2014b; MacAlister et al., 2007a). MUTE is required to terminate asymmetric division. In the absence of *MUTE*, meristemoids divide excessively and fail to make transition to guard mother cell (GMC). Another bHLH protein FAMA promotes the final phase as transition from GMC to guard cell (GC) (Pillitteri et al., 2007). Loss-of-function *fama* mutants revealed more than one symmetric division of GMC, resulting in the production of elongated cell clusters similar to the shape of caterpillars (Ohashi-Ito and Bergmann, 2006). SCRM and SCRM2, act broadly throughout the stomatal lineage and promote stomatal cell fates through forming heterodimers with SPCH, MUTE and FAMA (Kanaoka et al., 2008) (**Fig.1.4**).

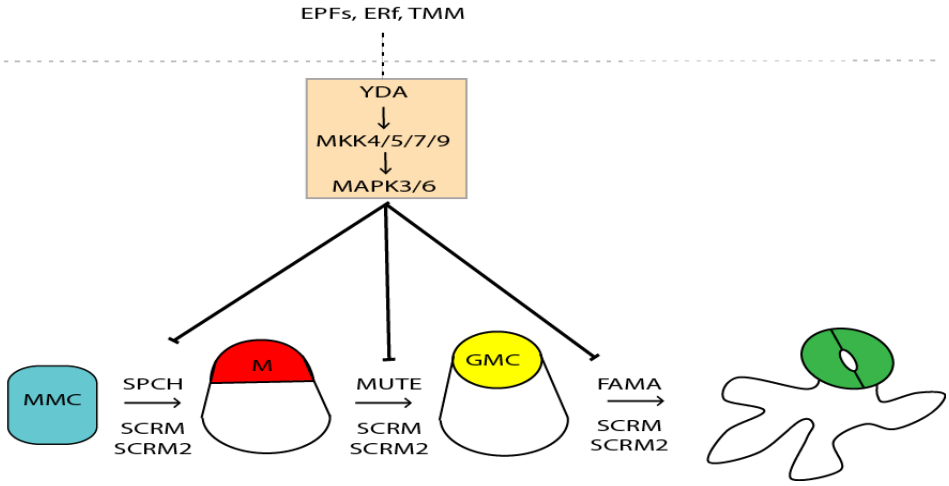

Fig. 1.4. Established signaling pathways of stomatal development.
Progression of *Arabidopsis* stomatal lineage cells is regulated by extrinsic signaling and transcription factor networks. Extracellular EPFs bind to plasma membrane receptors TMM and ERfs to transduce the signals to YDA MAPK cascade for inhibition on SPCH, MUTE and FAMA during specific cell fate transition (Dong and Bergmann, 2010).

Research goals

The identification of the BASL polarity protein in *Arabidopsis* stomatal lineage cells provided the first insights into polarity machineries that control divisional asymmetries in higher plants. How BASL polarization is initiated and maintained at the cortical membrane remains a major question to be addressed in our lab. My Ph.D. work focused on identifying new partners in the BASL polarity complex and investigating the molecular mechanisms for initiation and maintenance of cortical polarity.

CHAPTER 2. The MAPKKK YDA is a polarity partner of BASL in the stomatal lineage cells.

ABSTRACT

Cell polarization is one of the major mechanisms underlying asymmetric cell division (ACD) of plant stem cells. In *Arabidopsis*, BASL is polarized to control stomatal asymmetric division. A MITOGEN-ACTIVATED PROTEIN KINASE (MAPK) cascade comprised of the MAPKKK YODA(YDA)-MAPKK 4 and 5-MPK3 and 6 in *Arabidopsis* plays key roles in inhibiting stomatal production by promoting degradation of the bHLH transcription factor SPEECHLESS (SPCH). Here I show that BASL physically interacts with the MPKKK YODA (YDA) and YDA is polarized sub-cellularly to regulate stomatal ACD, functioning as a new component in the BASL-centered polarity complex. Beyond that, my collaboration with Dr. Ying Zhang and Dr. Pengcheng Wang demonstrated that cortically polarized BASL functions as a MAPK scaffold and recruits both YDA and MPK3/6 to spatially concentrate at the cortex, which leads to differential levels of SPCH in two daughter cells and thus differential cell fates. This represents a new mechanism for differential fate determination for ACD in plants, in striking contrast to the previously established mechanism- asymmetric cell fate specified by mobile transcription factors in root ACD.

INTRODUCTION

Polarity is a universal feature of cells and is required for a wide range of biological functions and behaviors, such as cell migration, cell morphogenesis, and asymmetric cell division (ACD). Multicellular organisms commonly use ACD to generate diverse cell types for developmental and morphogenetic patterning and to maintain stem cell population for tissue hemostasis (Knoblich, 2008). In animal systems, conserved polarity proteins, such as *Par*titioning Defective (PAR) proteins, regulate polarization of stem cells through uneven distribution at the cell cortex and specifies distinct daughter cell fates (Goldstein and Macara, 2007; Prehoda, 2009). Despite the fundamental structural differences between plant and animal cells, the *Arabidopsis* polarity protein BASL seemed to play conceptually similar roles as PAR proteins in the regulation of ACD in plants (Abrash and Bergmann, 2009b; Dong et al., 2009; Facette and Smith, 2012). Before ACD, BASL is initially observed in nuclei of Meristemoid Mother Cells (MMCs) and then accumulates to a polarized crescent at the cell periphery as MMCs expand prior to divisions. After ACD, the peripheral crescent is inherited by the larger daughter cells, whereas the nuclear localization of BASL is maintained in the self-renewing cells (Dong et al., 2009). The key functions BASL might play in the regulation of stomatal ACD are 1) to establish premitotic cell polarity and determine division orientation, and 2) to specify non-stomatal terminal differentiation in one of the daughter cells (Dong et al., 2009). However, how BASL polarity is established from its initial nuclear localization is one of the fundamental questions to be addressed.

The *M*itogen-*a*ctivated *p*rotein *k*inases (MAPK) signaling system regulates a wide range of cellular responses in all eukaryotes. It has been established that the MAPK cascade (composed of the MAPK Kinase Kinase *YODA*, YDA; the MAPK Kinase 4 and 5, MKK4/5; and the MAPK 3 and 6, MPK3/6) plays a key role in embryonic asymmetric cell division and stomatal development in *Arabidopsis* (Bergmann et al., 2004; Lukowitz et al., 2004; Wang et al., 2007). The MPKKK YDA is broadly expressed and has pleiotropic effects on plant development. The loss-of-function *yda* mutants have severe defects in the first asymmetric cell division and the basal lineage determination during embryonic patterning (Bayer et al., 2009). Besides, *yda* mutants also exhibit a severe epidermal phenotype involving over-proliferation of stomata, suggesting that YDA inhibits stomatal development and differentiation (Bergmann et al., 2004). Recently YDA was reported to function in promoting cell expansion and orienting the division plane in embryonic ACD (Smekalova et al., 2014), implicating its potential connection with BASL.

Previous analyses from Dr. Ying Zhang and Dr. Pengcheng Wang suggested that BASL polarization requires the MAPK signaling-mediated phosphorylation. After a fine-scale domain analysis of BASL, Dr. Ying Zhang identified three putative MAPK docking motifs, including two D-sites (named as D1 and D2) and one DEF-site (Murphy et al., 2002). Point mutations that disrupted the core docking sites failed to show cortical polar accumulation and cannot rescue *basl* stomatal phenotype, suggesting that the MAPK-docking motifs are critical for BASL polarity and functions. *In vitro* kinase assays by Dr. Pengcheng Wang demonstrated that BASL can be phosphorylated by activated MPK3 and MPK6. Mass spectrometry further identified, out of six predicted MAPK

substrate Ser sites, five of them were indeed phosphorylated. When all 6 Serine residues were converted into Alanine (phospho-deficient, A), BASL_123456A showed predominant localization in the nucleus with no cortical polarity formation and this version failed to rescue the stomatal defects in *basl-2*. However, when all 6 Serine were converted to Aspartic Acid (phospho-mimicking, D), BASL_123456D recovered polarization and its function to the wild-type level. These data thus indicated that BASL is phosphorylated by MPK3/6 in the nucleus, and then moves out of the nucleus to polarize at the plasma membrane (PM). But the purpose of BASL staying at the PM and how it drives cell polarity remains unknown. In addition, the lab had an important discovery that the YDA translational fusion line, YDA^{KI}-YFP, exhibited an obviously polarized pattern in the stomatal lineage cells. Based on all these data, I started exploring the functional connections of BASL with the MAPKKK YDA.

Here, I demonstrate that YDA physically interacts with BASL and localizes to the cell cortex of stomatal ACD cells. At the same time, BASL polarization from the nucleus to the cortical crescent also requires YDA MAPK activity, suggesting a positive feedback regulation between these two proteins in establishing cell polarity.

RESULTS

Promoter activity analysis of MAPKs

The *Arabidopsis* genome encodes 20 MAPKs, 10 MAPK kinase (MKKs) and 60 MAPK kinase kinase (MAPKKKs) (Group, 2002). Among them, only MKK4/5/7/9 and MPK3/6 have been implicated in the regulation of stomatal development through genetic approaches (Wang et al., 2007; Lampard et al., 2009). There was scarce knowledge about how many MAPK components may function in the stomatal lineage cells. To analyze their promoter activity, I isolated the promoter region of respective MAPKs (3, 4, 5, 11, and 12) or MKKs (4 and 5) and made a set of Yellow Fluorescent Protein (YFP)-fused marker lines to express in transgenic plants, followed by microscopy examination.

The promoters of *MPK3/6* and *MKK4/5* are all highly active in the early staged stomatal lineage cells, but excluded from mature guard cells (MKK4/5 are also expressed in pavement cells in the epidermis, **Fig. 2.1A**, **2.1C**, **2.1F-G**), While MPK4/11/12 are mainly active in mature guard cells (**Fig. 2.1B**, **2.1D-E**). Interestingly, MPK12 is newly found to be active in the early stomatal lineage cells, suggesting its potential roles in stomatal development and patterning.

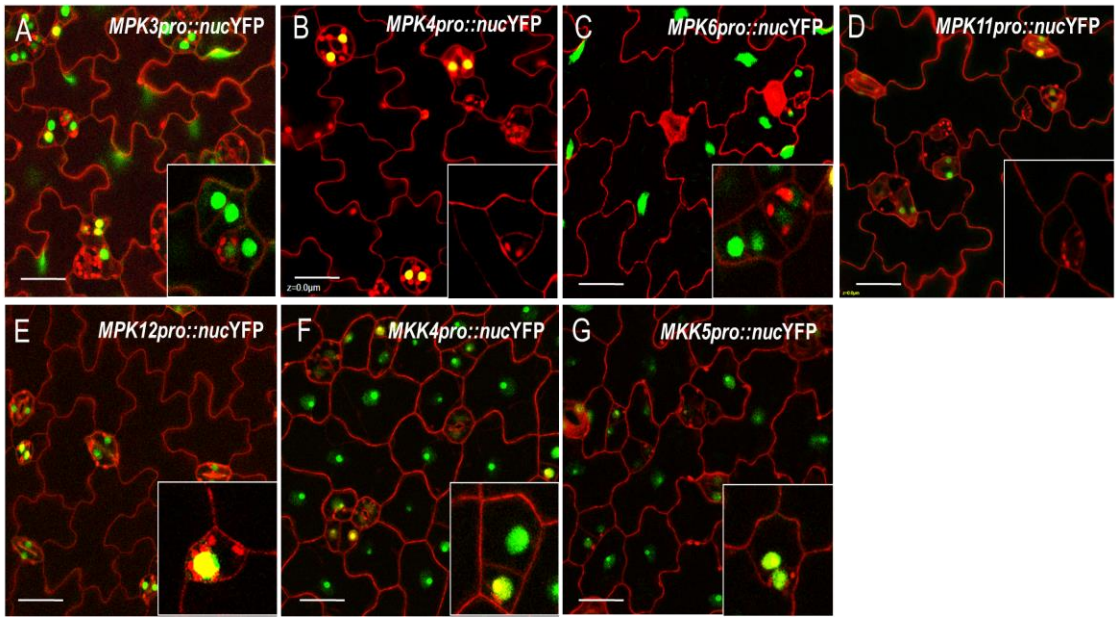

Fig. 2.1. Promoter activity of MAPKs and MKKs.
Confocal images of (**A**) *MPK3pro*::nucYFP (**B**) *MPK4pro*::nucYFP (**C**) *MPK6pro*::nucYFP (**D**) *MPK11pro*::nucYFP (**E**) *MPK12pro*::nucYFP (**F**) *MKK4pro*::nucYFP (**G**) *MKK5pro*::nucYFP. Cells are outlined with propidium iodide (red) and nucYFP is artificially colored by green in **(A-G)**. Scale bar: 25 μm. Insets showed enlarged localization in stomatal cell lineage.

The MAPKKK YDA is polarly localized

Based on the severe loss-of-function defects in asymmetric cell divisions and stomatal patterning, YDA is a particularly interesting candidate in stomata regulation. However, its translational expression pattern was not investigated. Our group generated transgenic plants expressing YFP-tagged YDA (driven by its endogenous promoter). YDA-YFP rescued loss-of-function *yda* mutants and showed localization at the plasma membrane, which broadly appeared in the leaf epidermal cells (**Fig. 2.2A**). To better visualize the localization of YDA-YFP in the stomatal ACD cells, we used the *SPCH* promoter for cell type-specific expression. Interestingly, YDA-YFP was found polarized at the cell cortex in stomatal lineage cells (**Fig. 2.2B**, 5/11 independent T2 plants showed visible

polarity). We quantified YDA polarity in these plants and found that 11.1% cells showed polar accumulation (n = 99 YFP positive cells). We also created a kinase inactive version of YDA (YDA^{KI}, K429R (Lampard et al., 2009)) fused to YFP, which displayed more obvious polar accumulation (26.8% cells show polarity, n = 302 YFP positive) (**Fig. 2.2C**). We suspect that the enhanced polarity of YDA^{KI} was likely due to its disrupted enzymatic activity and/or dynamics of localization. The orientation of the YDA^{KI}-YFP crescent was similar to that of YDA-YFP, both of which were reminiscent of BASL in the stomatal ACD cells (Dong et al., 2009).

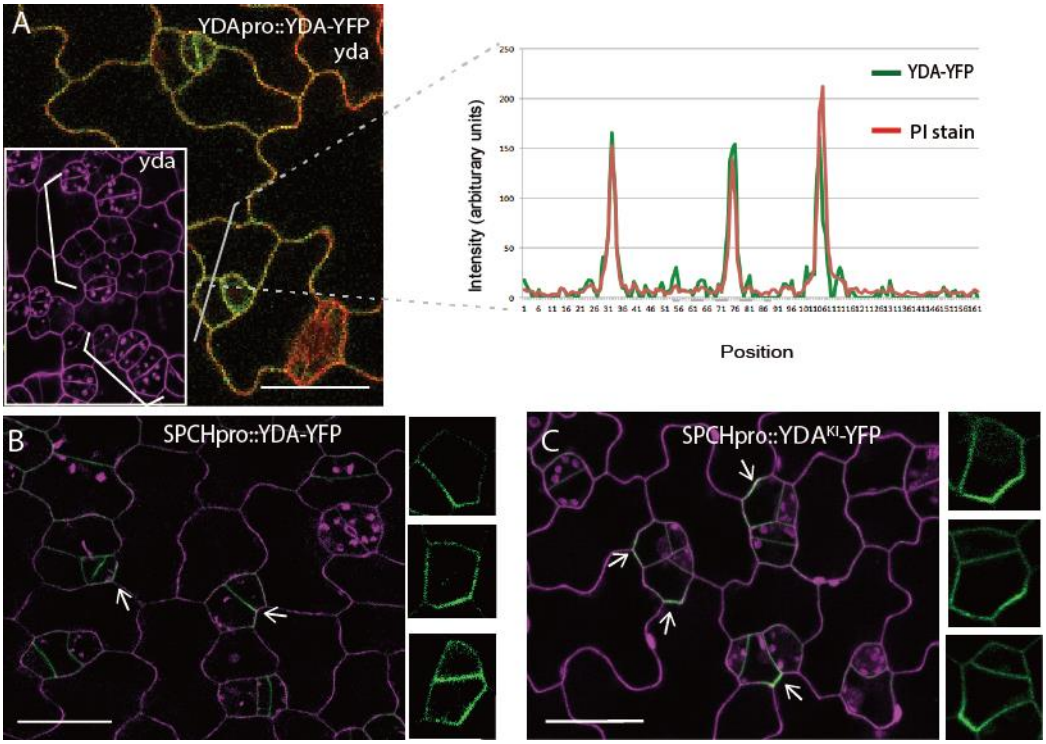

Fig. 2.2. Polar localization of MAPKKK YDA.

(A) Localization of YDA-YFP (green) driven by the endogenous promoter in a 2-dpg *yda* mutant. White brackets indicate *yda* mutant stomata clustering phenotype. Cell walls were stained with PI (red). Inset showing the loss-of-function *yda* (cells outlined with PI stain, magenta). Scale bar: 25 μm. The YFP (YDA) and PI (cell walls and the plasma membrane) intensity were plotted (by Image J) from the gray line.

(B) Confocal image showing YDA-YFP (green) localization in the stomatal lineage cells (driven by the *SPCH* promoter). Arrows indicate protein polar accumulation. Individual cells on right

demonstrate closer view of YDA polarization. Cell outlines are marked with PI (magenta). Scale bar = 25 μm, (D-F) at same scale.

(C) YDA^{KI}-YFP (green) polarization (arrows) in the stomatal lineage cells. Individual cells with green channel only (right) show detailed localization of YDA^{KI}. (A, B, and C were modified from Fig. 5 in Zhang et al. (2015) (Zhang et al., 2015)).

BASL recruits YDA to the polarity crescent

Since YDA polarized in a pattern which highly resembled BASL, we investigated their genetic and cellular connections. YDA^{KI} and BASL were observed co-polarized in stomata lineage cells harboring both YDA^{KI}-mRFP and GFP-BASL (**Fig. 2.3C**). Importantly, when YDA^{KI}-YFP was introduced into *basl-2* mutant plants, it was no longer polarized (**Fig. 2.3A**, polarity quantified in **Fig. 2.3B**), suggesting polarization of YDA depends on BASL. Additionally, YDA^{KI}-mRFP lost its polarity when combined with the expression of nuclear-only BASL_123456A when this BASL variant was expressed in the nucleus only (**Fig. 2.3D**). Similar phenomena as missing polarity happened when YDA^{KI}-mRFP coexpressed with myristylated BASL_123456A which has a short N-terminal myristoylation signal (Greenwood and Struhl, 1999) to artificially targets the attached protein to the plasma membrane (**Fig. 2.3E**), or BASL-def (MAPK docking-defective) with defected polarity (**Fig. 2.3F**). Thus, the MAPKKK YDA is polarized to the BASL crescent and its polarity requires BASL.

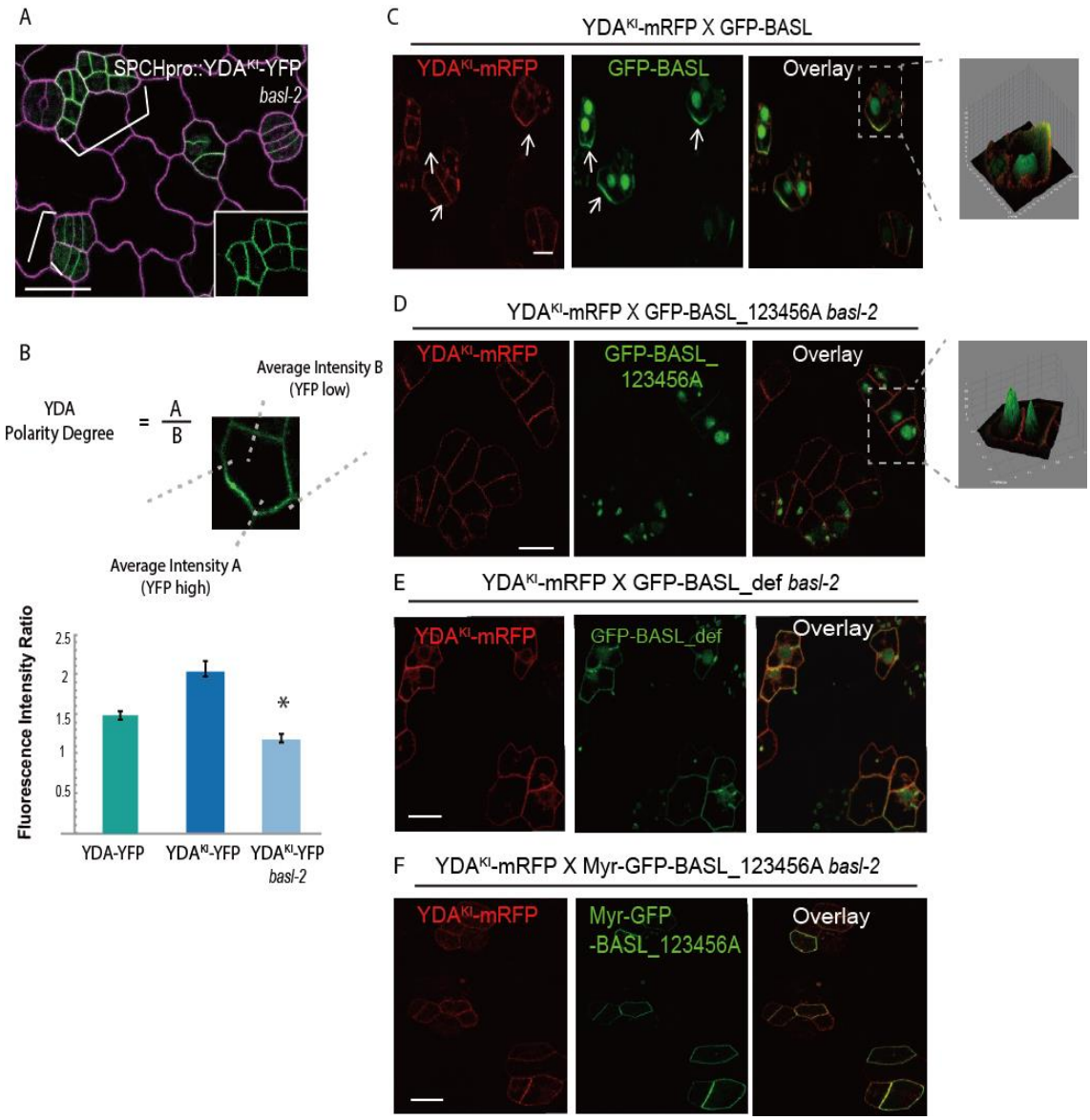

Fig. 2.3. BASL recruits YDA to the cell cortex.

(A) Localization of YDA^{KI}-YFP in *basl-2*. White brackets mark clustered stomatal lineage cells. The inset shows a closer view of YDA^{KI}-YFP (green channel only) in *basl-2*.

(B) Top panel: quantification of YDA and YDA^{KI} polarity. Protein polarity was determined by the ratio of average fluorescence intensity from the polarity site *vs.* that of the distal site (same length collected). Bottom panel: histogram shows the polarity quantification data. n = 50 YFP positive cells. Values are mean ± SD, * significantly different relative to YDA^{KI}-YFP in the wild-type (*t*-test, $P<0.0001$).

(C) Co-localization of YDA^{KI}-mRFP (red) and GFP-BASL (green), both driven by the *BASL* promoter, in a 2-dpg cotyledon. White arrows mark protein polar accumulation. The grey panel displays 3D surface plot of GFP and mRFP generated by Image J. Scale bar = 10 μm.

(D) Co-localization of YDA^{KI}-mRFP (red) and GFP-BASL_123456A (green), both driven by the *BASL* promoter, in a 2-dpg *basl-2* adaxial cotyledon. The grey panel (right) displays a 3D surface plot of GFP and mRFP. Scale bar = 10 μm.

(E) Co-localization of YDA^{KI}-mRFP (red) and BASL_def in a 2-dpg *basl* cotyledon. Scale bar: 10 μm. Others at the same scale.

(F) Co-localization of YDA^{KI}-mRFP (red) and Myr-GFP-BASL_123456A (green) in a 2-dpg *basl* mutant cotyledon. Scale bar: 10 μm. Others at the same scale. (A-D were modified from Fig. 5 and E-F from Fig. S5 in Zhang et al. (2015, Dev. Cell)).

YDA physically interacts with BASL

Inspired by the co-polarization and genetic data, we further investigated the physical connection between BASL and YDA. *In vitro* pull-down assays with recombinant proteins were performed by Dr. Pengcheng Wang to test their physical interaction. We observed a direct interaction between recombinant 6×His-tagged BASL and Maltose Binding Protein (MBP)-tagged YDA *in vitro* (**Fig. 2.4A**). We further confirmed their physical association using the yeast two-hybrid (Y2H) system and showed that BASL interacts with the N-terminal regulatory domain of YDA (Lukowitz et al., 2004; Wu et al., 2006) (**Fig. 2.4B** and **2.4C**). Since the polarization of BASL requires phosphorylation, we assessed whether this modification affects its interaction with YDA. By Y2H, YDA displayed a stronger interaction with BASL_123456D than with BASL_123456A, suggesting that phosphorylation stabilizes YDA's association with BASL (**Fig. 2.4C**). We also assessed BASL mutants defective in MAPK-docking, since these motifs are critical for BASL cortical polarity. These mutants displayed a weaker interaction with YDA in both *in vitro* pull-down and Y2H assays (**Fig.2.3A** and **Fig.2.3D**). Thus, our results strongly suggest that the MAPK-docking motifs mediate the BASL-YDA and BASL-MPK3/6 interactions, and that BASL phosphorylation enhances its interaction with YDA.

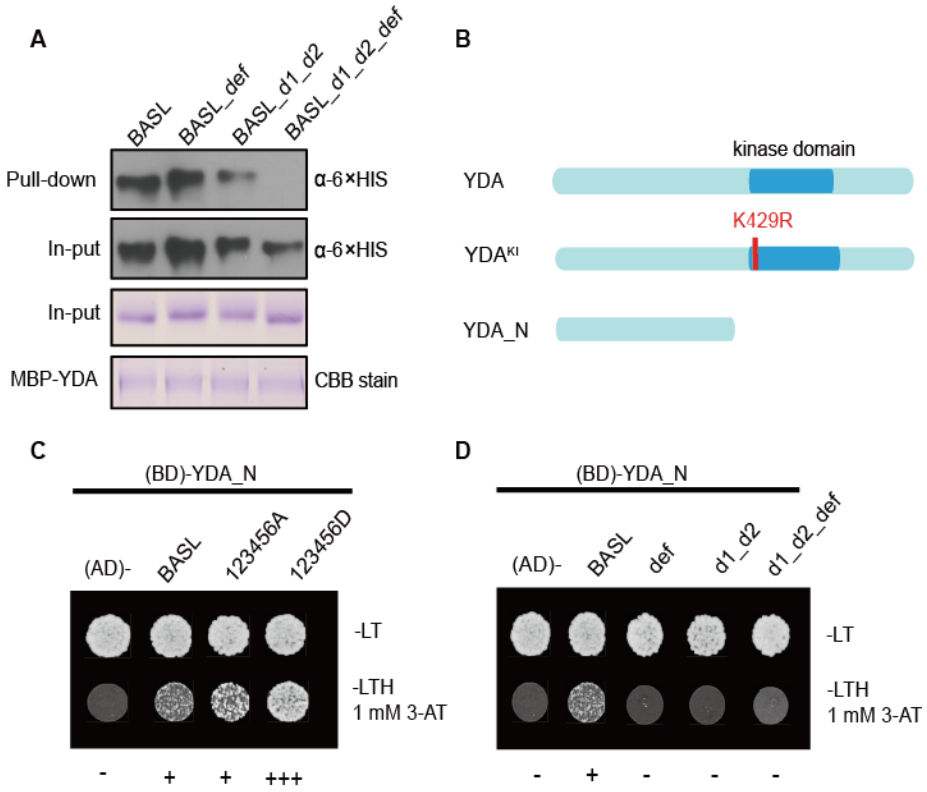

Fig. 2.4. BASL interacts with YDA at the cell cortex.

(A) *In vitro* pull-down assays using recombinant proteins show interactions between MBP-tagged YDA and BASL variants (HIS-tagged). CBB, Coomassie Brilliant Blue stain. Immunoblots were visualized with anti-6 X HIS antibody. Data produced by Dr. Pengcheng Wang.

(B) Schematics show protein structure of YDA and variants. Mutating Lys429 to Arg (K429R) renders YDA kinase-inactive (YDA^{KI}). YDA_N, the N-terminal domain of YDA, without the kinases domain.

(C) Y2H assays of YDA_N with BASL and phospho-variants (123456A and 123456D). Top row, growth control (-Leu-Trp). Bottom row, interaction test (-Leu-Trp-His with 3-AT). Interaction strength low to high: - to +++.

(D) Yeast two-hybrid assays demonstrating the physical interaction between YDA_N and BASL variants. BASL_def, d1_d2, def_d1_d2 have mutations in the respective MAPK-docking motifs. Top panel, yeast growth control (-LT). Bottom panel, interaction test (-LTH supplemented with 1 mM 3-AT). (A-C were modified from Fig. 5 and D from Fig, S5 in Zhang et al. (2015, Dev. Cell))

Compromised MAPK signaling leads to defective polarization of BASL

To genetically assess the role of YDA and MAPK signaling on BASL localization,

GFP-BASL was introduced into MAPK signaling-defect mutants. GFP-BASL displayed

nucleus localization and cortical polarization defects in *yda* loss-of-function plants (**Fig. 2.5A**). The width of the BASL crescent expanded greatly, and the occupancy along the cell periphery increased from 24.3% in the wild-type to 57.8% in *yda* (**Fig.2.2D**), We also evaluated the role of YDA upstream receptor, the ERECTA receptor-like kinases (Shpak et al., 2005a), on BASL polarity. Consistently, the BASL crescent spread wider in the loss-of-function triple mutants *er erl1 erl2* (**Fig.2.2B**, quantified in **2.2D**). In combination, these data strongly suggest that YDA MAPK signaling is required for BASL polarization at the cell cortex.

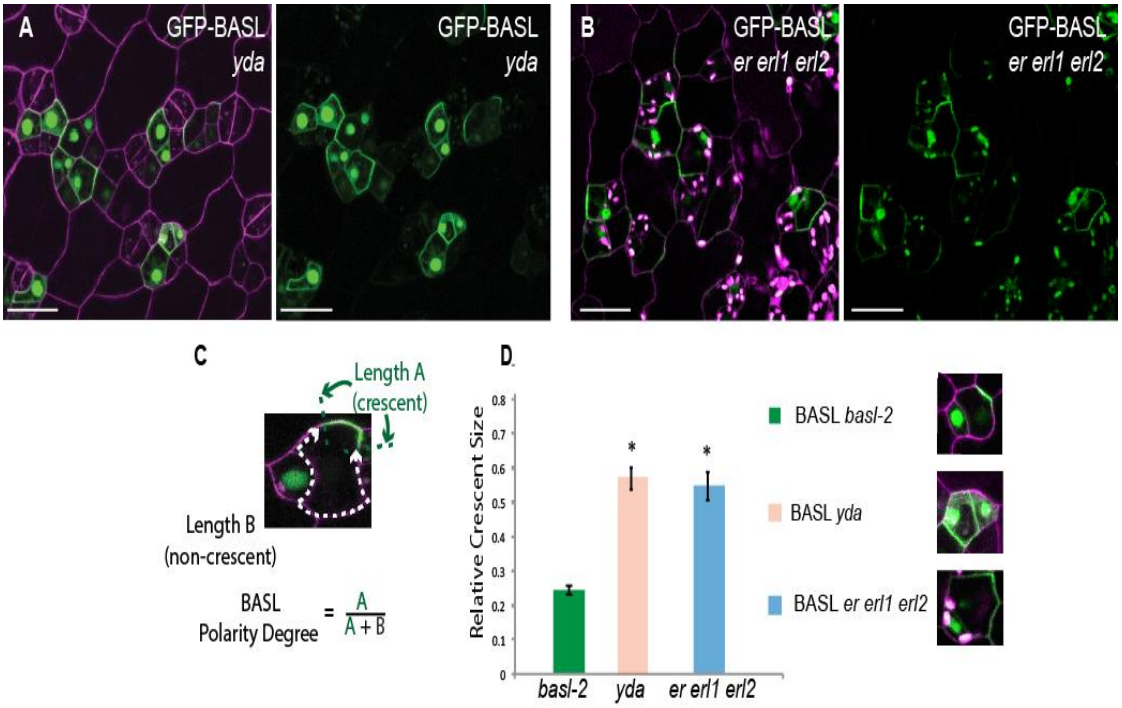

Fig. 2.5. Defective BASL polarity due to compromised MAPK activities.

(A) Left: localization of GFP-BASL (green) in *yda*. Confocal images taken from a 2-dpg cotyledon. Cell walls were stained with PI (magenta). Scale bar: 25 μm. Right: GFP channel only.

(B) Left: confocal image showing the localization of GFP-BASL (green) in *er erl1 erl*. Right: GFP channel only. Scale bar: 25 μm.

(C) Diagram of a confocal image of GFP-BASL showing the quantification of BASL polarity by crescent length.

(D) Quantification of BASL polarity in loss-of-function *yda* plants and in *er erl1 erl* mutants. Representative localizations in individual cells are shown (right). Values are mean ± SD (n = 50 GFP-BASL positive cells), *significant differences (*t*-test, *P*<0.0001). (A, C, and D were modified from Fig. 4 and B from Fig. S4 in Zhang et al. (2015, Dev. Cell)).

DISCUSSION

The findings presented here have several important implications. First, our studies provide unique insights into a universal signaling MAPK pathway being integrated into a specific cellular event, the BASL-centered polarization process during stomatal ACD. Second, we provided strong evidence to demonstrate a forward feedback loop between the polarity protein BASL and the MAPK signaling pathway as a molecular basis for cell polarity and ACD (**Fig. 2.6**). Third, we demonstrate that the physical interaction of two proteins (BASL and YDA) is sufficient to trigger a spontaneous polarization process, a mode of action critical for cell polarity that is scarcely documented in plants.

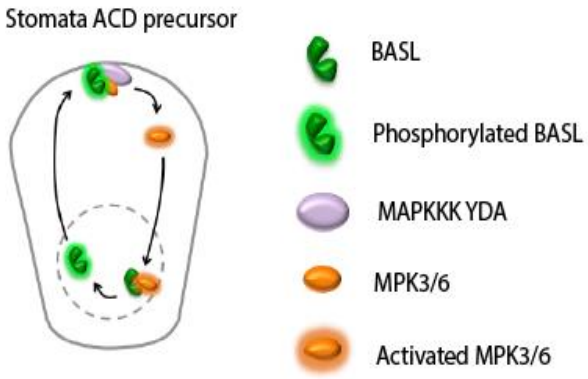

Fig. 2.6. Models for the feedback loop between BASL and the YDA MAPK pathway. BASL and the YDA MAPK cascade form a feedback loop, which reinforces cell polarity in stomatal ACD precursor cells. This model does not exclude the possibility of MAPKs or other kinases phosphorylating BASL in the nucleus, cytoplasm and/or at the plasma membrane.

The MAPK docking motifs for BASL-YDA interaction

The major types of MAPK docking motifs, D domains and DEF domains, have been identified in many MAPK-interacting proteins for signaling efficiency and specificity (Cargnello and Roux, 2011). Diffuse cytoplasmic localization of BASL_d1_d2_def is

consistent with the frequent overlap between MAPK docking motifs and the nucleus localization signal (NLS) (Cargnello and Roux, 2011), and further supports our hypothesis the MPK3/6-mediated phosphorylation of BASL occurs in the nucleus. Unexpectedly, our data indicated that these docking motifs also mediate BASL's interaction with the MAPKKK YDA. Although BASL_d1_d2_def lost its binding ability with YDA in our pull-down and Y2H assays (**Fig. 2.4A** and **Fig. 2.4D**), BASL polarity was dampened but still noticeable in *yda* mutants (**Fig. 2.5A**), suggesting that these three motifs might be needed for BASL's interaction with other regulators in polarity formation.

Based on the evidence that BASL interacts with YDA, MKK5 and MPK3/6 (BASL interaction data with MKK5 and MPK3/6 by Dr. Ying Zhang were not shown here), we propose that BASL may function as a new MAPK scaffold protein in plants. Scaffold proteins are well recognized as hubs for shaping information flow and achieving signaling specificity in animal systems (Good et al., 2011). However, the putative MAPK scaffolding functions in plants were revealed by two MAPKKKs (from alfalfa and *Arabidopsis*) for their direct binding to the downstream MAPKs (Nakagami et al., 2004; Suarez-Rodriguez et al., 2007). In addition, the polarity protein BASL's scaffolding function would provide a new layer of appreciation about how specific spatial-temporal control of MAPK signaling is achieved in plant stem cell asymmetric divisions.

The positive feedback loop between BASL and the YDA MAPK pathway

The MPK3/6-mediated phosphorylation of BASL and the BASL-mediated redistribution of the YDA-MPK3/6 signaling (polarity assays in tobacco cells by Dr. Ying Zhang were not shown here) rendered a positive feedback model (**Fig. 2.6**). In addition, as BASL binds to the N-terminal autoinhibitory domain of YDA (**Fig. 2.4C**), we hypothesize that YDA activity would be elevated by the interaction with BASL, thus further promotes activated MAPKs in the nucleus to phosphorylate BASL for polarization.

Positive feedback loops amplify a small disturbance to an increased magnitude of the perturbation and have been widely accepted as a general principle to reinforce initial polarity cue and maintain cell polarity (Thompson, 2013). The well-studied symmetry breaking events mediated by small GTPases, Cdc42 in yeast and ROPs in plants, rely on cytoskeleton-dependent and -independent positive feedback loops (Johnson et al., 2011; Slaughter et al., 2009a; Yang, 2008). Recent advances established that the phytohormone auxin forms a positive feedback loop with the ROP signaling during interdigitating polar growth of pavement cells in *Arabidopsis* (Xu et al., 2010; Yang and Lavagi, 2012). Our discovery of the BASL-YDA polarity module would encourage future investigation of whether and how MAPK upstream signaling molecules, e.g. the EPF ligands, and downstream cytoskeletal regulators (Komis et al., 2011) may function in feedback loops to establish cellular asymmetry during plant ACD.

Phosphorylation-dependent BASL polarization

Phosphorylation-triggered or involved protein polarization seems to be commonly found in both animal and plant cell systems. In polarized epithelial cells, basolateral localized PM protein AQP2 (aquaporin 2) is phosphorylated by PKA kinase, which is activated by cAMP signaling in dehydration stress. Phosphorylated AQP2 is then transcytosed from the basal PM to the apical PM through endomembrane activities (Fushimi et al., 1997; Katsura et al., 1997). It is not quite clear yet whether phosphorylation of BASL is related to endomembrane trafficking for the polarity orientation (some hints in Chapter 3), but this is an interesting direction to follow up in the future.

On the other hand, differential phosphorylation sites on a polarity protein could play antagonistic regulation on protein localization. The PKA-dependent phosphorylation of S256 (Serine 256) activates AQP2 for translocation, while phosphorylation of S269 by another unknown kinase stabilized AQP2 in the apical PM. In plant root cells, the apical-to-basal polarity shift of the PIN1 auxin effluxer relies on phosphorylation mediated by the Serine/threonine kinase PINOID (PID) (Friml et al., 2004). This process is antagonized by a PP6-type phosphatase and the coordinated activity of PID and phosphatases dynamically determine the phosphorylation status of PINs (Dai et al., 2012; Michniewicz et al., 2007). Interestingly, among the six phosphorylation sites of BASL, different sites seem to fulfill distinct, even antagonistic biological functions in protein localization and function (Zhang et al., 2016b). In addition, other kinases beyond MAPKs and potential phosphatases for dynamic BASL

activation/deactivation, as well as possible phospho-lipases for BASL PM association and polarization are fascinating topics to explore.

Taken together, my studies in this chapter show that the MAPK scaffold protein BASL and the MAPKKK YDA are partners of the cortical polarity complex. Since the YDA MAPK pathway broadly functions in plant development, e.g. embryonic asymmetric cell division (Lukowitz et al., 2004), root apical meristem integrity (Smekalova et al., 2014), and inflorescence patterning (Meng et al., 2012), the spatial organization of MAPK signaling could be commonly used to control division orientation, regional cell proliferation and fate diversification in plants.

METHODS

Plant materials and growth conditions

Arabidopsis thaliana plants were grown at 22°C on half-strength MS plates or in soil with 16-hr light/8-hr dark cycles. The ecotype Columbia (Col-0) was used as the wild-type unless otherwise noted. Mutants and alleles used in this study were: *basl*-2 (Dong et al., 2009), *yda* (Salk_105078 from the *Arabidopsis* Biological Resource Center, ABRC) and *er erl1 erl2* (Shpak et al., 2005a).

Plasmid construction

Gateway cloning technology (Invitrogen) was used for most DNA manipulations unless otherwise specified. BASL, YDA YDA^{KI} and YDA-N sequences were described previously (Bergmann et al., 2004; Dong et al., 2009; Lampard et al., 2009). The

promoter sequences of *MPK3, MAP4, MPK6, MPK11, MPK12, MKK4, MKK5* and *YDA* were amplified by the listed primers (Table listed) and integrated into pENTR/D or pDONR-P4-P1R before recombination into binary vectors. The coding sequences of YDA, YDA^{KI} and YDA-N (N terminal regulatory domain) were cloned into pENTR/D vector (courtesy of Dr. Kyoko Ohashi-Ito). The *BASL* and *SPCH* promoter sequences can be found in (Dong et al., 2009) and (MacAlister et al., 2007b) and were subcloned into pDONR-P4-P1R, respectively (courtesy of Dr. Diego Wengier). Double LR recombination reactions using LR Clonase II (Invitrogen) were performed to integrate coding sequences and promoters into the R4pGWB vectors (Nakagawa et al., 2008) to generate transgenic *Arabidopsis* plants. To generate constructs for yeast two-hybrid analysis, pENTR/D vector containing the coding region of YDA-N was recombined into the pGBKT7 vector (Clontech) for expressing protein fused to the GAL4 DNA-binding domain.

Primers used in this study are listed as below.

Primers	**Forward**	**Reverse**
MPK3 promoter	CACCCTGATCGAAAATAGCTTACTTAAAAATC	TTCTCTCTCAATTGATCAAAGTCG
MPK4 promoter	CACCTCAATCGGTGCTAAGCTATAACT	GTTGTGAGGAATTTTGCTCCG
MPK6 promoter	CACCCCTGCAAGATCCAATGTGTCA	GACCGGTAAAGATGAAAGCTTTTGAGG
MPK11 promoter	CACCAACTGCTGCTAGATCCGTATTATC	AAACAGAGGAGATTTTGGCGTG
MPK12 promoter	CACCGTGACGAGAGAAACATCACTAGG	CGTTACTAGTCTGGCTCTTGC
MKK4 promoter	CACCCTAAGCACATACGTGGAGAATC	CGCTTTTGGAATCAAAAGTTC
MKK5 promoter	CACCGACGGCAAAGAAGGCAAAC	GGCTTTTAGAAGAAGAGGGAATC
YDA promoter	CACCGGTCAACGGTACGAAGCAAGG	CTTCTTCCCACAAACCAAGAGGC
YDA CDS	CACCATGCCTTGGTGGAGTAAATC	GGGTCCTCTGTTTGTTGATCC

YDA^{KI}	TAGAGTAACCTCTCTCATGGC ACACATCTCCCCA	TGGGGAGATGTGTGCCATGAGA GAGGTTACTCTA
YDA-N	CACCATGCCTTGGTGGAGTAA ATC	TCGCGATCCAGGGCTAACCGTAG CCTC

Confocal imaging and image processing

Confocal images were captured by Leica TCS SP5 II. The Excitation/ Emission spectra for various fluorescent proteins are: CFP 458 nm/480-500nm, YFP 514 nm/ 520-540 nm, GFP 488 nm/501-528 nm, mCherry 543 nm/600-620 nm, mRFP 594 nm/ 600-620, and Propidium Iodide (PI) 543 nm/ 591-636 nm. All imaging processing was performed by Fiji software (http://fiji.sc/Fiji) and figures were assembled with Adobe Illustrator CS6.

Yeast two-hybrid analysis

Matchmaker II yeast two-hybrid System (Clontech) was used to detect protein-protein interactions. The manufacturer's protocols were followed. The bait and prey plasmids were sequentially or co-transformed into yeast strain AH109. To inhibit the self-activation of YDA_N, 1mM 3-Amino-1, 2, 4-triazole was used. In addition, X-alpha-Gal (Clontech) was added into the growth medium to indicate the interaction strength.

Protein polarity quantification in *Arabidopsis*

For quantitative analysis of GFP-BASL polarization, confocal images were taken from 2-dpg adaxial cotyledons of 10 representative seedlings (cell outlines were imaged with PI staining). GFP-BASL forms distinctive crescent in the stomatal lineage cells. To

quantify the polarity degree of BASL, the length of GFP crescent (A) and the whole-cell perimeter (A+B, marked by PI) were measured Protein polarity was determined by the ratio of crescent width over the cell perimeter (A/A+B, **Fig. 2.5D**). Total 50 individual cells expressing cortical BASL were selected and scored for polarity. For YDA^{KI} (**Fig. 2.2C** and **Fig. 2.3A**), the mean values of fluorescence intensity at the plasma membrane were measured from two segments with the same length; one from the YDA^{KI} (A) and the other one from the distal side (B). Polarity degree was determined by A/B. Measurements were conducted on 50 cells collected from 3-dpg adaxial cotyledons of 5 individual plants.

CHAPTER 3. Intracellular trafficking of the BASL-YDA polarity complex

ABSTRACT

Plasma membrane-residing proteins are constantly subjected to various regulations in order to precisely coordinate cellular responses to external stimuli. These proteins can be internalized by endocytosis, sorted to different endosomal compartments, so that they are recycled back to the plasma membrane or sent to vacuole for degradation. Vesicle trafficking plays important roles in the establishment and maintenance of polarized proteins, e.g. the auxin efflux carrier PINs in plants. Whether the plasma membrane-associated polarity proteins, BASL and YDA, are regulated by the endomembrane system and vesicle trafficking has not been studied. Here I provided cytological evidence that YDA and BASL are regulated by the endomembrane system. Besides its association with the PM, YDA was also found to localize to intracellular punctate structures that largely overlap with FM4-64-positive endosomes. The interference of MVB and vacuolar targeting by chemical inhibitors resulted in abnormal accumulation of BASL and YDA, suggesting that these two components of the polarity complex are delivered to the vacuole for degradation. Thus, vesicular trafficking provides a means of down regulation of the BASL-YDA positive feedback signaling at the plasma membrane.

.

INTRODUCTION

In eukaryotic cells, the endomembrane system consists of nuclear envelope, endoplasmic reticulum (ER), the Golgi apparatus, endosome vesicles, vacuole/lysosomes and the plasma membrane (PM) (Morita and Shimada, 2014) (**Fig. 3.1**). Although many membrane components and regulators are conserved in different life styles, the plant endomembrane system possesses some unique characteristics, e.g. the combined functionality of the trans-Golgi network (TGN) with early endosomes in protein sorting and recycling (Peer, 2011).

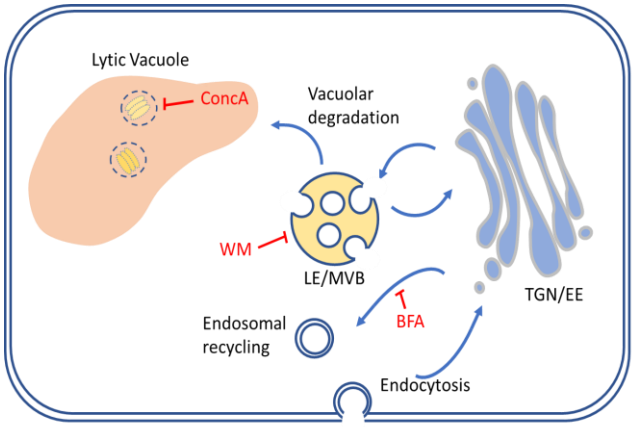

Fig.3.1. Diagram of the subcellular endocytic pathway in plants. Three inhibitors including BFA, Concanamycin A (ConcA), and Wortmannin (Wm) are indicated in red, adjacent to specific trafficking routes.

Decades of research revealed that the endomembrane trafficking pathway has essential functions in establishing cell polarity (Belanger and Quatrano, 2000). Some PM-embedded polarity proteins, after being synthesized in the cytoplasm, are directional delivered to the PM by the TGN/EE vesicles. Alternatively, some PM proteins begin with even distribution initially, followed by endocytosis and subsequent directional recycling to achieve PM polarity (Offringa and Huang, 2013).

In plant cells, the well-studied PIN auxin efflux carriers polarly localized at PM and facilitate intercellular auxin transport. Newly synthesized PIN proteins are initially secreted to the PM in an apolar manner and their subsequent polarity formation heavily rely on the regulation of endomembrane system. Mechanisms underlying apical (shootward), basal (rootward) or lateral polar PIN deposition involve constitutive clathrin-mediated endocytosis, endocytic polar recycling and restriction of lateral diffusion by lipid raft (Dhonukshe et al., 2007; Geldner et al., 2003; Kitakura et al., 2011; Willemsen et al., 2003). The ADP Ribosylation Factor Guanine nucleotide Exchange Factor (ARF-GEF) GNOM promotes endosomal recycling and plays a key role in establishing basal polarity of PIN1 in root stele or PIN2 in root cortex (Geldner et al., 2003; Kleine-Vehn et al., 2008a). Inhibition of the BFA-sensitive endosomal recycling pathway induces PIN abnormal aggregation, often called "BFA compartments" (Geldner et al., 2003; Kleine-Vehn et al., 2008a). On the other hand, the apical polarity of PIN2 in root epidermis is formed in a GNOM-independent manner and recently was linked to the regulation of small GTPase RabA proteins (Kleine-Vehn et al., 2008a; Li et al., 2017). In addition, the recycling of PIN2 was found Microtubule (MT)-dependent and regulated by the connected functions of the MT-associating protein CLASP and the retromer component soring nexin 1, SNX1 (Ambrose et al., 2013).

Endocytic degradation is essential for maintaining the proper spatiotemporal signaling of PM proteins. The turnover of *Arabidopsis* PIN2 protein is mainly triggered by ubiquitylation, which then induce PIN2 endocytosis and vacuolar proteolysis (Leitner et al., 2012). A putative conserved BLOC-1 protein complex, which facilitates vesicle

trafficking from endosomes to lysosomes in animal systems, was recently found to mediate vacuolar targeting of PIN2 in plants. Differing from PINs, BASL and YDA do not contain transmembrane domains; their attachment to the PM is presumably achieved through protein-protein and/or protein-lipid interactions (Zhang et al., 2016a). Whether cortically polarized BASL and YDA are regulated by endocytic trafficking is a fundamental question, but has not been addressed yet. Here we show that polarized BASL and YDA are internalized by the membrane system and delivered to the endosome, MVB and vacuole for degradation in the stomatal lineage cells.

RESULTS

The PM-associated YDA and BASL are regulated by endomembrane trafficking

Since both BASL and YDA are PM-associated proteins (Zhang et al., 2015), we assessed whether these two proteins are associated with and regulated by the endomembrane system. Careful examination of Z-projected confocal images showed that YDA-YFP distributes unevenly along the PM and often accumulates into PM foci and cytoplasmic puncta (**Fig. 3.2A**). This localization pattern is more obvious and robust when YDA^{KI} was expressed in the stomatal lineage cells driven by the promoter of *BASL* or *SPEECHLESS* (*SPCH*) (MacAlister et al., 2007b). Both N- and C- terminal GFP/YFP fusions produced similar localization pattern and induced anticipated stomatal phenotype (**Fig. 3.2B**, **3.2C**). We, therefore, used GFP- or YFP-tagged YDA^{KI} as a tool for detailed cell biological characterization.

First, we applied the endocytic tracer FM4-64 on seedlings expressing YDA^{KI}-YFP for 20-min and found that the intracellular YDA^{KI} puncta largely overlap with the FM4-64-stained endosomes (66.0%, n = 51 cells), suggesting that YDA molecules are endocytosed from the PM (**Fig. 3.2D)**. When FM4-64 treatment was employed on GFP-BASL, no obvious intracellular colocalization was observed (**Fig. 3.2E**). However, by using Brefeldin A (BFA) to disrupt an ARF-GEF-based endocytic recycling of proteins from endosomes to the PM in plant cells (Geldner et al., 2003), we found that, besides an obvious loss-of-polarity phenotype, GFP-BASL accumulated into BFA-induced FM4-64 endosomal aggregations (**Fig. 3.2F**), often referred to “BFA compartments”

(Lam et al., 2009), but the nuclear pool of BASL was not dramatically affected. These data suggest that cortical BASL is indeed regulated by endocytosis and endosomal recycling, and the polarity maintenance may require ARF-GEF-mediated cellular processes, as for other polarized proteins (Barbosa et al., 2014; Geldner et al., 2003; Takano et al., 2010).

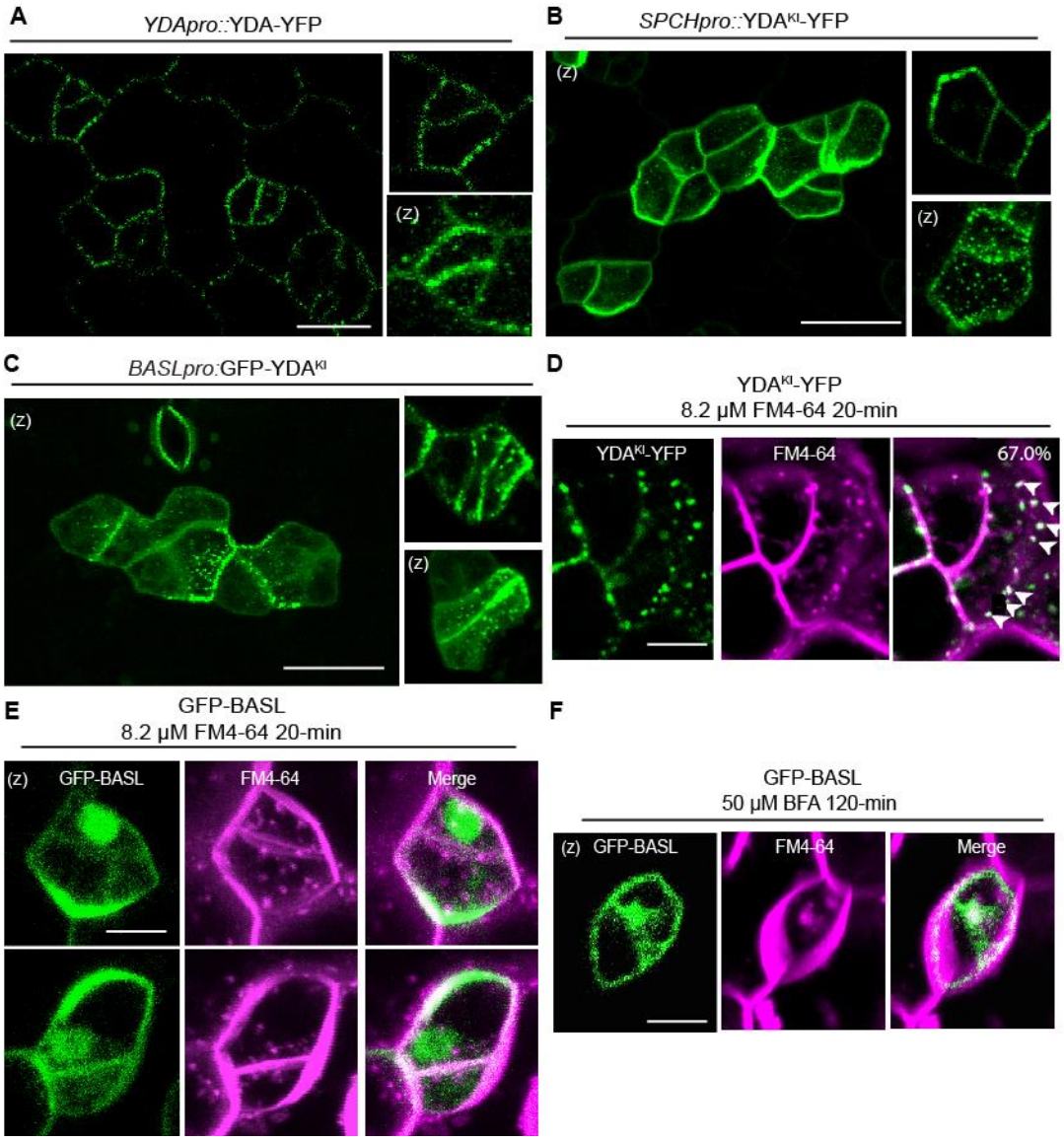

Fig. 3.2. The PM-associated YDA and BASL are regulated by endomembrane trafficking.
(A) Localization of YDA-YFP driven by the endogenous promoter in 3-dpg *Arabidopsis* cotyledons. Representative individual cells are shown in the inset. Top inset shows a middle

layer of YDA localization and polarity at cell cortex. Bottom inset shows a z-projection view of cortical dense puncta. Z, z-projection. Scale bar: 25 μm.

(B) Localization of *SPCHpro::*YDA^{KI}-YFP in the stomatal lineage cells. Representative individual cells are shown in the inset. Top inset shows strong protein polar accumulation. Bottom inset shows a z-projection view of cortical dense puncta. Scale bar = 25 μm.

(C) Localization of *BASLpro::*GFP-YDA^{KI}. Similar localization patterns were observed. Scale bar = 25 μm.

(D) Confocal images of *SPCHpro::*YDA^{KI}-YFP (green) after 20-min of 8.22μM FM4-64 uptake (Magenta). White arrowheads indicate colocalization of YDA^{KI} -YFP with FM4-64 labeled endosome. Scale bar: 10 μm.

(E) Z-projection images of *BASLpro::*GFP-BASL (green) after 20-min of 8.22μM FM4-64 uptake (Magenta). Scale bar: 10 μm.

(F) Z-projection images of GFP-BASL (green) after 20-min of 8.22μM FM4-64 uptake (Magenta) and 120-min of 50μM BFA treatment. Note the BFA body in the cytosol. Scale bar: 10 μm.

YDA and BASL are transported through WM-sensitive late endosomes

To examine whether BASL and YDA are targeted to the LE/MVB pathway, we treated *Arabidopsis* seedlings with 33 μM Wortmannin (WM), an inhibitor of phosphatidylinositol 3-kinases, induces homotypic fusion and swelling of late endosomes or multivesicular bodies (MVBs) in plant cells (Wang et al., 2009). Apparently, 4-hr of WM treatment of YDA^{KI}-YFP and GFP-BASL triggered both proteins to internalize and accumulate into the enlarged endosomal structures, and no abnormalities were found in the mock DMSO treatment (**Fig. 3.3A**, **3.3B**). The WM-induced internal distribution of BASL (54.9% abnormal, n=122 cells) and YDA (99.3% abnormal, n=144 cells) was similar to the bubble-like vacuolated structures formed by the late endosomal marker SNX1 in response to WM in the stomatal lineage cells (**Fig. 3.3C),** recapitulating what was reported for SNX1 in young root cells (Hirano et al., 2015b; Jaillais et al., 2006). These results indicated that BASL and YDA transit through the WM-sensitive late endosomes.

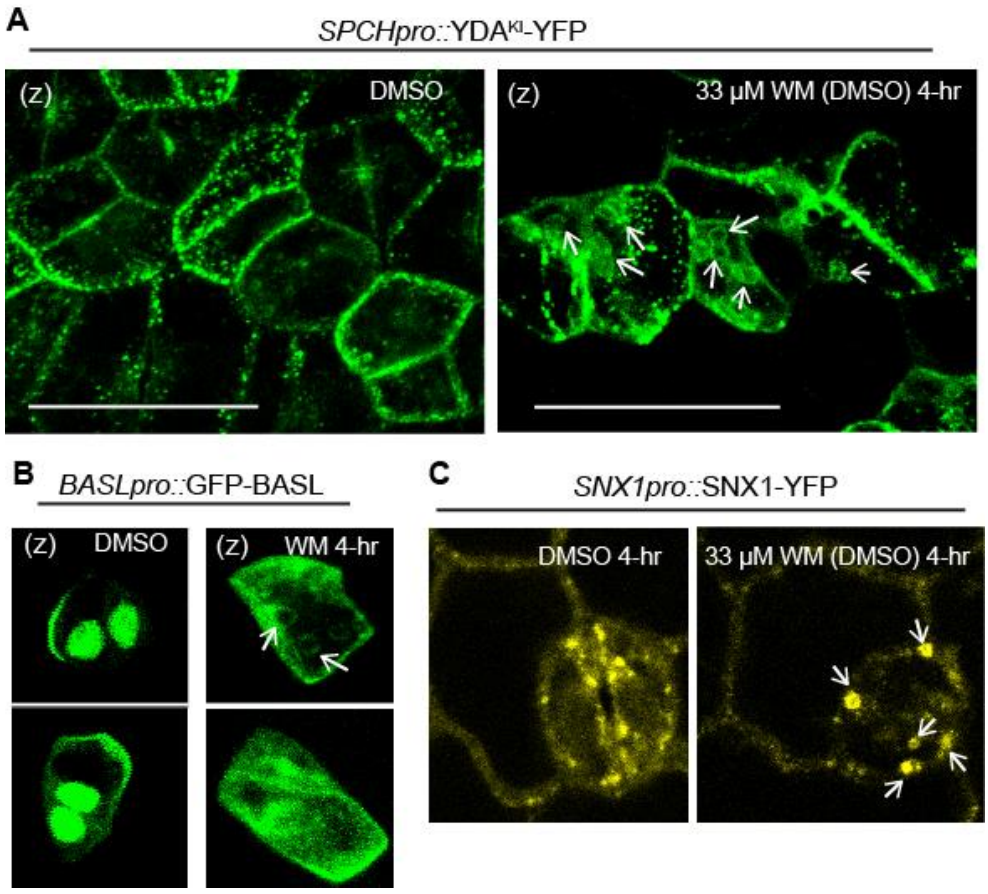

Fig. 3.3. Transport of YDA and BASL is dependent on WM-sensitive late endosomes.
(A) Left: Z-projection image of *SPCHpro::*YDA^{KI}-YFP after 0.33% DMSO for 4-hr in leaf epidermis. Right: A Z-projection image of *SPCHpro::*YDA^{KI}-YFP after 33µM Wortmannin treatment for 4-hr. Arrows indicate wortmannin-induced bubble-like vacuolated compartments. Scale bar: 25 µm, others at the same scale.
(B) Left: Representative individual stomatal lineage cells showing z-projected *BASLpro::*GFP-BASL after 0.33% DMSO for 4-hr. Right: Representative individual cells showing z-projected *BASLpro::*GFP-BASL after 33µM Wortmannin treatment for 4-hr. Arrows indicate wortmannin-induced compartments.
(C) Left: Confocal image of *SNX1pro::*SNX1-YFP after 0.33% DMSO for 4-hr in stomatal lineage cells. Right: 33µM Wortmannin treatment on *SNX1pro::*SNX1-YFP for 4-hr. Arrows indicate wortmannin-induced compartments.

YDA is highly colocalized with FAB1A-decorated late endosomes

To characterize the internalized YDA-associated vesicles in the cytoplasm, we co-expressed YDA^{KI}-YFP with a number of endomembrane marker lines (Geldner et al.,

2009), including endosome, late endosome/MVB, and Golgi, in tobacco epidermal cells and in *Arabidopsis* stomatal lineage cells, In tobacco cells, YDA^{KI}-YFP showed similar distribution as it was in the stomatal lineage (**Fig. 3.2B**, **3.4A**), forming discrete speckles along the PM (small) and larger puncta in the cytoplasm **(Fig. 3.4A)**. Along the PM, the small speckles of YDA^{KI}-YFP seemed to partially overlap with endosomal markers (RabC1, RabA1e, and RabA1G), but once internalized, no significant co-location with any of the three endosomes/recycling endosomes were detected (**Fig. 3.4B**, **3.4C**, **3.4I**). On the other hand, the large cytoplasmic puncta of YDA^{KI}-YFP showed pronounced co-localization with FAB1A late endosomes of (**Fig. 3.4E**, **3.4H**, 98.7%, n=103 cytoplasmic dots) and partially overlapped with endosomes decorated by RabF2b/Ara7 (**Fig. 3.4F**, 63.6%, n=57 cytoplasmic dots) and RabG3c (**Fig. 3.4D**, 33.6%, n=112 cytoplasmic dots).

The SNX1 endosomes were previously demonstrated to highly co-localize with FAB1A in *Arabidopsis* roots (Hirano et al., 2015b), and we found FAB1A co-localizes with YDA in leaf epidermal cell, but surprisingly we did not find significant co-localization of YDA^{KI} and SNX1 in both tobacco and *Arabidopsis* (**Fig. 3.4G** and **Fig. 3.4M**). Furthermore, no Golgi markers (Got1p, SYP32 and MEMB12) were found to co-localize with YDA^{KI}-YFP (**Fig. 3.4J**, **3.4K**, **3.4L**). Taken together, our results show that the PM-associated YDA gets internalized, although we were not able to specify which early endosomes it associates with, we found close connections between YDA and FAB1 late endosomes.

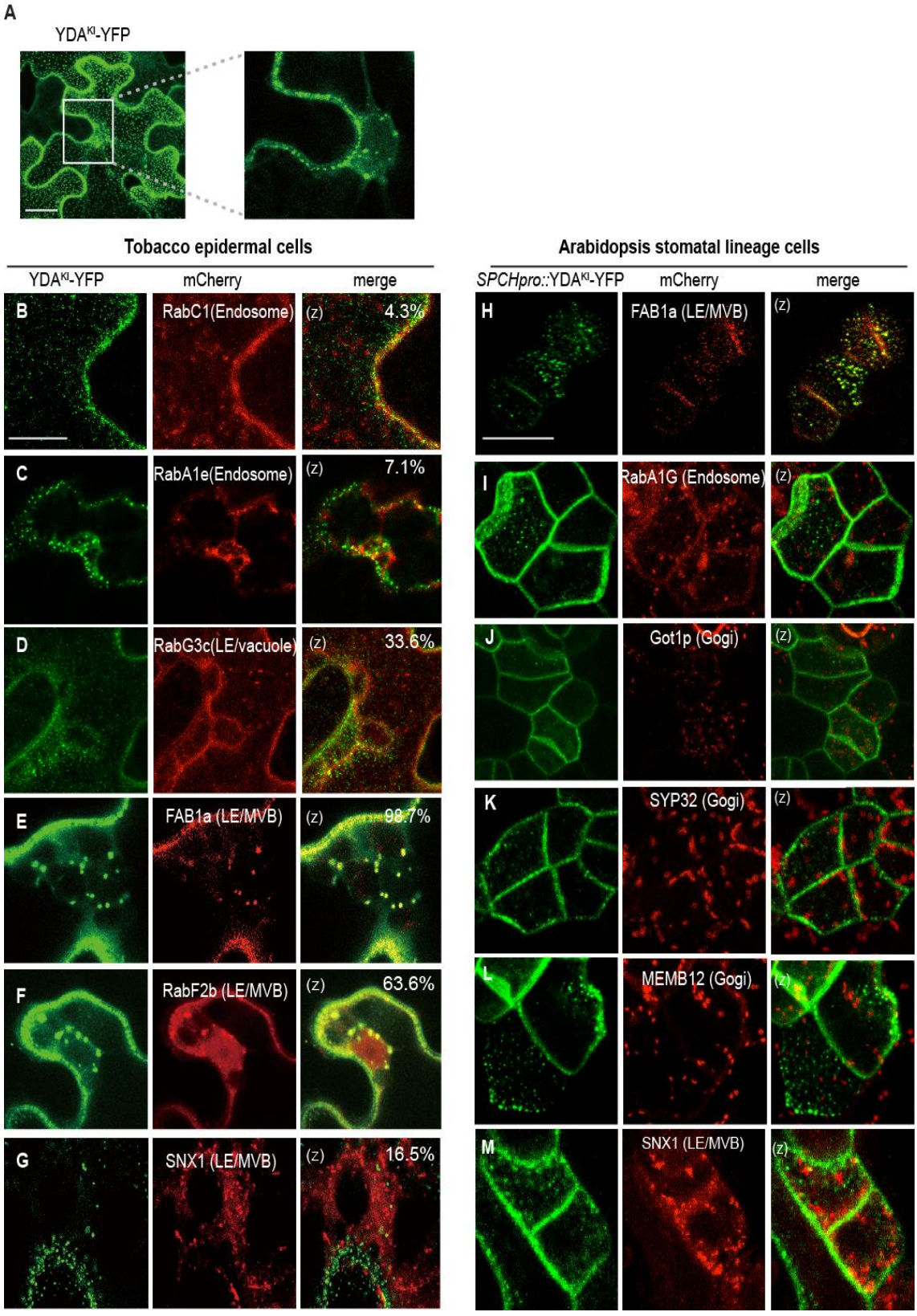
A
YDA^KI-YFP
Tobacco epidermal cells
YDA^KI-YFP
mCherry
merge
B
RabC1(Endosome)
(z)
4.3%
C
RabA1e(Endosome)
(z)
7.1%
D
RabG3c(LE/vacuole)
(z)
33.6%
E
FAB1a (LE/MVB)
(z)
98.7%
F
RabF2b (LE/MVB)
(z)
63.6%
G
SNX1 (LE/MVB)
(z)
16.5%
Arabidopsis stomatal lineage cells
SPCHpro::YDA^KI-YFP
mCherry
merge
H
FAB1a (LE/MVB)
(z)
I
RabA1G (Endosome)
(z)
J
Got1p (Gogi)
(z)
K
SYP32 (Gogi)
(z)
L
MEMB12 (Gogi)
(z)
M
SNX1 (LE/MVB)
(z)

Fig. 3.4. Colocalization of YDA with endosome markers in both tobacco cells and *Arabidopsis* stomatal lineage cells.

(A) Representative confocal z-projected image of YDA^{KI}-YFP overexpression (green) in tobacco epidermal cells. Enlarged region on right demonstrates a closer view of punctate structures of YDA^{KI}.

(B-G) Co-expression of YDA^{KI}-YFP (green) and a mCherry-tagged organelle markers (red) in tobacco epidermal cells. Percentages in merged images represent colocalization rates of two fluorescent proteins captured from at least five images of five cells. Images were captured 3-4 days after infiltration**. (B)** Endosome/recycling endosome marker mCherry-RabC1. **(C)** Post-Golgi/endosome marker mCherry-RabA1e. **(D)** Late endosome/vacuole marker mCherry-RabG3c. **(E)** Late endosome/vacuole marker mCherry-FAB1a. **(F)** Late endosome/vacuole marker mCherry-RabF2b. **(G)** Late endosome/vacuole marker mCherry-SNX1.

(H-M) Co-expression of YDA^{KI}-YFP (green, driven by the *SPCH* promoter), with a mCherry-tagged organelle markers (red) in the *Arabidopsis* stomatal lineage cells. **(H)** Late endosome/vacuole marker mCherry-FAB1a. **(I)** Endosome/recycling endosome marker mCherry-RabA1G. **(J)** Golgi marker mCherry-Got1p. **(K)** Golgi marker mCherry-SYP32. **(L)** Golgi marker mCherry-MEMB12. **(M)** Late endosome/vacuole marker mCherry-SNX1.

BASL and YDA are targeted in the vacuole for degradation

Next, we investigated whether BASL and YDA, after transiting through the MVBs, are delivered to the lytic vacuole for degradation. Concanamycin A (ConcA) is a well-established and specific inhibitor of vacuolar H^+-ATPase (V-ATPase) that raises the pH values in the TGN/EE and the vacuole thus preventing protein degradation (Luo et al., 2015; Matsuoka et al., 1997). We applied ConcA to seedlings expressing GFP-BASL and YDA^{KI}-YFP with PIN2-GFP being used as a control protein that is targeted to the vacuole (Leitner et al., 2012). The fluorescence signals of both PIN2 and YDA^{KI} aggregated into dot-like compartments after 16-hr of ConcA incubation (**Fig. 3.5A**, **3.5B**), while GFP-BASL was found much more diffused in the cytoplasm (**Fig. 3.5C, 3.5D**, note abundant GFP accumulation in the cell "cortical" region). As ConcA also interferes TGN/EE endocytic trafficking (Dettmer et al., 2006), we conducted a less invasive experiment, dark treatment that allows protein stabilization in the vacuole

(Tamura et al., 2003). Indeed, both PIN2-GFP and YDA^{KI}-YFP appeared in the vacuole-like structures after 16-hr of dark treatment (**Fig. 3.5A**, **3.5B**). GFP-BASL again showed diffused accumulation at the cell cortex (**Fig. 3.5C, 3.5D**). The results demonstrated that YDA is transported to the vacuole for degradation and that BASL, although not strongly revealed in the vacuole (likely due to its large nuclear pool as a storage/buffer zone (Dong et al., 2009)), is regulated by the vacuolar degradation pathway.

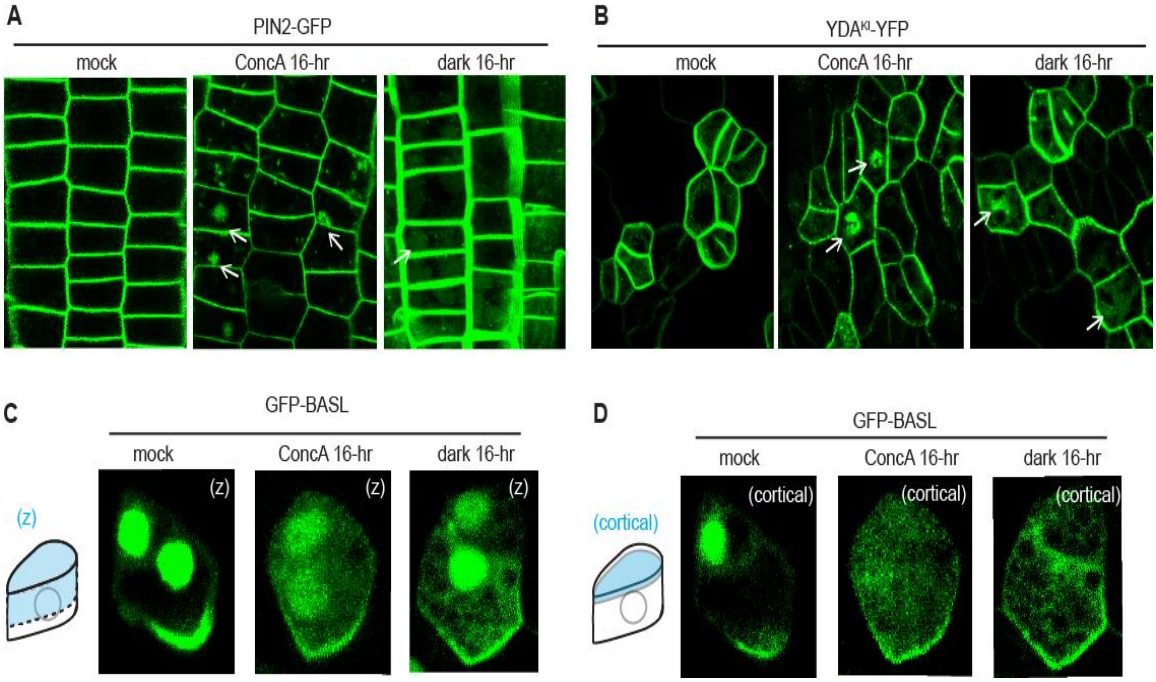

Fig. 3.5. BASL and YDA are targeted in the vacuole.

(A) Left: PIN2-GFP localization at the plasma membrane in untreated epidermal root cells. Middle: Appearance of GFP signal in lytic vacuoles in PIN2-GFP-expressing seedlings after 1 μM concanamycin A treatment for 16-hr. Right: PIN2-GFP localization in lytic vacuoles after incubation 16-hr in the dark. Arrowheads indicate the vacuolar occurrence of GFP signals.

(B) Left: YDA^{KI}-YFP -expressing transgenic lines showing YDA^{KI} localization at the plasma membrane in untreated stomatal lineage cells. Middle: YDA^{KI}-YFP degradation in lytic vacuoles after 1 μM concanamycin A for 16-hr. Right: Appearance of diffuse vacuolar GFP signal in YDA^{KI}-YFP -expressing cells after dark treatment for 16-hr. Arrowheads indicate the vacuolar occurrence of GFP signals.

(C) Left panel: Diagram of the captured cell layers of a single stomatal lineage cell for z-projection. Right panel: Representative GFP-BASL localization at the nuclear, plasma membrane and endocytic intracellular compartments in leaf epidermal cells. Diffused GFP-BASL signals were observed in lytic vacuoles after 1 μM concanamycin A for 16-hr (Middle) or dark incubation for 16-hr (Right).
(D) Left panel: Diagram of the captured single cortical cell layers of stomatal lineage cells. Right panel: Representative GFP-BASL localization showed strikingly diffused GFP-BASL signal in the lytic vacuoles after 1 μM concanamycin A for 16-hr (Middle) or dark incubation for 16-hr (Right).

DISCUSSION

Endomembrane trafficking pathway has been reported with essential functions in polarity establishment and maintenance. Here, our data demonstrate that the PM-associated BASL and YDA are endocytosed with membranes. Furthermore, polarized BASL and YDA are internalized and delivered from the late endosome to lytic vacuole for degradation. This data for the first time suggested polar PM proteins BASL-YDA are dynamically regulated by endocytic trafficking.

Differing from the well-studied PM proteins PINs, BASL and YDA do not contain transmembrane domains. Thus, other membrane-embedded partners are potentially involved to recruit BASL and YDA so that vesicular trafficking routes can be employed to establish their asymmetric localizations. Further investigation on new partners of BASL-YDA polarity complex in cell polarity will be helpful for understanding their molecular mechanisms.

To dissect the major trafficking pathways that BASL-YDA polarity complex involves in, several trafficking inhibitors were employed to modulate endomembrane system. After blocking the recycling routes using BFA, the cortical BASL polarity got

diminished, suggesting that, similar as polarized PIN proteins, the polarity maintenance of BASL may also require ARF-GEF-mediated endosomal recycling pathway. The ARF-GEF GNOM was found to regulate PIN recycling to the basal PM regions (Geldner et al., 2003; Kleine-Vehn et al., 2008a). Since BASL rarely shows punctate endosome localization, possibly because of its high dynamics and strong masking from nuclear sub-portion, it become more difficult to directly examine the transit patterns of BASL. Genetic analysis and applications of specific trafficking inhibitors would be helpful for further investigation.

Although BASL and YDA share same LE/MVB pathway and both are degraded in the lytic vacuole, they may also respectively participate in unique endocytic routes. YDA and BASL were observed to accumulate into swelling late endosomes or multivesicular bodies (MVBs) after Wortmannin (WM) treatment. Furthermore, dampened polarization of BASL and YDA was induced by WM inhibition, suggesting vacuolar trafficking of BASL-YDA is possibly interdependent, yet molecularly distinct, to their polar translocation to the plasma membrane. Thus, the precisely coordinated endo-trafficking pathways modulate BASL-YDA protein abundance as well as their polar localizations.

The endocytic machinery has been identified to efficiently control the availability and levels of activated receptors at the cell surface. The brassinosteroid (BR) receptor BRI1 is endocytosed in early endosomal compartments, and the increasing endosomal localization of BRI1 enhances the activation of BAK1-BZR1 to control BR response (Geldner et al., 2007). On the other hand, endocytosis of the Ste2p pheromone receptor

in yeast appears to be necessary for termination of the signaling transduction. In plants, the boron receptor BOR1 is transported by endocytic trafficking to the vacuole to avoid boron toxicity upon high boron supply (Takano et al., 2010). Similarly, a number of integral plasma membrane proteins, e.g. PIN2, the brassinosteroid receptor BRI1, and the aquaporin PIP2, were found being targeted to the vacuole for degradation, suggesting a tight posttranslational regulation during plant development (Kleine-Vehn et al., 2008b). Our findings about the endocytosis, transport and degradation of BASL-YDA polarity complex provide insights into the relevance of subcellular compartmentation of signaling components for the regulation of plant polarity module.

METHODS

Plant materials and growth conditions

Arabidopsis thaliana plants were grown on ½ MS media in 22 ℃ with 16-hr light/8-hr dark cycles. Young expanding cotyledons were imaged at 3–4 days. Columbia-0 ecotype plants were used as wildtype. Previously published lines used in this study are *BASLpro::*GFP-BASL (Dong et al., 2009), *SPCHpro::*YDA^{KI}-YFP, *YDApro::*YDA-YFP (Zhang et al., 2015), *PIN2pro::*GFP-PIN2 (Wisniewska et al., 2006), WAVE lines including *35S::*mCherry-RabF2b, *35S::*mCherry-RabC1, *35S::*mCherry -RabG3c, *35S::*mCherry-RabA1e, *35S::*mCherry -Got1p, *35S::*mCherry -MEMB12 and *35S::*mCherry-SYP32 (Geldner et al., 2009). Transgenic endosome marker lines in *SPCHpro::*YDA^{KI}-YFP overexpressing background were generated by pollination cross.

Plasmid construction

The coding region of *SNX1* was amplified by PCR using primers listed in the table, and cloned into pENTR/D/TOPO entry vectors through AscI/NotI digestion and insertion. *SNX1* and *FAB1A* sequences were described previously (Hirano et al., 2011b; Jaillais et al., 2006). The promoter sequences of *SNX1* was PCR amplified by the listed primers and subcloned into pDONR-P4-P1R vectors. For YDA^{KI} localization, different orientations of GFP/YFP tag were used. *BASL* promoter in pDONR-P4-P1R (Dong et al., 2009) was combined with *YDA^{KI}* cDNA in R4pGWB vectors (Nakagawa et al., 2008) using LR Clonase II (Invitrogen).

To generate transient protein expression constructs in tobacco, the pENTR/D vectors containing coding sequences of *FAB1A* (courtesy of Dr. Masa H Sato), *SNX1* were recombined into the pH35GY or pH35CG, pH35GC. The constructed binary vectors were electrotransformed into *Agrobacterium tumefaciens* strains GV3101 for tobacco leaf infiltration.

Primers used in this study

Purpose	**Primer name**	**Sequence**
SNX1 CDS	SNX1_F	GCTCCGCGGCCGCCATGGAGAGCACGGAGCAG
	SNX1_R	AGGCGCGCCCGACAGAATAAGAAGCTTCAAGTTTGG
SNX1 promoter	SNX1pro_F	GCTCCGCGGCCGCCGGAAGAAGCCTGTTTCTTCTTAG
	SNX1pro_R	CCCTCGAGTTAGACAGAATAAGAAGCTTCAAGT

Microscopy and Image Analysis

Confocal images of 3-days seedlings were captured using Leica TCS SP5 II. Seedlings were counter-stained with 10 μg/μL Propidium iodide (PI, Invitrogen) to visualize cell outlines as needed. Following excitation (Ex) and emission (Em) wavelengths (Ex/Em) were used: GFP 488 nm/501–528 nm; mCherry 543nm/600–620 nm, CFP, 458 nm/480–500 nm; YFP, 514 nm/520–540 nm; mRFP, 594 nm/600–620 nm; PI 543 nm/591–635 nm. All imaging processing was performed with Fiji software (https://imagej.net/Fiji), and figures were assembled with Adobe Illustrator.

Drug Treatment

Plants were grown on ½ MS media as described above. For treatment, seedlings were gently removed from plates and placed in tubes containing endomembrane dye or trafficking-inhibition drugs. FM4-64 (8.2 μM), BFA (100 μM in DMSO), Wortmannin (33 μM in DMSO) and Concanamycin A (1 μM) with respective final concentrations were performed for the times indicated in figure legends before observation. Corresponding concentrations of DMSO treatment were used as the controls.

Transient expression in *Nicotiana benthamiana*

Agrobacterium tumefaciens strains GV3101 harboring binary vectors were cultured in 10ml LB overnight and harvested at 4500 rpm for 10 min. Concentrated cells were then washed with 10 ml of 10mM MgCl2 twice and sit at room temperature for 3 h prior to infiltration. Equal volumes of cell culture and p19 which suppress gene silencing (Voinnet et al., 2003) were mixed with an OD600=0.5 and infiltrated into the 4-week-old tobacco expanding leaves. The leaf disks were excised and mounted on slides for confocal imaging 2-3 days after the infiltration.

CHAPTER 4. Microtubule-associated ICR1 attenuates the BASL-YODA polarity proteins through vacuolar degradation

ABSTRACT

The plasma membrane integrates the cell with external cues and internal responses. Signaling components at the plasma membrane operate within a delicate balance between propagation and restriction. The initiation and maintenance of cell polarity in *Arabidopsis* stomatal asymmetric cell division involves a positive feedback loop between a canonical YDA MAPK cassette and the scaffold protein BASL. Here we describe that a restriction mechanism, which is achieved by the microtubule (MT)-associated protein ICR1 and by the vesicle trafficking, attenuates the propagating BASL-YODA signaling at the plasma membrane. The inhibition of the vacuolar/endosomal trafficking leads to disturbed subcellular distribution and accumulation of BASL and YDA. Elevated expression of ICR1 and the late endosome maturation factor FAB1/PIKfyve in the stomatal lineage triggered the vacuolar degradation of BASL and YDA. Interestingly, ICR1 is functionally dependent on the binding to MTs, and FAB1 and YDA colocalize to the endosomes that align on the ICR1-decorating MTs. These results reveal a novel function of MTs in the regulation of endosome/vacuole activity for protein degradation in plant cells.

INTRODUCTION

Cell polarization is a fundamental feature of almost all cellular organisms. The asymmetric distribution of intracellular structures and functions within a cell plays critical roles in plant development, growth and responses to environmental stimuli. Our previous work established a positive feedback loop between the polarity protein BASL (BREAKING OF ASYMMETRY IN THE STOMATAL LINEAGE) and the YDA MAPK pathway, the components of which constitute a novel polarity complex at the cell cortex to regulate stomatal asymmetric cell division (Zhang et al., 2015). Yet, how this self-amplifying, feed-forward signaling system is maintained and attenuated in plant cells remains unknown.

The Rho-family small GTPases are conserved molecular switches in the establishment of cell polarity (Hodge and Ridley, 2016) and in plants, Rho-like GTPases (ROPs) govern the plethora processes of cytoskeletal organization and vesicular trafficking to control cell polar growth and morphogenesis (Craddock et al., 2012). Downstream of the active ROP signaling was an Interactor of Constitutive-active ROPs 1 (ICR1) that links vesicle trafficking to the polarization of interdigitated pavement cells and pollen tubes in *Arabidopsis* (Lavy et al., 2007; Li et al., 2008a). The function of ICR1 was further linked to the regulation of exocytosis or endocytic recycling of the PIN proteins back to the PM *via* interacting with the exocyst subunit SEC3A (Hazak et al., 2010). In addition, the PM recycling of PIN proteins was found Microtubule (MT)-dependent and regulated by the connected functions of the MT-associating protein CLASP and the retromer component sorting nexin 1, SNX1 (Ambrose et al., 2013).

Here, we report a novel function of ICR1 in alleviating the abundance of the polarity proteins BASL and YDA in a MT-dependent manner in the stomatal lineage cells. In Chapter 3, we showed that polarized BASL and YDA are internalized by the membrane system and delivered to the endosome, MVB and vacuole for degradation in the stomatal lineage cells. Here we further discovered that this process is facilitated by the ROP effector ICR1 protein. Surprisingly, ICR1 has to bind to the MTs for this function, suggesting an interesting and new role of MT cytoskeleton in the regulation of late endosomal activities in plant cells. Furthermore, we demonstrate that internalized YDA localizes to the FAB1/PIKfyve (Phosphatidylinositol 3-phosphate 5-kinase)-positive endosomes and both associate with the ICR1-decorating MT tracks. Consistent with the functions of FAB1 in promoting endosome maturation (Hirano et al., 2015b), FAB1b overexpression in the stomatal lineage triggers the degradation of BASL and YDA in *Arabidopsis*. Thus, our study discovers a novel function of the MT-associated ICR1, likely through cooperating with the late endosome maturation factor FAB1, to promote the vacuolar degradation of BASL-YDA, so that the positive feedback signaling of the polarity site can be dampened at the PM.

RESULTS

Promoter activity of the ICRs family

Research in our lab disclosed a set of candidate genes that are involved in stomatal ACD, and ICR1 (Interactor of Constitutively Active ROPs) was enlisted. In *Arabidopsis*, the *ICR* gene family consists of five family members, whose homologs were also found in other plant species, including tobacco, potato, and rice, but not in yeast and animals

(Li et al., 2008b). All five ICR members contain coiled-coil domains that may mediate protein-protein interactions. Based on the phylogenetic tree by the full-length proteins, the five members can be divided into three subgroups, with group 1 consisting of ICR1 and ICR4, group 2 consisting of ICR2, ICR3 and group 3 containing ICR5 (**Fig. 4.1A**). All five ICRs share a relatively high similarity in amino acid sequence at their N and C-termini: an N-terminal QEEL motif required for oligomerization and a C-terminal QWRKAA motif responsible for the interaction with ROPs and other proteins (Li et al., 2008b). The ICR family members seem to perform various functions by interacting with unique protein partners. ICR1 was reported to link vesicle trafficking to the polarization of interdigitated pavement cells and pollen tubes in *Arabidopsis* (Lavy et al., 2007; Li et al., 2008a). ICR3 (also known as MIDD1) regulates the formation of secondary cell wall pits in xylem cells. It was shown to localize to the MT by interacting with kinesin13A, which functions to locally sever or depolymerize MT filaments (Oda and Fukuda, 2013; Oda et al., 2010). However, there was limited knowledge about how ICR members function and whether they are expressed in the stomatal lineage cells.

To analyze the expression pattern of individual ICR members, a set of transcriptional fusion makers (nuclear Yellow Fluorescent Protein, nuYFP, driven by the endogenous promoters) were generated to transform into *Arabidopsis* WT plants. Interestingly, all five *ICR* members are highly transcribed in the early staged stomata lineage cells (e.g. Meristermoid, SLGC) (**Fig. 4.1B-F**). The promoter of *ICR1, 2, 4,* and *5* also showed activity in pavement cells (**Fig. 4.1B-F**). The broad expression pattern of *ICR* family in the leaf epidermis suggested their potential functions in stomatal development and patterning.

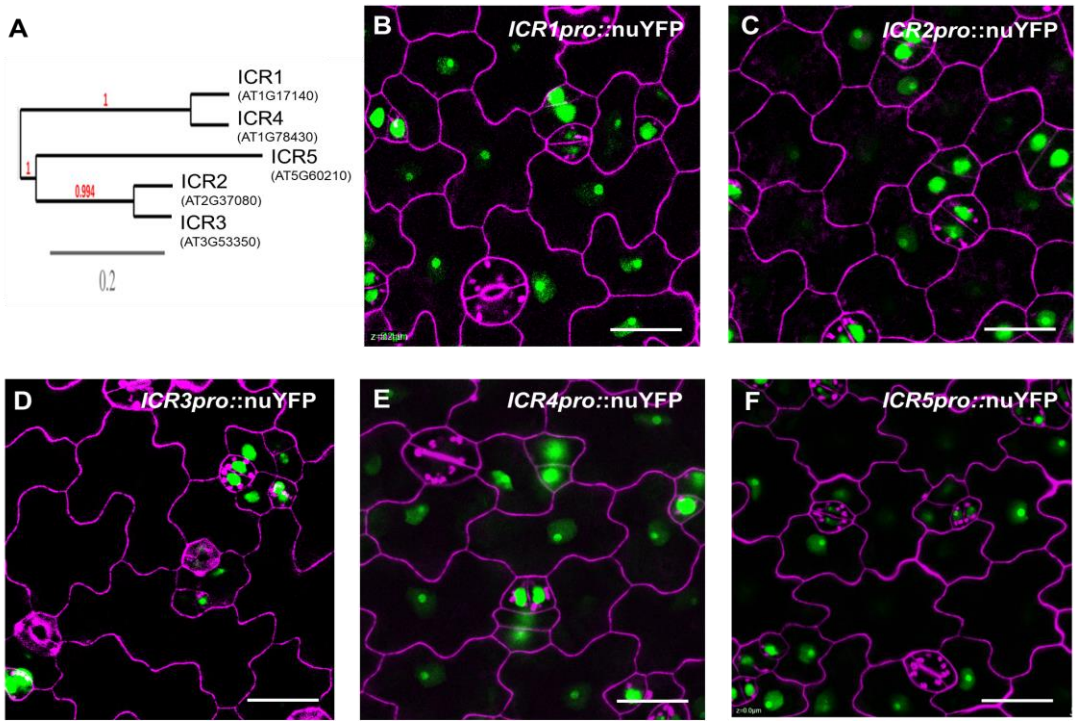

Fig. 4.1. Phylogenetic tree and promoter activity of *ICR* members.
(A) The phylogenetic tree of ICRs based on amino acid sequence similarity. Red numbers next to branch nodes are bootstrap values. Branch scale =0.2.
(B-F) Confocal images of **(B)** *ICR1pro::*nuYFP, **(C)** *ICR2pro::*nuYFP, **(D)** *ICR3pro::*nuYFP, **(E)** *ICR4pro*::nuYFP, **(F)** *ICR5pro::*nuYFP that show their promoter activities in *Arabidopsis*. Cells are outlined with Propidium Iodide staining (magenta) and nuYFP (nuclear YFP) is artificially colored with green in **(B-F)**. Scale bar in (B) =25μm, others at the same scale.

ICR proteins are associated with the microtubule cytoskeleton

Recent studies reported the protein localizations of ICR1 and ICR3. ICR1 was observed to localize in the cytosol and at the plasma membrane in leaves and roots (Hazak et al., 2014; Lavy et al., 2007). ICR3 is associated with cortical microtubules in xylem cells (Oda and Fukuda, 2013; Oda et al., 2010). To systematically analyze protein localizations of the ICR family, GFP-tagged ICR proteins driven by their endogenous promoters were introduced in *Arabidopsis* for expression examination. All five ICR

proteins were found to localize to MT-like filamentous structures at the cell cortex in the *Arabidopsis* stomatal lineages (**Fig. 4.2A-E**).

Consistently, when expressed transiently in tobacco epidermal cells, GFP-ICR fusions showed association with microtubule-like filaments. More interestingly, individual ICR members exhibited distinct distribution patterns along the filaments, suggesting that they may contribute to different biological processes at the subcellular level (**Fig. 4.2F-J**).

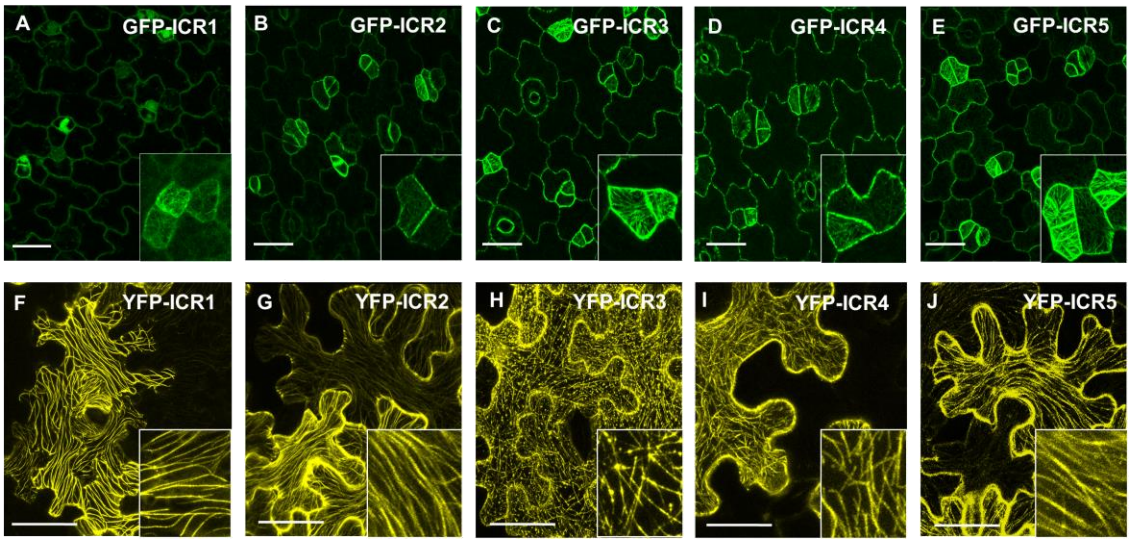

Fig. 4.2. Expression of fluorescent protein-tagged ICRs in plant cells.
(A-E) Confocal images showed that GFP-ICRs consistently localize to filamentous structures at the cell cortex in the *Arabidopsis* stomatal lineages. Z-projected individual cells are shown in the insets. Scale bars in (A) = 50μm, others are at the same scale.
(F-J) Confocal images of transiently expressed YFP fused ICRs in the tobacco leaf epidermal cells. Z-projected microtubule structures are shown in the insets Note, they all seem to associate with the microtubule cytoskeleton, but with distinct patterns. Scale bars in (F) = 50μm, others are at the same scale.

Genetic redundancy of the *ICR* gene family

To study their biological functions, we collected single *icr* mutants, each of which harbors a large piece of T-DNA fragment so that the gene function is presumably disrupted. Using a PCR-based genotyping approach, we verified the T-DNA insertion sites in *ICR1, ICR2, ICR3,* and *ICR5* (described in **Fig. 4.3A)**. The T-DNA insertional single mutants were assessed for stomatal phenotypes and none of the single mutants (*icr1-t, icr2, icr3* and *icr5*) showed obvious stomatal patterning defects.

These single mutants were crossed together to obtain high order mutants. Currently, we have confirmed the homozygous mutants of quadruple *icr1-t;icr2;icr3;icr5* that did not generate obvious stomatal patterning defects (**Fig. 4.3C-D**), except for the cubical morphology of pavement cells, which was a typical feature of the *icr1-t* single mutants (*icr1* mutants are described later).

In the process of generating high order mutants, in particular, to create an *icr4* loss-of-function allele, we employed the CRIPSR/Cas9 system for targeted gene mutagenesis (Mao et al., 2013). We simultaneously targeted all five *ICR* gene sites by co-transforming three CRISPR/Cas9 constructs, each of which contained one or two sgRNA expression cassettes (**Fig.4.3B,** sgRNA-1.1, 4, sgRNA-2, 5, and sgRNA-3). Out of 30 primary transformants (T1), 8 plants were randomly selected for mutation identification using T7 Endonuclease I digestion (**Fig. 4.3E**). The results showed that sgRNAs targeted to *ICR2*, *ICR4* and *ICR5* worked efficiently and we were able to find 3 single mutants (**Fig. 4.3E**, #3 *icr5*, #4 *icr4,* and #5 *icr5*) and 2 double mutants (#1 *icr2 icr5* and #6 *icr4 icr5*) out of 8 T1 plants, but none of them showed obvious stomatal

phenotype. Their progenies will be further characterized and crossed with the other T-DNA mutants to generate quadruple and quintuple loss-of-function mutants.

In summary, our data show that all five *ICR* genes are expressed in the stomatal lineage cells suggesting their potential function there. We will have to combine T-DNA mutants with CRISPR/Cas9 mutations to fully establish quadruple and/or quintuple mutants for thorough phenotype examination and genetic analyses in order to understand the functions of *ICR* family in stomatal development.

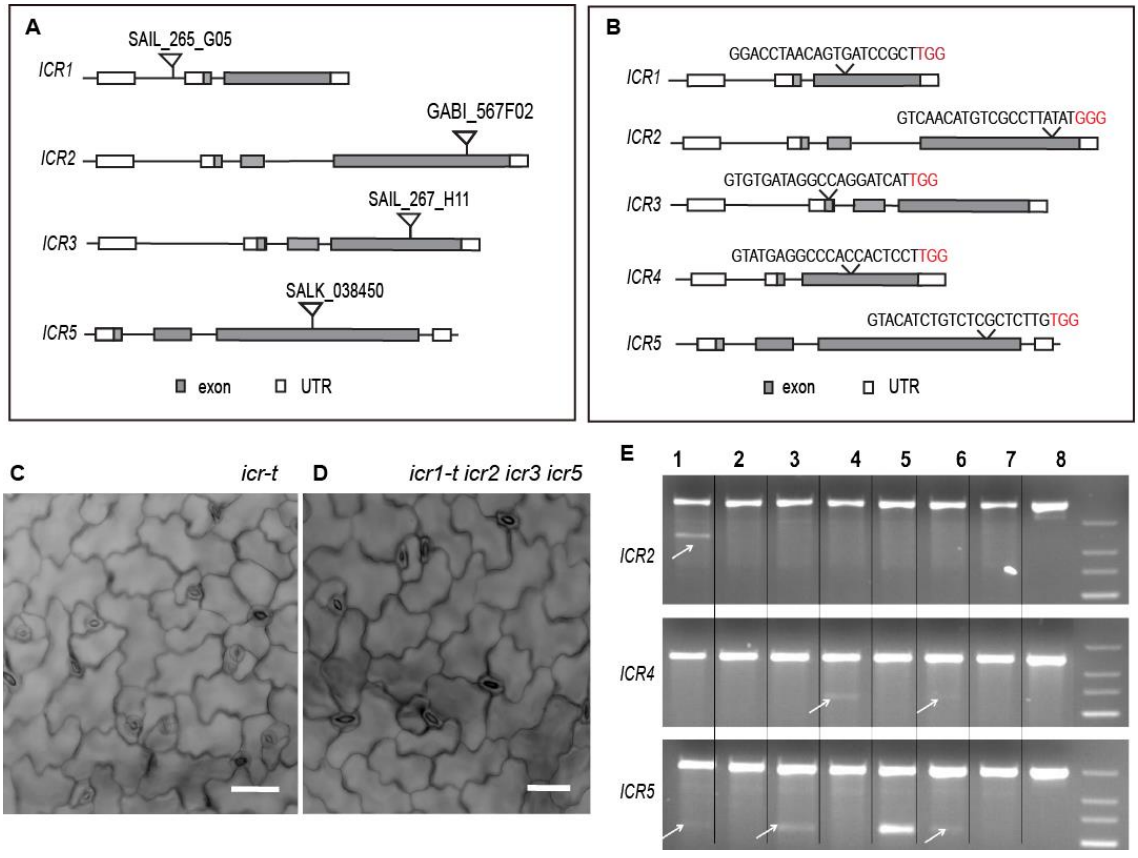

Fig. 4.3. Genetic redundancy of the *ICR* family.
(A) A schematic representation of T-DNA insertion sites on *ICR1*, *ICR2*, *ICR4* and *ICR5*, respectively.
(B) A schematic diagram of sgRNA designs of CRISPR/Cas9 targeted *ICR1-5*. Red highlights the PAM region.
(C-D) Confocal images of 5dpg adaxial cotyledons stained with propidium iodide to mark cell outlines. (**C**) *icr1-t*. (**D**) *icr1-t icr2 icr3 icr4*. Scale bars: 50 μm.

(E) 2.0% agarose DNA gel showing mutation identification with T7 Endonuclease I treatment. 8 T1 *Arabidopsis* seedlings were digested as labeled. Arrows indicate extra DNA fragments resulted from T7 endonuclease cleavage at DNA mismatches, suggesting potential mutations on indicated genes.

ICR1 overexpressor resembles the loss-of-function *basl* mutants

To analyze how *ICR1* functions in stomatal development, we generated overexpression lines by using the *BASL* promoter to drive the expression of YFP-fused ICR1. Interestingly, the ICR1 overexpressors displayed proliferated stomatal lineage divisions and clustered guard cells (shaded with magenta and cyan, respectively, in **Fig. 4.4A, 4.4B**), strikingly resembling the phenotype of the loss-of-function *basl-3* mutant (**Fig. 4.4F**) (Dong et al., 2009). This phenotype was recapitulated when the expression of *ICR1* was elevated by the ubiquitous *CaMV 35S* promoter (**Fig. 4.4D**) or by the endogenous *ICR1* promoter in the wild-type (WT, Col) background (**Fig. 4.4E**), in which the ICR1 transcript levels were elevated by 1.5 to 2 folds based on quantitative PCR (**Fig. 4.4C**). Then, *BASLpro::* ICR1-YFP was introgressed into *basl-3* to determine their genetic interaction. We found that, while *BASLpro::* ICR1-YFP (**Fig. 4.4B**) was comparable to *basl-3* (**Fig. 4.4F**), the progeny of *BASLpro::* ICR1-YFP *basl-3* (**Fig. 4.4G**) phenocopied either of the parental lines (quantified in **Fig. 4.4H**), suggesting that *BASL* and *ICR1* function in the same genetic pathway and overexpressing ICR1-YFP might have interfered the BASL function.

We previously reported that BASL regulates an intrinsic cell polarity pathway during stomatal ACD (Dong et al., 2009), which is independent of the extrinsic signaling pathway mediated by the receptors of Too Many Mouth (TMM) (Nadeau and Sack,

2002b) and the ERECTA (ER) family (Shpak et al., 2005a). We also introgressed the ICR1-YFP overexpression line into the null *er105* and *tmm-1* mutants. The results showed that overexpressing ICR1-YFP created an additive phenotype in the absence of *TMM* and *ER* (**Fig. 4.4I-J** and **Fig. 4.4K-L**, quantification in **Fig. 4.4M**), highly similar to the double mutants of *tmm basl* and *er105 basl* (Dong et al., 2009). These data further suggested that *ICR1* functions independent of *TMM* and *ER*, but in the same pathway with *BASL*.

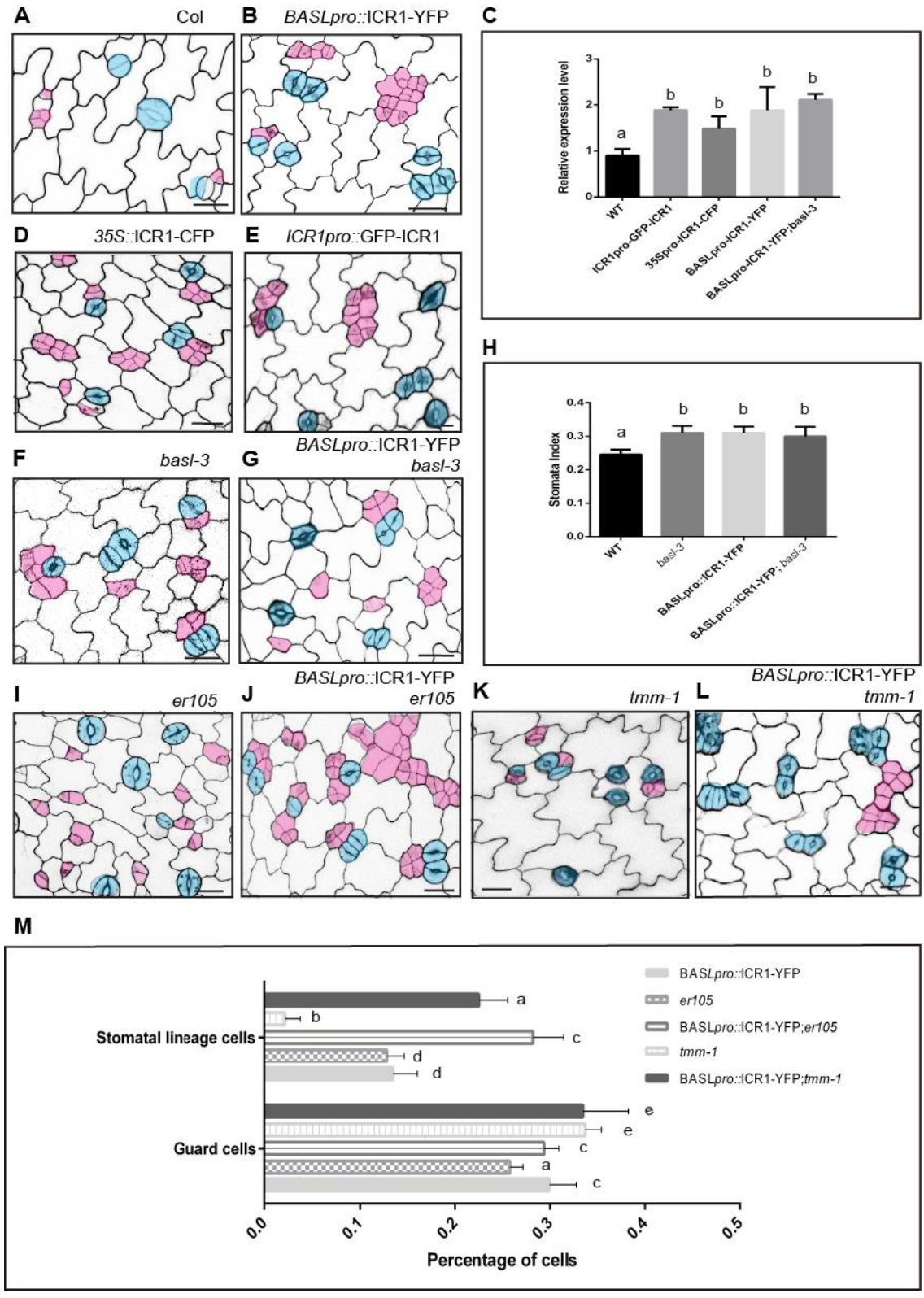

Fig. 4.4. Overexpression of ICR1 resembles loss-of-function *basl* mutants.
(A-B) Representative confocal image of a 2-dpg (day post germination) adaxial cotyledon of **(A)** WT, **(B)** *BASLpro::*ICR1-YFP. Light blue highlights guard cells and pink highlights early

stomatal lineage cells (Meristemoid, SLGC, Guard Mother cells). Note abnormal divisions and clustered guard cells in the ICR1 overexpressing lines. Cell walls were stained with propidium iodide (PI) and this applies to all the other figures. Scale bars, 25 μm.

(C) Quantitative PCR of ICR1 transcript level. Histograms demonstrate the real-time PCR data that confirms ICR1 overexpression among the different transgenic populations. Bars represent the mean values of three independent replicates normalized with the reference gene AtACT2 ± SE. Letters indicate significant differences determined by Holm-Sidak's multiple comparisons test, $p<0.005$.

(D-G) Representative confocal image of a 2-dpg (day post germination) adaxial cotyledon of **(D)** *35Spro::*GFP-ICR, **(E)** *ICR1pro::*GFP-ICR1, **(F)** *basl-3*, **(G)** *BASLpro::*ICR1-YFP; *basl-3.* Scale bars, 25 μm.

(H) Quantification of the stomatal index using 5-dpg adaxial cotyledons. Data are mean ± SD. Letters indicate significant differences determined by Holm-Sidak's multiple comparisons test, $p<0.005$.

(I-L) Representative confocal image of **(I)** *er105*, **(J)** *BASLpro::*ICR1-YFP; *er105*, **(K)** *tmm-1*, **(L)** *BASLpro::*ICR1-YFP; *tmm-1*. Scale bars, 25 μm.

(M) Quantification of the stomatal index using 5-dpg adaxial cotyledons. Data are mean ± SD. Letters indicate significant differences determined by Holm-Sidak's multiple comparisons test, $p<0.005$.

Analysis of *icr1* mutants

To further characterize the function of *ICR1* in stomatal development, a previously reported T-DNA mutant *icr1-t* (SAIL_265_G05) (Lavy et al., 2007) was obtained. Through PCR-based characterization, we confirmed that the T-DNA insertion site is located in the 5'-UTR intron region, 176 bp upstream of the start codon of *ICR1* (**Fig. 4.5A,** Top panel). Real-time PCR using primers flanking the 3'-UTR region demonstrated that *ICR1* was transcribed at a lower level and *icr1-t* is a knockdown mutant (**Fig. 4.5B**). The *icr1-t* mutant exhibited cubical pavement cells in leaf epidermis (**Fig. 4.5C-D**) and short primary roots with numerous adventitious roots (Lavy et al., 2007).

To confirm this phenotype, we created more *icr1* mutant alleles by CRISPR/Cas9. Among three *sgRNAs* we designed to target *ICR1*, only *sgRNA2* was proven to work

and the obtained transgenic plants were designated as *icr1-crispr2*. As shown by the T7 endonuclease I digestion, *icr1-crispr2* mutations were successfully created (**Fig. 4.5E**), but these plants did not show obvious developmental defects in both pavement cells (**Fig. 4.5F**) and roots.

At the moment, it still needs to be clarified whether the developmental defects of *icr1-t* were caused by *ICR1* loss-of-function. The phenotype discrepancies will be addressed by analyzing different mutant alleles and by successful functional complementation eventually.

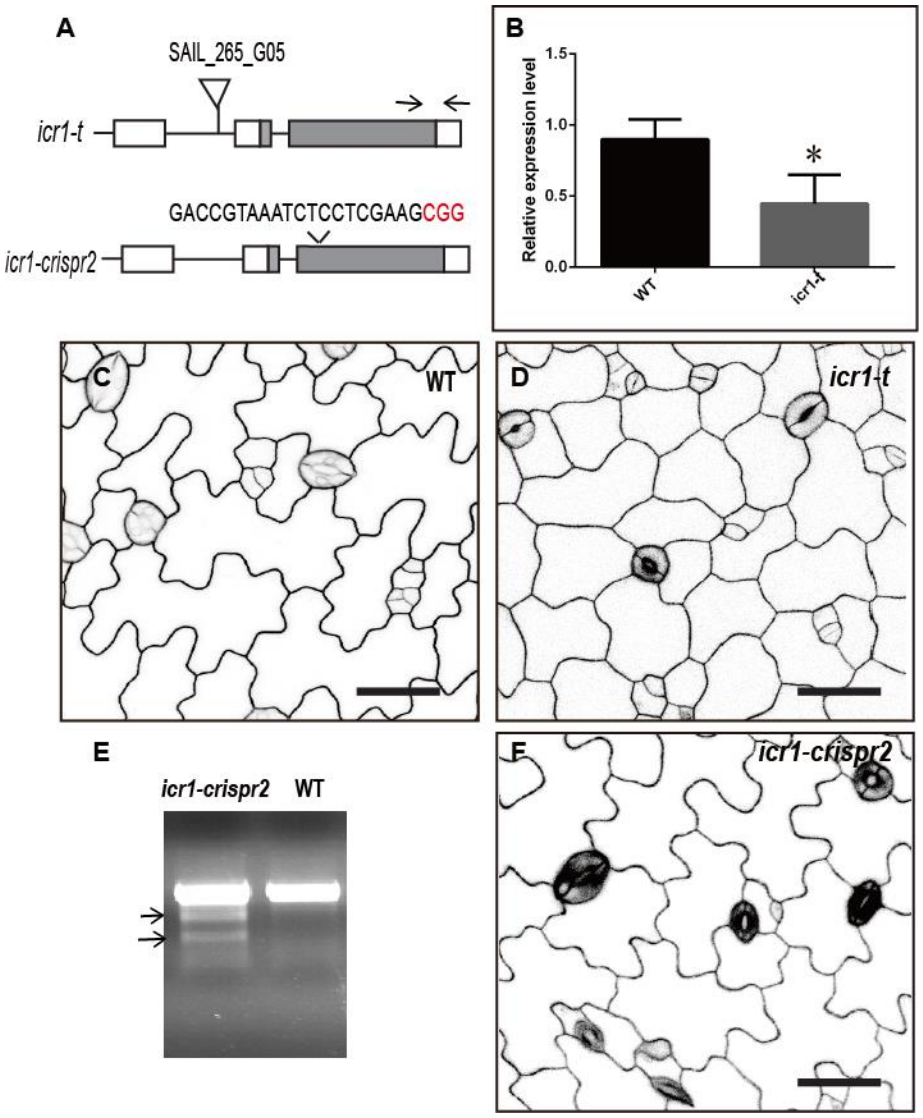

Fig. 4.5. *ICR1* mutant phenotype in leaf epidermis.

(A) Top: A schematic representation of T-DNA insertion site of *icr1-t* mutants. Arrowheads point to the location of designed primers for realtime PCR. Bottom: sgRNA design of CRISPR/Cas9 targeted *ICR1*. Red highlights the PAM region.

(B) Realtime PCR of *ICR1* transcripts level. Bars represent the mean values of three independent replicates normalized with the reference gene AtACT2 ± SE. * indicate significant difference. (t test, $p<0.005$)

(C-D) Confocal images of 5dpg adaxial cotyledons stained with propidium iodide to mark cell outlines. **(C)** WT. **(D)** *icr1-t*. Scale bars: 50 μm.

(E) Mutation identification with T7 Endonuclease I treatment. Arrows indicate extra DNA fragments resulted from T7 endonuclease cleavage at DNA mismatches, suggesting potential mutations on *ICR1*.

(**F**) Confocal images of 5dpg cotyledons of *icr1-cripst2*. Propidium iodide was used to mark cell outlines. Scale bars: 50 μm.

ICR1 overexpression induces protein degradation of both BASL and YDA

To investigate whether ICR1 overexpression changes BASL polar localization, we crossed the well-established maker line *BASLpro::*GFP-BASL (Dong et al., 2009) with the *35S::*ICR1-CFP overexpression plants. Surprisingly, we found that the fluorescence intensity levels of GFP-BASL were drastically reduced by *ICR1* overexpression, therefore barely detectable under the confocal microscope (**Fig. 4.6A, 4.6B,** 38.4% n=232 of GFP-positive cells, compared to 81.0% n=218 in the WT). Careful observation showed that the BASL polarity did not seem to be drastically affected; in the cells with detectable levels of GFP, BASL cortical polarization was evident (**Fig. 4.6B**). Similar effects were recapitulated when the overexpression of ICR1 was induced by estradiol in the 2-dpg (days post germination) seedlings of GFP-BASL marker line (**Fig. 4.6D**). The lowered expression of GFP-BASL was found to occur at the protein level because the quantitative PCR data demonstrated that *BASL* transcripts in *35S::*ICR1-CFP plants were comparable to those in the WT (**Fig. 4.6C**).

Because the MAPKKK YDA physically interacts and co-polarizes with BASL at the PM (Zhang et al., 2015), we also examined whether ICR1 affects YDA protein accumulation. Similar results were found; the fluorescence intensity of YDA-YFP was much lowered in the *ICR1* overexpression plants than it was in the WT (**Fig. 4.6G, 4.6H**), while the transcript level of *YDA* was not reduced (**Fig. 4.6I**). The degradation of YDA protein did not appear to depend on its kinase activity, as the kinase inactive YDA protein (K429R (Lukowitz et al., 2004), YDA^{KI}-YFP) was similarly reduced by elevated *ICR1* expression (**Fig. 4.6E, 4.6F**).

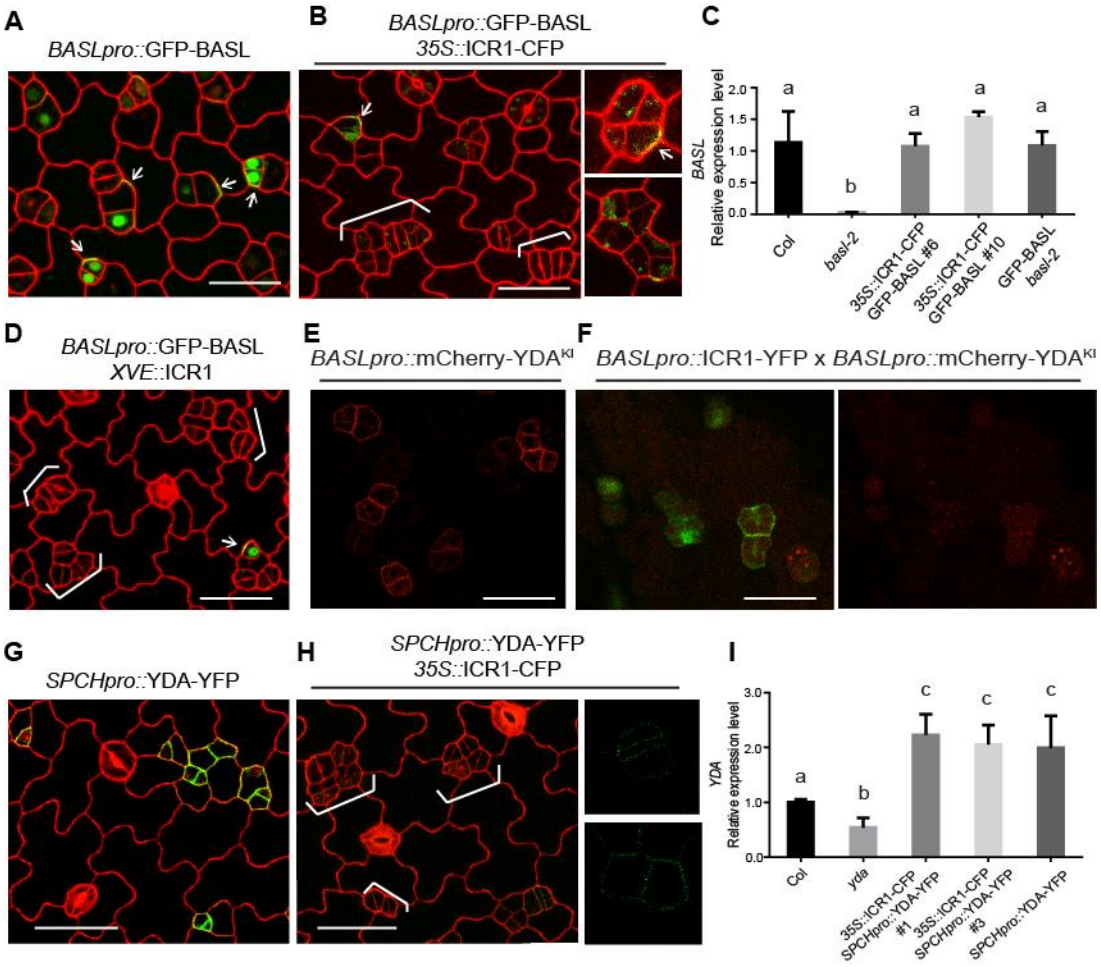

Fig. 4.6. ICR1 overexpression induces YDA and BASL protein turnover.

(A) Confocal images of *BASLpro::*GFP-BASL (green) localization. Arrows indicate dual localization of BASL in both nuclear and cortical polar regions. Red, propidium iodide (PI)-stained cell walls. White brackets indicate clustered stomatal lineage cells which resemble *basl*. Scale bar = 25 μm, others at the same scale.

(B) Localization of diminished *BASLpro::*GFP-BASL at both nuclear and plasm membrane (indicated by arrows) in ICR1 overexpressing lines. Insets show a closer view of weak GFP-BASL.

(C) Quantitative PCR of *BASL* transcript level. 4 day-post-germination *Arabidopsis* seedlings of Col-0, *basl-2* mutant, two independent cross lines of ICR1-CFPXGFP-BASL and GFP-BASL were used to extract total RNA. cDNA was generated and gene-specific primers were used to determine expression levels of BASL. Bars represent the mean values of three independent replicates normalized with the reference gene AtACT2 ± SE. Letters indicate significant differences determined by Holm-Sidak's multiple comparisons test, $p<0.005$.

(D) Diminished BASL localization by β-estradiol induced ICR1 expression. BASL marker lines bearing *XVE::*ICR1 were treated with 10 μM β-estradiol for 72 h to induce ICR1 expression. White brackets indicate clustered stomatal lineage cells generated by overexpressing ICR1. Arrows indicate remaining weak nuclear localization of BASL.

(E) Confocal images of *BASLpro::*mCherry-YDA^{KI} (red) localization.

(F) Confocal images of *BASLpro::*mCherry-YDA^{KI} (red) localization in ICR1-overexpressing background (green). Note the striking reduced level of YDA^{KI} expression when introducing ICR1.
(G) *SPCHpro::*YDA-YFP (green) localization in WT.
(H) Localization of diminished *SPCHpro::*YDA-YFP in ICR1 overexpression plants. White brackets indicate clustered stomatal lineage cells generated by overexpressing ICR1. Red, propidium iodide (PI)-stained cell walls. Insets show a closer view of barely observed YDA-YFP (YFP channel only).
(I) Quantitative real-time PCR of YDA transcript level. 4 day-post-germination *Arabidopsis* seedlings of Col-0, *yda*, two independent cross lines of ICR1-CFPXYDA-YFP and YDA-YFP were used to determine expression levels of YDA. Bars represent the mean values of three independent replicates normalized with the reference gene AtACT2 ± SE. Letters indicate significant differences determined by Holm-Sidak's multiple comparisons test, $p<0.005$.

PINs are not downregulated by ICR1

A previous study reported that ICR1 promotes the recruitment of the auxin efflux transporters, PIN-FORMED 1 (PIN1) and PIN2, back to the polarized domain at the PM in *Arabidopsis* roots and embryos (Hazak et al., 2010). We further tested whether overexpression of ICR1 may induce the degradation of PIN proteins. The protein abundance of GFP-tagged PIN1, PIN2 and PIN3 were not obviously affected by ICR1 overexpression (**Fig. 4.7A, 4.7B, 4.7C**); this is also reflected by the negligible developmental defects in *35S::*ICR1-CFP plants at the whole plant level (**Fig. 4.7D**). Thus, ICR1-mediated protein degradation does not seem to universally affect all membrane proteins, including PINs, and its function in the down-regulation of BASL-YDA is likely a selective process in *Arabidopsis*.

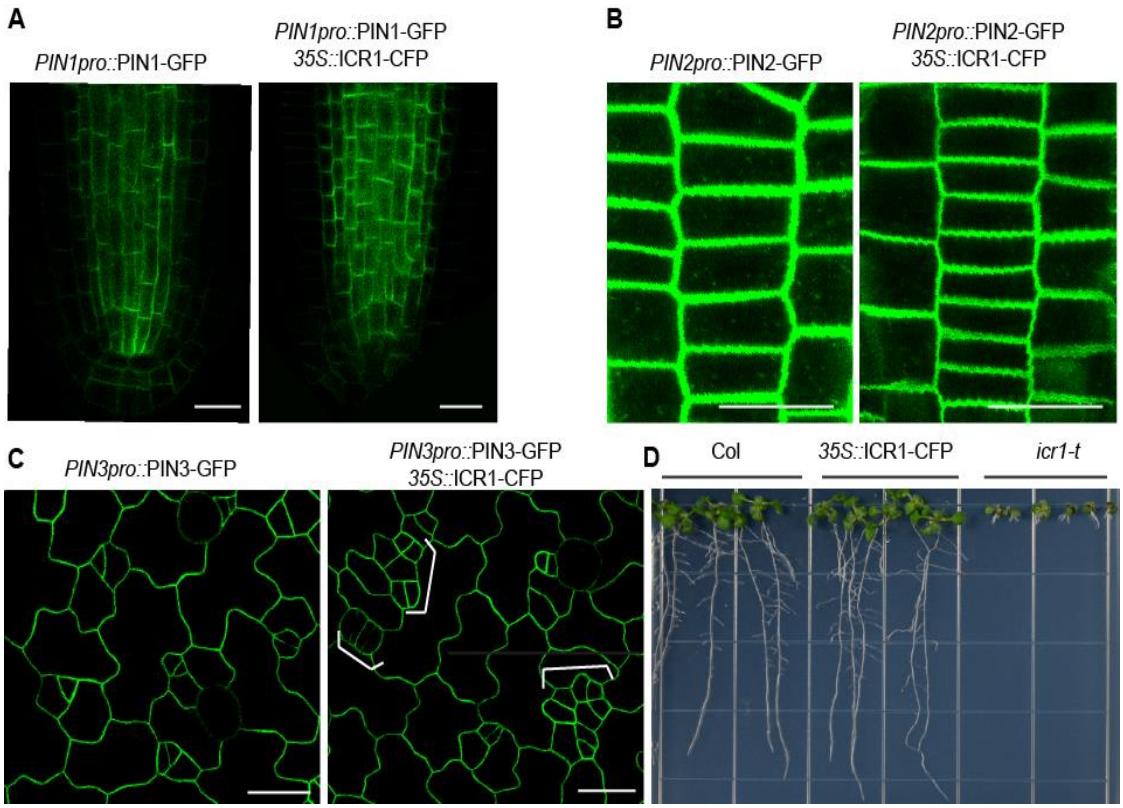

Fig. 4.7. PINs are not downregulated by ICR1
(A) Representative confocal images of *PIN1pro::*PIN1-GFP localization in root tip of 4-dpg WT (Left) and *35Spro::*ICR-CFP (Right). Scale bar = 25 μm, others at same scale.
(B) *PIN2pro::*PIN2-GFP localization in root tip of 4-dpg WT (Left) and *35Spro::*ICR-CFP (Right).
(C) *PIN3pro::*PIN3-GFP localization in leaf epidermis of 3-dpg WT (Left) and *35Spro::*ICR-CFP (Right). White brackets indicate clustered stomatal lineage cells generated by overexpressing ICR1.
(D) Whole-plant level phenotype of WT, *35S::*ICR1-CFP and *icr1-t* mutants.

ICR1 promotes BASL and YDA targeting towards the vacuole.

As ICR1 seemed to promote BASL and YDA vacuolar targeting for degradation, we assayed how GFP-YDA^{KI} and GFP-BASL are localized in the absence *ICR1*. We found that the localization of YDA was very sensitive to the *icr1-t* T-DNA mutation (SAIL_265_G05). Strikingly differing from its dominant PM-association pattern in the WT background, GFP-YDA^{KI} was much more accumulated in the cytoplasm in *icr1-t*

(**Fig. 4.8A, 4.8B**), possibly suggesting that with lowered expressed *ICR1*, the internalized YDA molecules failed to get degraded. On the other hand, the localization of GFP-BASL did not show obvious changes in *icr1-t* mutants (**Fig. 4.8E**). However, in a more sensitized system where the MVB inhibitor WM was applied, the response of GFP-BASL was much less sensitive in *icr1-t* than in the WT (**Fig. 4.8C, 4.8D**). Specifically, 4-hr WM treatment of 3-dpg (day-post-germination) seedlings expressing GFP-BASL resulted in the association of GFP-BASL with WM-triggered abnormal MVB structures (**Fig. 4.8C**, 54.9% of GFP-positive cells, n = 122). By contrast, in *icr1-t* mutants, the association of BASL with MVB no longer occurred under the same WM treatment (**Fig. 4.8D**, 8.1% of GFP-positive cells, n = 123). These findings indicate that ICR1 functions as a positive regulator in targeting both YDA and BASL to the MVBs and vacuoles. Considering the physical association of YDA with late endosomes and its translocation in *icr1-t*, we suspect that YDA is more tightly controlled by the ICR1 function.

If ICR1 promotes YDA degradation, we would anticipate the YDA MAPK activity to be elevated in the loss-of-function *icr1-t* mutants. To biochemically evaluate the YDA MAPK signaling strength, Dr. Xiaoyu Guo used a p44/42 antibody for Western blotting of total proteins from 3-dpg *icr1-t* mutants and ICR1 overexpression plants, respectively. Her data demonstrated that more phosphorylated MPK3/6 accumulated in *icr1-t* mutants but less in ICR1 overexpression plants (**Fig. 4.8F**), compared to the wild-type Col, supporting ICR1 as a negative regulator of the YDA MAPK activity in *Arabidopsis* plants.

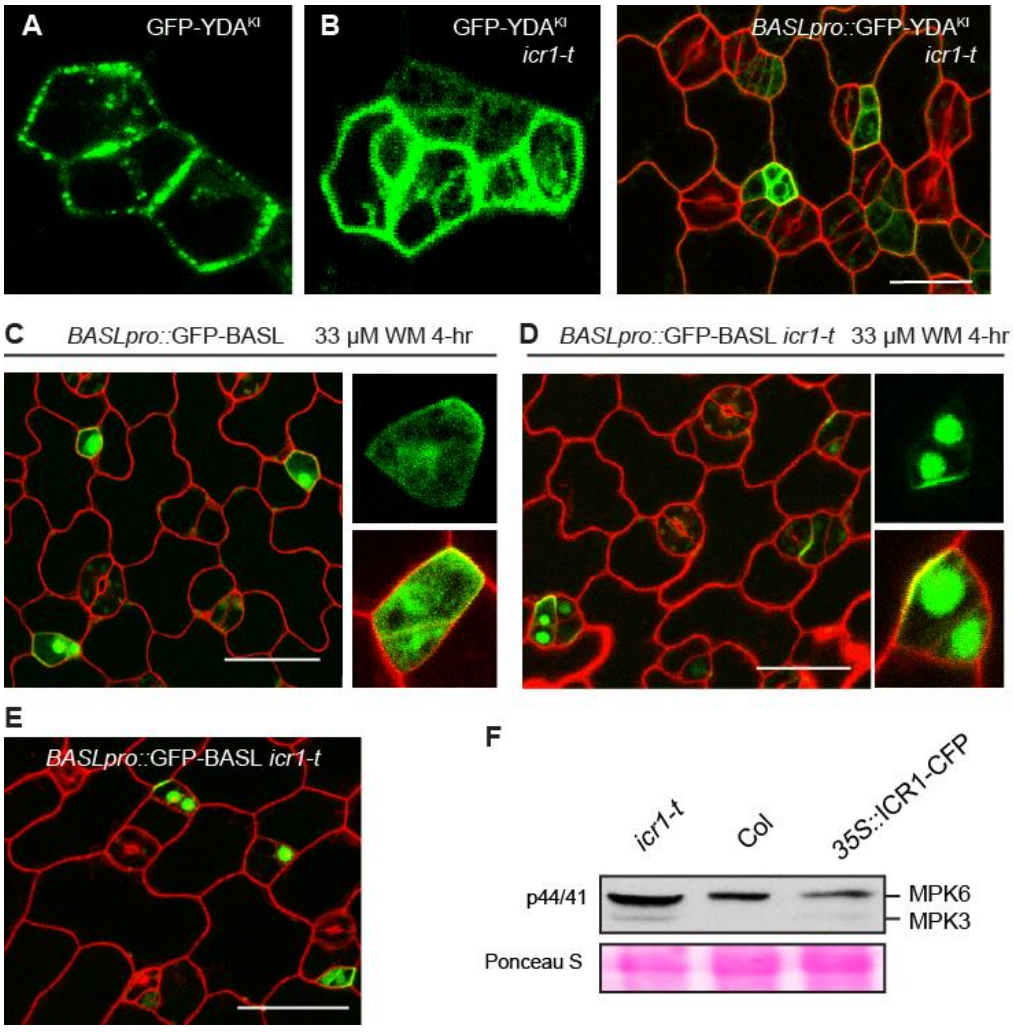

Fig. 4.8. ICR1 promotes BASL and YDA targeting towards the vacuole.
(A-B) Expression of *BASLpro::*GFP-YDA^{KI} (green) in **(A)** WT and **(B)** *icr1-t*, respectively. Individual cells with cytoplasmic accumulation of YDA^{KI} were shown on the left panel. Cell walls were stained with PI (Red). Scale bar = 25 μm.
(C) *BASLpro::*GFP-BASL treated with 33uM Wortmannin for 4hr. Inserts showed individual cells with GFP-BASL localized to wortmannin-induced abnormal MVB compartments.
(D) 33μM Wortmannin treatment on *BASLpro::*GFP-BASL in *icr1-t* mutant background for 4hr.
(E) *BASLpro::*GFP-BASL in *icr1-t*.
(F) Western blots evaluate MPK3/6 kinase activity in designated genetic backgrounds. Twenty micrograms of total proteins from 3-dpg seedlings were used for detection of active MPK3 and MPK6 by a p44/42 MAPK antibody. Protein loading is visualized by Ponceau S staining. Data produced by Dr. Xiaoyu Guo.

ICR1 associates with the microtubules

To gain further insights into ICR1's expression pattern and biological function, we assayed its promoter activity and protein localization in *Arabidopsis* plants. As previously shown, *ICR1* promoter is highly active in the early stomatal lineage cells and less so in pavement cells (**Fig. 4.1B**). The protein fusions *ICR1pro::*GFP-ICR1, besides showing the previously reported cytoplasmic and PM localization (Lavy et al., 2007), were also detected in the nucleus and along the MT-like filaments at the cell cortex (**Fig. 4.9A**). By using the MT-depolymerization drug Oryzalin, we found that the filamentous localization of GFP-ICR1 disappeared and protein diffused in the cytoplasm after 30-min of 1 μM Oryzalin treatment (**Fig. 4. 9B**). The ICR1 association with the MT cytoskeleton was further confirmed by co-expressing ICR1-YFP with a MT-binding protein MAP65-3 (Steiner et al., 2016) in tobacco epidermal cells (**Fig. 4.9G**). Similarly, Oryzalin treatment dissembled the MT-association pattern of ICR1-YFP (**Fig. 4.9D-F**).

ICR1 protein contains a stretch of Serine, Proline and Arginine residues at the N-terminus that was recognized as a S/R rich microtubule-binding domain (Al-Bassam and Chang, 2011). We deleted the N-terminal domain and constructed GFP-ICR1_d29 driven by the endogenous promoter to check its localization. The results showed that GFP- ICR1_d29 lost its localization to the cortical MTs (**Fig. 4.9C**), suggesting the short motif of 29 amino acids mediate ICR1 binding to MTs. Furthermore, elevated expression of *ICR1pro::*GFP-ICR1_d29 in the WT failed to produce the stomatal clustering phenotype (12 out of 12 lines of primary transformants), while *ICR1pro::*GFP-ICR1 in WT did (7 out of 15 primary transformants), further suggesting

that the ICR1-mediated BASL and YDA degradation relies on its association with the MTs.

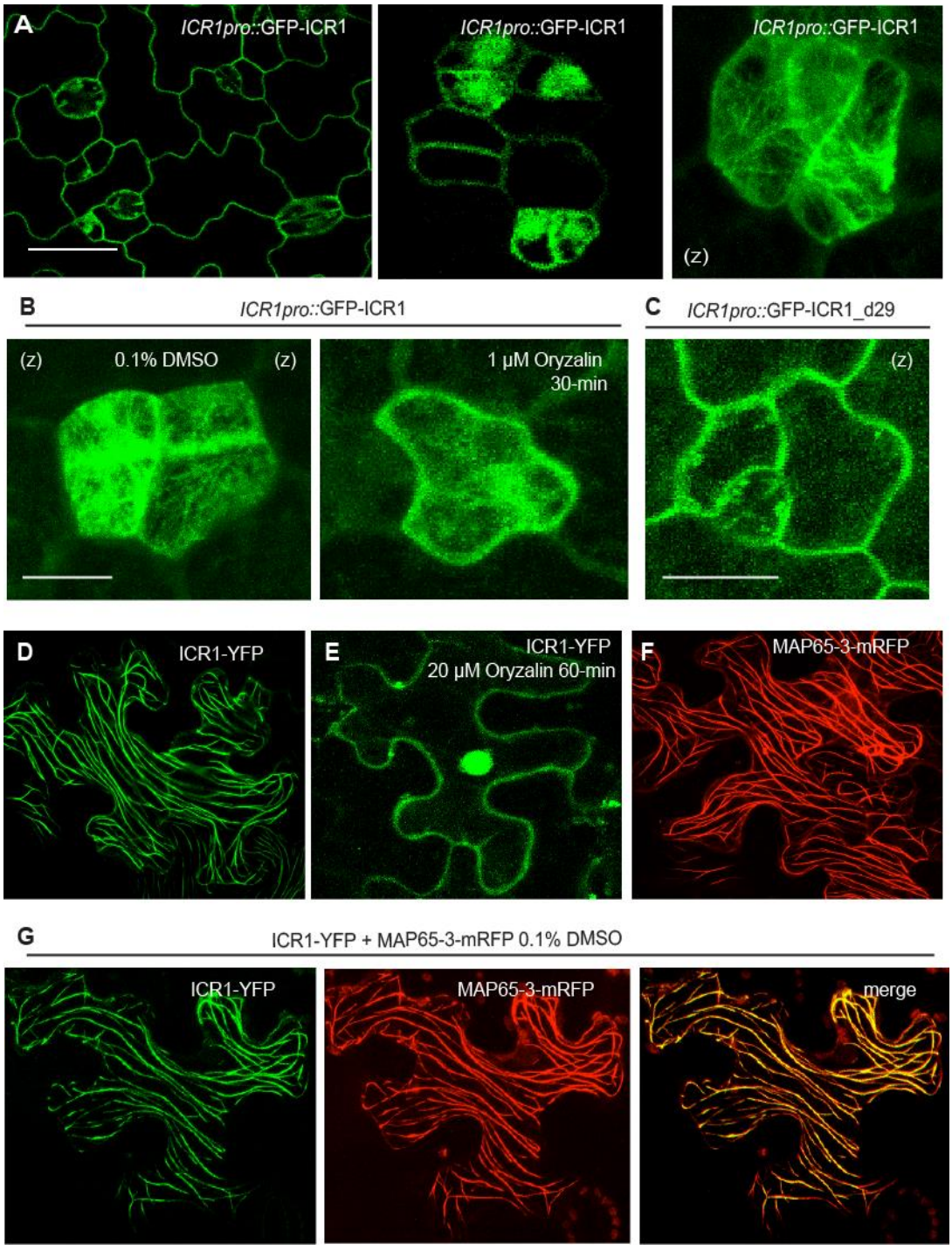

Fig. 4.9. Cellular localization of ICR1 reveals direct MT-binding.
(A) GFP-labeled ICR1 (green, driven by the *ICR1* promoter) localization in 3-dpg *Arabidopsis* adaxial cotyledons. Individual cells on right demonstrate nuclear and cytoplasmic accumulation (Middle) and a z-projection of ICR1 localization as filamentous structures (Right). Scale bar = 25 μm, others at same scale.
(B) Oryzalin treatment on *ICR1pro::*GFP-ICR1. Microtubule dissociation of GFP-ICR1 were observed after treated with 1μM oryzalin for 30-min. 0.1% DMSO for same 30-min serves as control. Note MT-dissociated GFP-ICR1 diffused in the cytoplasm after short-time oryzalin treatment.
(C) Representative Z-projected confocal image of *ICR1pro::*GFP-ICR1_d29.
(D-F) Tobacco leaf epidermis expressing **(D)** ICR1-YFP. **(F)** MT-binding protein mCherry-MAP65-3. 20 μM Oryzalin were infiltrated and incubated for 60-min. **(E)** Dissociation of ICR1 from MT to cytoplasm were observed after oryzalin-induced MT depolymerization.
(G) Mock treatment of transiently co-expressed ICR1-YFP (green) with mCherry-MAP65-3 (red) in the tobacco leaf epidermal cells.

ICR1 physically interacts with YDA.

The enhanced degradation of BASL-YDA in ICR1 overexpression plants prompted us to test whether ICR1 directly interacts with YDA and/or BASL. Bimolecular Fluorescent Complementation (BiFC) assays in tobacco epidermal cells were first employed. While no signals were found in negative controls (**Fig. 4.10A**), when ICR1 (ICR1-nYFP) was paired with YDA (YDA^{KI}-cYFP), the YFP signal was recovered at the PM and along the MT structures (**Fig. 4.10B**), suggesting that the interaction of ICR1-YDA occurs at both places. No discernable YFP signals were detected for the ICR1-BASL pair (data not shown). Dr. Xiaoyu Guo also produced the recombinant proteins of His-ICR1 and MBP-YDA for *in vitro* pull-down assays. An anti-MBP antibody was used to detect His-ICR1 partners after being pulled down by the Ni-NTA affinity resin. The results showed that, again, a direct protein-protein interaction was detected between ICR1 and YDA (**Fig. 4.10C**), but not between ICR1 and BASL (**Fig. 4.10C**). Pair-wise yeast two-hybrid assays confirmed the physical association of ICR1-YDA and further suggested that the interaction occurs at the C-terminal kinase region

(YDA-C), but not at the YDA regulatory N-terminus (Lukowitz et al., 2004) (**Fig. 4.10D**).

Intrigued by the MT-association of interacting ICR1-YDA, we examined the individual and co-expression patterns of ICR1-CFP and YDA^{KI}-YFP. YDA^{KI}-YFP in tobacco cells showed typical puncta along the PM and in the cytoplasm (**Fig. 4.10E**) and ICR1-CFP was localized to the nucleus and along the MTs (**Fig. 4.10E**). When co-expressed, interestingly, the seemingly randomly distributed YDA^{KI}-YFP foci became obviously aligned to the ICR1-decorating MTs (**Fig. 4.10F**, time-lapse movies in **Fig. 4.10G**), suggesting that in the presence of ICR1 protein, YDA may translocate to the MTs through interacting with ICR1.

We further examined the consequence of disrupting microtubules to YDA localization. Intriguingly, 1 μM of Oryzalin treatment of 3-dpg seedlings for 4-hr resulted in an obvious vacuole-like accumulation of YDA^{KI}-YFP (**Fig. 4.10H**), phenocopying its localization in *icr1-t* mutants (**Fig. 4.8A**). Higher concentration of Oryzalin (20 μM for 1-hr) enhanced the abnormal accumulation of YDA^{KI}-YFP in the endomembrane system (**Fig. 4.10H**). This suggests that the membrane-associated YDA^{KI}-YFP trafficking may depend on the MTs. Taken together, the interaction between YDA and ICR1 occurs at the MT and the vacuolar degradation of YDA may require ICR1-mediated MT activity.

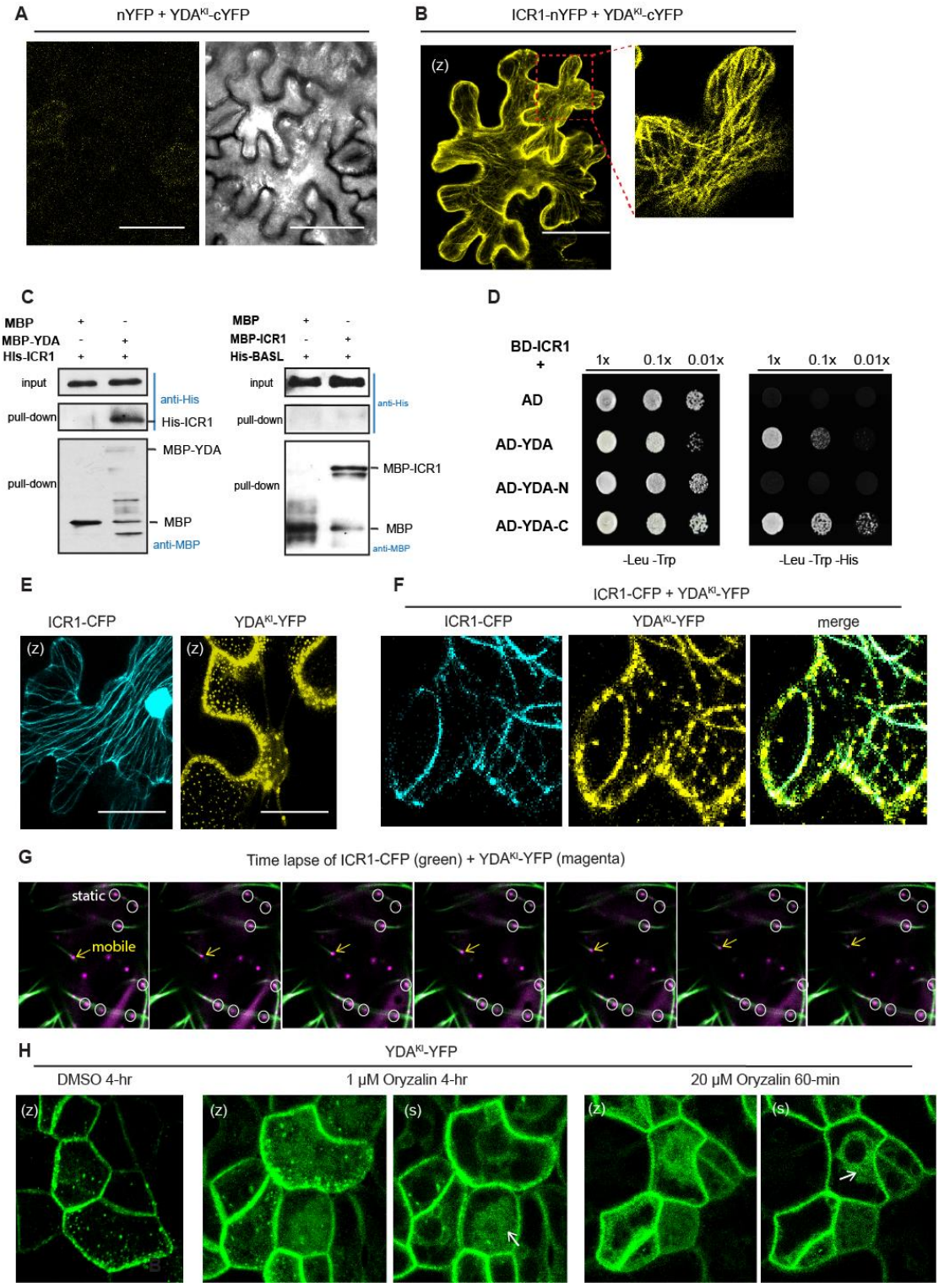

Fig. 4.10. ICR1 physically interacts with YDA.

(A-B) Bimolecular fluorescence complementation (BiFC) assays testing ICR1 (ICR1-nYFP) with YDA^{KI} (to avoid YDA expression-induced cell death) in the tobacco leaf epidermis. **(A)** Negative control, YDA^{KI}-cYFP with nYFP did not emit any YFP signal. **(B)** Recovered

split YFP signal suggests the positive interaction. Enlarged region on right demonstrates a closer view of protein interaction on MT. Scale bar = 25 μm.

(C) *In vitro* pull-down assays using recombinant proteins. Left panel: Direct interactions detected between MBP-tagged YDA and His-tagged ICR1. Right panel: No interactions detected between MBP-tagged ICR1 and His-tagged BASL. Immunoblots were visualized with Anti-MBP antibody. Data produced by Dr. Xiaoyu Guo.

(D) Pair-wise Y2H analyses demonstrate the interactions between ICR1 and YDA. ICR1 interacts with YDA, particularly with YDA catalytic kinase domain on C terminus, not the N-terminus regulatory domain. Left panel, yeast growth control (-Leu-Trp). Right panel, interaction test (-Leu-Trp-His) with 1X, 0.1X, 0.01X dilution.

(E) Representative z-projected confocal image of transient protein expression in tobacco epidermal cells. (Left) ICR1-CFP (cyan). Note the MT association. (Right) YFP-YDA^{KI} (yellow). Note the punctate structures in the cytoplasm. Image captured 2–3 days after infiltration. Scale bar = 10 μm.

(F) Co-expression of ICR1-CFP (cyan) and YDA^{KI}-YFP (yellow). Note the YDA^{KI} distribution change to ICR1-labeled MT.

(G) Time-lapse movie of co-expression of ICR1-CFP (green) and YDA^{KI} -YFP (magenta), scanned every 20 s over a period of 120 s. YDA^{KI} reside on ICR1-labeled MT when co-expressed. Arrows indicate mobile YDA^{KI} puncta which trafficked along MT, meanwhile circles label static YDA^{KI} puncta.

(H) Oryzalin treatment on *SPCHpro::* YDA^{KI}-YFP in 3-dpg *Arabidopsis* leaf epidermis. Compared with mock (Left panel, 0.1% DMSO for 4 h), obvious vacuole-like accumulations of YDA^{KI}-YFP were observed after long-time Oryzalin treatment at low concentration (Middle panel, 1μM Oryzalin for 4-hr) or short-time treatment at a higher concentration of (Right panel, 20 μM for 60 min). Arrows indicate vacuole accumulation of YDA^{KI}. Z, Z-projected image stacks. S, the single central layer of the cells.

FAB1 localize to ICR1-decorating MTs

ICR1 belongs to the ROP Interactive Partners (RIP) family, the members of which seem to function as scaffold proteins. By binding to Kinesin-13A, MIDD1/ICR3 could induce local disassembly of cortical MTs to initial secondary cell wall patterning in xylem cells (Mucha et al., 2010). ICR1/RIP1 itself was found to bind to the SEC3A exocyst subunit for polarized exocytosis in pavement cells and pollen tubes (Bloch et al., 2016; Lavy et al., 2007). For the vacuolar degradation process, we considered a few candidates in the endomembrane system that may function with ICR1 to regulate BASL and YDA. The SNX1 retromer component was found to act in the degradation PIN2 during

gravitropism response (Jaillais et al., 2006). The BLOC complexes promote endosome maturation and lysosome biogenesis in mammals (Dell'Angelica, 2004), and BLOS1, a putative BLOC-1 subunit in *Arabidopsis*, was suggested to interact with SNX1 to promote PIN1/2 vacuolar degradative transport (Cui et al., 2010). In addition, the FAB1/PIKfyve kinases produce PI(3,5)P2 from PI3P to mediate the late endosome maturation in yeast, animals (Jean and Kiger, 2012) and plants (Hirano et al., 2015b). To test the functional relevance of BLOS1, SNX1, and FAB1 in the regulation of BASL and YDA, we overexpressed these three proteins in the stomatal lineage cells. Driven by the *BASL* promoter, neither *BLOS1* nor *SNX1* induced abnormal stomatal division and patterning (data not shown), but both members of the FAB1 family (FAB1A and FAB1B) triggered overproduction and clustered stomatal lineage cells (FAB1B shown in **Fig. 4.11A**), recapitulating that of *ICR1* overexpression and *basl or yda* loss-of-function.

Similar to what has been reported (Hirano et al., 2015b), mCherry-FAB1B was localized to the PM and endosomal-like compartments that seemed to align into tubular clusters at the stomatal cell cortex (**Fig. 4.11A**). Such tubular alignment did not appear when individual FAB1B was obvious in tobacco epidermal cells (**Fig. 4.11B**); however when ICR1 was introduced into these cells, a significant amount of FAB1B particles translocated to the ICR1-MTs (**Fig. 4.11C**), suggesting that ICR1 has a potential to recruit FAB1B onto the MTs. We expanded the ICR1 co-expression assay to a few other late endosomal markers (FAB1A, RabF2b/ARA7 (Lee et al., 2004), RabG3c (Bozkurt et al., 2015), and SNX1), interestingly all of which showed moderate levels of co-localization on the ICR1-decorating filaments (**Fig. 4.11D, 4.11E, 4.11G** and **4.11F**).

It is therefore possible that ICR1 may provide a general scaffolding function for late endosomes to attach to the MT.

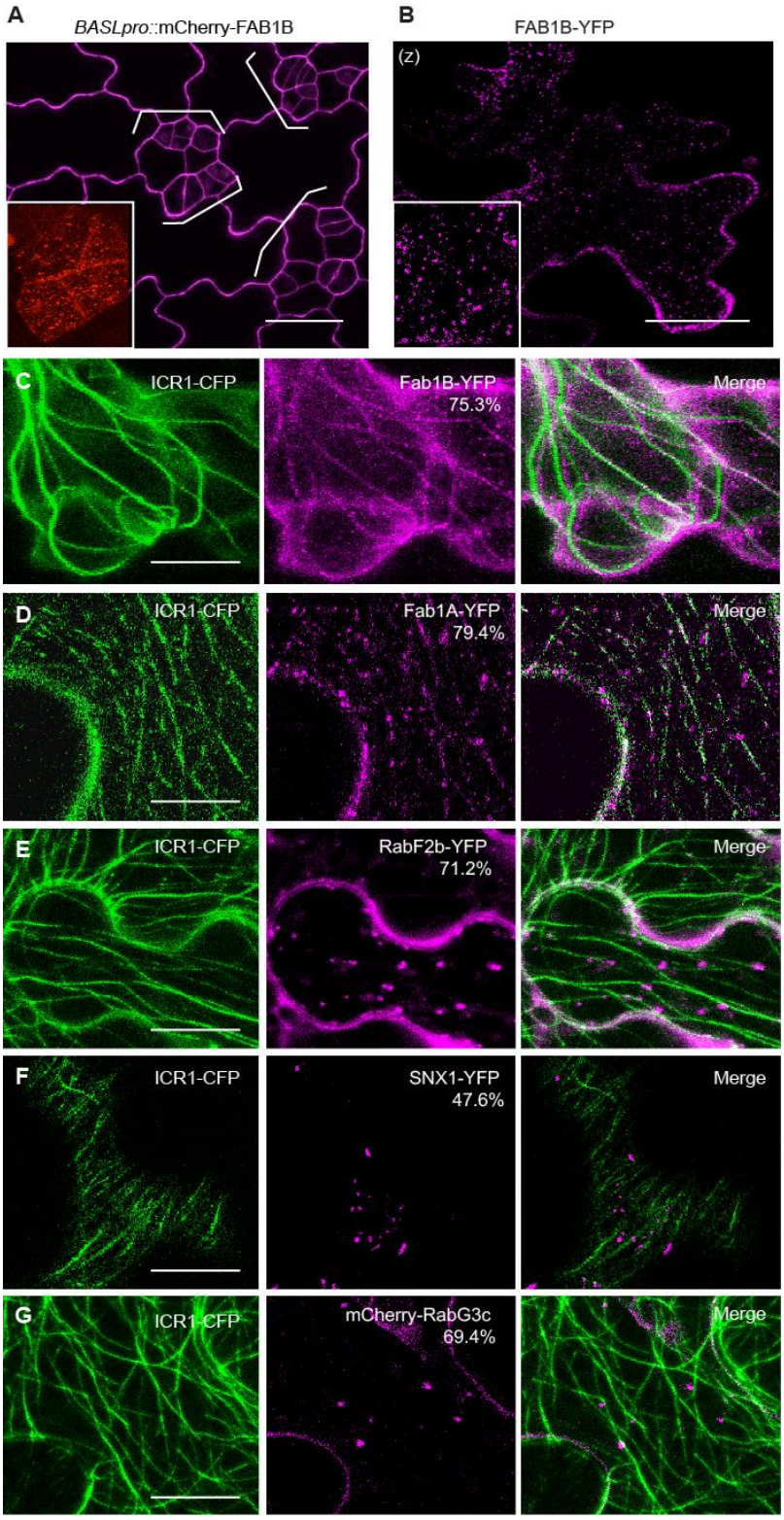

Fig. 4.11 FAB1 localized to ICR1-decorating MTs. **(A)** Confocal images of *BASLpro::*mCherry-FAB1B in 3-dpg adaxial cotyledons. Cell walls were stained with PI (Magenta). Inserts showed FAB1B localization (Red) as endosome-like compartments in stomatal lineage cells. White braces indicate the typical clustered stomata resembling *basl* null mutants. Scale bar = 25 μm. **(B)** Z-projected confocal image of transient FAB1B-YFP(Magenta) in tobacco epidermal cells. (Left) ICR1-CFP (cyan). Scale bar = 25 μm. **(C)** Co-expression of ICR1-CFP (green) and FAB1B-YFP (Magenta). Note the FAB1B-YFP translocation to ICR1-labeled MT. Colocalization percentage is shown as indicated. Scale bar = 10 μm. Others at same scales. **(D-G)** Co-expression of ICR1-CFP (green) and a YFP or mCherry tagged late endosome/vacuole markers (magenta) in tobacco epidermal cells. **(D)** FAB1A-YFP. **(E)** RabF2b-YFP. **(F)** SNX1-YFP. **(G)** mCherry-RabG3c. Percentages in merged images represent colocalization rates of two fluorescent proteins. 80-100 cytoplasmic dots were calculated from at least five images of five cells.

FAB1 promotes BASL-YDA degradation.

To further understand the stomatal phenotypes created by FAB1B overexpression, we assayed how the localization pattern of YDA-YFP and GFP-BASL could be changed by elevated FAB1B expression in the stomatal lineage. In a segregating population, we observed a very consistent expression pattern: when mCherry-FAB1B is strongly expressed, YDA-YFP and GFP-BASL could barely be detected and these plants show clustered stomatal lineage cells (**Fig. 4.12A** and **Fig. 4.12B**, respectively), whereas in the plants highly expressing YDA-YFP or GFP-BASL only, no mCherry-FAB1 could be observed, nor the stomatal phenotype (**Fig. 4.12A** and **Fig. 4.12B**, respectively). The results suggested that, similar to ICR1, elevated expression of FAB1B results in the degradation of YDA and BASL protein, hinting that FAB1-mediated endosome maturation might be one of the processes regulated by ICR1 and the related MT activities.

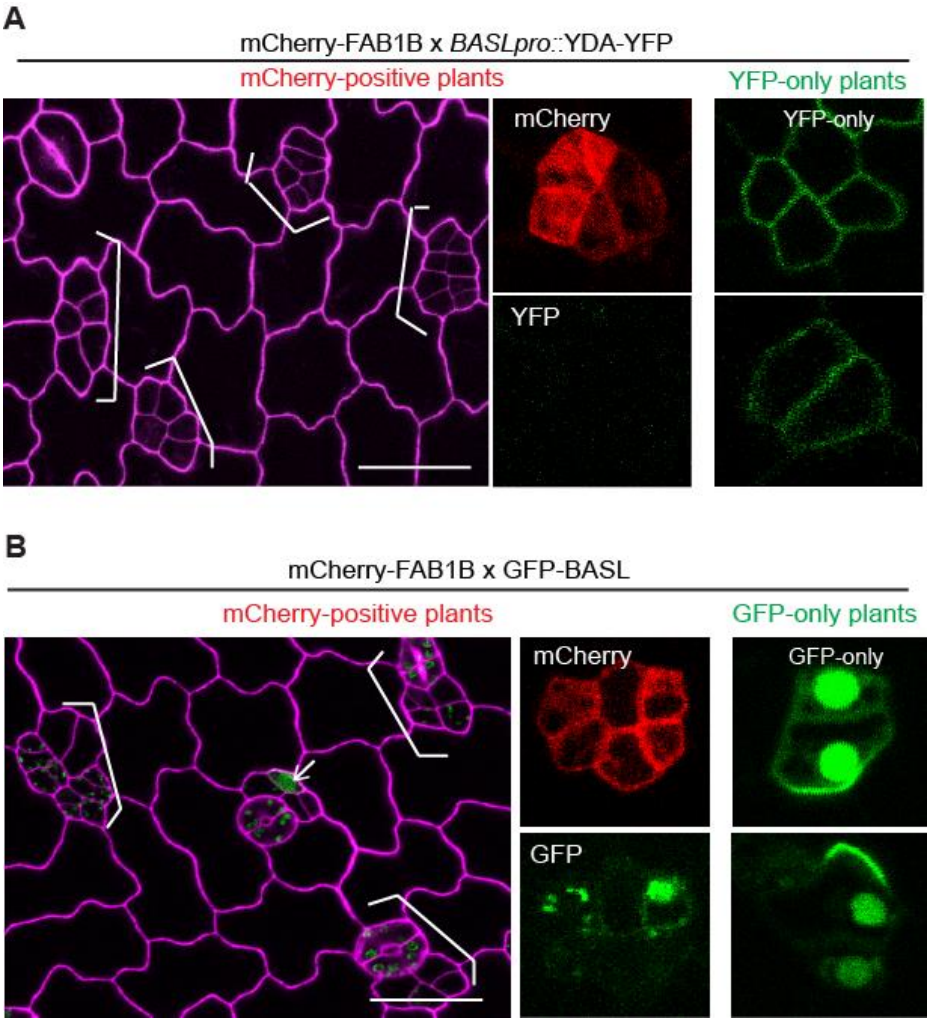

Fig. 4.12. ICR1 physically interacts with YDA.

(A) Left: Reduced *BASLpro::*YDA-YFP (green) level in FAB1B-overexpressing lines. White braces indicate typical clustered stomata induced by FAB1B overexpression. Magenta, propidium iodide (PI)-stained cell walls. Insets show a closer view of co-expresssed mCherry-FAB1B and undetected YDA-YFP. Right: Segregating lines only bearing with *BASLpro::*YDA-YFP. Scale bar = 25 μm.

(B) Left: Reduced *BASLpro::*GFP-BASL (green) level in FAB1B-overexpressing lines. White braces indicate typical clustered stomata induced by FAB1B overexpression. Insets show a closer view of co-expressed normal mCherry-FAB1B and weak GFP-BASL expression. Arrows indicate remaining weak BASL level. Right: Segregating lines only bearing with *BASLpro::*GFP-BASL. Scale bar = 25 μm.

DISCUSSION

In summary, our study identifies the ICR1 Rho scaffold protein-centered cellular machinery that downregulates the polarity partners, BASL and YDA in the stomatal lineage cells. The PM-associated BASL and YDA are internalized into the endosome and targeted for vacuolar degradation. This process is promoted by ICR1, its binding activity to the MTs, as well as the function of the FAB1 kinases that govern endosome maturation (**Fig. 4.13**).

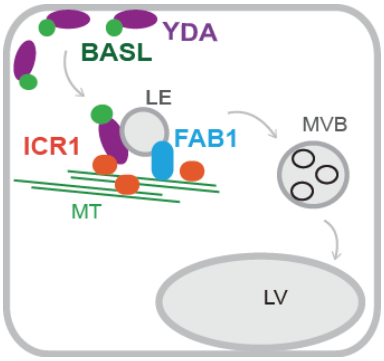

Fig. 4.13. Hypothetical model of downregulation mechanisms of ICR1 on BASL-YDA polarity complex.

After BASL-YDA polarity established at the cell cortex through the positive feedback loop, microtubule-associated ICR1 interact with internalized YDA for recruitment of BASL-YDA vesicles on microtubules. FAB1B kinase further promotes the late endosome maturation and directional target for degradation in the vacuole. LE, Late Endosome. MVB, Multi-Vesicular Body. LV, Lytic Vacuole.

Downregulation of the positive feedback loop at the plasma membrane

Positive feedback loops are widely used by eukaryotic cell systems in the establishment of cell polarity (McCaffrey and Macara, 2012). Yet essentially, the induction of positive feedback activity needs to be precisely balanced by negative regulation, to maintain stringent control of signal intensity and duration for long-term cell fate decisions. Despite of the great importance, the attenuation of positive signals remains poorly understood. Here we demonstrated a novel mechanism that attenuated components of the BASL-YDA positive feedback loop in plant cells through protein internalization and degradation in endomembrane system. To some extent, this negative regulatory

mechanism resembles that of the tip concentrated Ste5-Ste11 feedback loops (the MAPKKK Ste11 with the MAPK scaffolding protein Ste5) in yeast (Sette et al., 2000; van Drogen et al., 2000), where accelerated turnover and ubiquitin-dependent endocytosis of Ste11 were observed to terminate and disassemble the self-amplifying polarity signaling (Esch and Errede, 2002).

Possible functions of ICR1 in MT organization

We showed that ICR1 binds to MT, where it might provide a scaffolding function for BASL-YDA-associated late endosomes to dock on. However, whether and how ICR1 may regulate MT organization is unknown. The ICR members were demonstrated to distribute differently along MT filaments and seem to function distinctly in MT organization. MIDD1/ICR3 mainly accumulates at the MT plus ends during shrinkage to promote local MT disassembly in xylem cell wall pattern (Mucha et al., 2010; Oda et al., 2010). On the other hand, based on *in vitro* assays, ICR2 directly binds to the MTs to promote MT bundling (data not shown, from our collaborator), but how ICR2 contributes to cell function has not been studied *in vivo*. Future analyses on the ICR1 regulation of MT stability and/or organization, both *in vitro* and *in vivo*, will be necessary to further understand the biological roles of ICR1. In addition, our study identified the S/R rich microtubule-binding domain in ICR1. This should shed lights on the possibility of other ICR members' direct interaction with the MTs.

Possible functions of MT in endomembrane trafficking

Membrane trafficking, organelle movement and other intracellular motility in plant cells have been predominantly linked to the actin filaments network (Wang and Hussey, 2015). The potential roles of the microtubule cytoskeleton in endomembrane organization and regulation of cell signaling were barely understood (Brandizzi and Wasteneys, 2013). The MT-binding protein CLASP tethers the SNX1-associated retromer to cortical MTs and promotes the PM recycling of polarly localized auxin efflux carrier PIN2 (Ambrose et al., 2013; Cui et al., 2010). However, in mammalian cells, microtubule and associated motor proteins, e.g. dyneins and kinesins, play key roles in Golgi integrity and ER dynamics (Friedman et al., 2010; Ward and Brandizzi, 2004). Our discovery of the microtubule-dependent function of ICR1 in vacuolar targeting suggested a novel role of MTs in endomembrane trafficking in the plant system. We also showed evidence that late endosomes associating with the MTs might be a common phenomenon in plant cells, by which the versatile MT responses to external cues can be integrated to diverse cellular responses that require vesicle trafficking.

FAB1/PIKfyve-involved vacuolar degradation

The phosphatidylinositol 3-phosphate 5-kinase FAB1 and/or its products PI(3,5)P2 were hypothesized to recruit various late endosomal effector proteins, e.g. the Rab5 GTPases ARA7, to the endosomal membranes to promote the transition to late endosomes and to facilitate vacuolar sorting (Hirano et al., 2011a; Hirano et al., 2015a). Interestingly, the association of FAB1 with endosomes also depends on proper function

and organization of the MTs (Hirano et al., 2015a). Here, we observed the ICR1-induced MT-association of FAB1 endosomes in tobacco cells, suggesting that ICR1 might promote the tethering of FAB1 onto the MTs and the subsequent vacuolar sorting. Indeed, similar to ICR1, elevated expression of FAB1B induced degradation of YDA and BASL (**Fig. 4.12A, 4.12B**), likely in a MT-dependent manner.

Taken together, we conclude that ICR1 promotes the protein turnover of BASL-YDA polarity complex in a tissue-specific manner. The working model **(Fig. 4.13)** is that membrane associated BASL-YDA are internalized and, facilitated by ICR1, delivered to late endosomes for vacuolar degradation. In this process, the MT-associated FAB1, likely through promoting late endosome maturation, positively affects vacuolar degradation of BASL-YDA. Whether FAB1 is functional dependent or independent of ICR1 needs further exploration. This mechanism provided new insights into how the self-amplifying BASL-YDA signaling system is maintained and attenuated at the plasma membrane.

METHODS

Plant Materials and Growth Conditions

Arabidopsis thaliana plants were grown on ½ MS media in 22°C with 16hr light/8hr dark cycles. Young expanding cotyledons were imaged at 3–4 days. Columbia-0 ecotype plants were used as wildtype. Previously published lines used in this study are *icr1* (Lavy et al., 2007), *basl-2*, *BASLpro::*GFP-BASL (Dong et al., 2009), *er105* (Torii et al., 1996), *tmm-1* (Nadeau and Sack, 2002b), *yda* (Salk_105078 from the *Arabidopsis* Biological Resource Center; ABRC), *SPCHpro::* YDA^{KI}-YFP, *YDApro::*YDA-YFP (Zhang et al., 2015), *PIN1pro::*GFP-PIN1 (Heisler et al., 2005), *PIN2pro::*GFP-PIN2 (Wisniewska et al., 2006), *PIN3pro::*GFP-PIN3 (Laskowski et al., 2008), WAVE lines (Geldner et al., 2009).

Plasmid construction

The coding sequences of *ICR1, ICR2, ICR3, ICR4, ICR5* were amplified by PCR using primers listed in table below, and cloned into pENTR/D/TOPO entry vectors by following the manufacturer's protocol (Invitrogen). Sequences of *YDA, YDA^{KI}, BASL, FAB1A, FAB1B* and *BLOS1* were described previously (Cui et al., 2010; Dong et al., 2009; Hirano et al., 2011b; Lampard et al., 2009; Wang et al., 2007). The promoter sequence of *ICR1* was amplified by the listed primers and the KpnI/PmeI sites were used to replace the *35S* promoter in the binary vector pMDC43 (Hirano et al., 2011b) for the purpose of GFP-tagged expression of ICR1 in *Arabidopsis* plants. The endogenous promoters of *ICR2, ICR3, ICR4, ICR5* were amplified with listed primers

and subcloned into pDONR-P4-P1R, which is subsequently recombined with their respective coding sequences fused with GFP in R4pGWB vectors (Nakagawa et al., 2008) using LR Clonase II (Invitrogen). pENTR/D vectors with coding sequences of *FAB1B* (courtesy of Dr. Masa H Sato), *BLOS1* were recombined with *BASL* promoter and integrated into the R4pGWB vectors (Nakagawa et al., 2008) to generate transgenic *Arabidopsis* plants.

To generate BiFC constructs in tobacco, the pENTR/D vectors containing coding sequences of ICR1, YDA, YDA^{KI} were recombined into pXNGW and/or pXCGW vectors (Yuan et al., 2013). For transient protein expression constructs, pENTR/D vectors with FAB1A, FAB1B (courtesy of Dr. Masa H Sato), ICR1, ICR2, ICR3, ICR4, ICR5, YDA, YDA^{KI}, were recombined into the pH35YG, pH35GY or pH35GC (Kubo et al., 2005). The constructed binary vectors were electro-transformed into *Agrobacterium tumefaciens* strains GV3101 for tobacco leaf infiltration.

To generate CRISPR/Cas9 targeted mutagenesis, one sgRNA oligo was designed for each gene of the *ICR* family (primer sequences were listed in the table). The phosphorylated and annealed oligos were ligated to pAtU6-sgRNA-pAtUBQ-Cas9 vector (Mao et al., 2013) by BbsI digestion. PCR-based cloning of the CRISPR target cassette was then performed and two target cassettes were combined and ligated into the destination vector pCAMBIA1300 (courtesy of Jian-Kang Zhu) by HindIII/EcoRI for stable transformation.

To generate cell-type specific induction of ICR1, inducible system driven by stomata specific promoter was built through *BASLpro* insertion into p1R4:ML-XVE entry vector

(Siligato et al., 2016). Unique AscI/KpnI sites were utilized to clone *BASL* promoter (by Xueyi Xue). Entry clones of *BASLpro::* XVE (L4-R1), ICR1 in pENTR/D vectors (L1-L2) and terminator nosT (R2-L3) are then recombined with a destination vector containing *att*R4 and *att*R3 sites in a single MultiSite Gateway reaction (Invitrogen).

To express recombinant proteins in *E. coli*, the coding regions of *ICR1*, *YDA* and *BASL* were cloned into pET28a or pMAL-c2x and introduced into E. coli BL21 (DE3) cells.

Primers used in this study.

Purpose	**Primer name**	**Sequence**
ICR1 CDS	ICR1_F	CACCATGCCAAGACCAAGAGTTTC
	ICR1_R	CTTTTGCCCTTTCTTCCTCCAC
ICR2 CDS	ICR2_F	CACCATGCAGACTCCAAAACCTAG
	ICR2_R	TTTCTGACTTTTCTTCAGTAACACACC
ICR3 CDS	ICR3_F	CACCATGCAGACTCCAAAATCAAGG
	ICR3_R	CTTATGGTTTTTCTTGAGTAACACACC
ICR4 CDS	ICR4_F	CACCATGCCAAAACCAAGTATTAGAG
	ICR4_R	TATTATATCACTTCATTTCTGCCC
ICR5 CDS	ICR5_F	CACCATGCAGACCCAAAAGGC
	ICR5_R	TTTCTGAGGCTTCTTCCAC
FAB1B CDS	FAB1B_F	CACCATGGGTACAAGAGATAGTAA
	FAB1B_R	CTCTGCTTGTGTACCGGCTTGAG
BLOS1 CDS	BLOS1-F	CACCATGAATACGCCGATGTCACT
	BLOS1-R	TTATTGTTGATCTTCATGAATGTTTCG
ICR1 promoter	ICR1pro_F	CAAGAAAGGACGACAAAAATG
	ICR1pro_R	TTTGATTTCGTGTTGAGG
	ICR1pro_F_PmeI	AGCTTTGTTTAAACCAAGAAAGGACGACA AAAATG
	ICR1pro_R_KpnI	CGGGGTACCTTTGATTTCGTGTTGAGG
ICR2 promoter	ICR2pro_F	GATTATAATATGCTTGCAAGTCG
	ICR2pro_R	TGCTTGAGATTAGAGTTCTAAAAC
ICR3 promoter	ICR3pro_F	TTCAGTTAACCTTTTTTAATCC
	ICR3pro_R	TTTTGGAGTTTAAAAACC

ICR4 promoter	ICR4pro_F	CAGCTTCTTTAATTCTTTGTGG
	ICR4pro_R	TCTGATTTATGCAAAGTTGC
ICR5 promoter	ICR5pro_F	GGCGATTTTGTTTTTGTTG
	ICR5pro_R	ACTGTAATATTACTTCTCCAAAACAC
Icr1 (SAIL_265_G05) genotyping	SAIL_265_G05-LP	ACAAAAGAATGAAACATGCGG
	SAIL_265_G05-RP	AGTGATCAGACGGTTGGAATG
Icr2 (GABI_567_F02) genotyping	GABI_567_F02-LP	CATCAGTGGAAGAGCTCAAGG
	GABI_567_F02-RP	CACGATAGGCAACAAAAACATG
Icr3 (SAIL_267_H11) genotyping	SAIL_267_H11-LP	CAACGTGCATTTACCTGAACC
	SAIL_267_H11-RP	TGTGAAAACGTTCCCTGTTTC
Icr4 (SAIL_780_G08) genotyping	SAIL_780_G08-LP	AAATATGTCCTACACGGTGCG
	SAIL_780_G08-RP	CTGAAGGTCCAAACAGAGCAG
Icr5 (SALK_038450) genotyping	SALK_038450-LP	CCTGTCTCTGAGGTATGAGCC
	SALK_038450-RP	GAACGCGTCTTGTACATCTGTC
SgRNA1 oligo targeted *ICR1*	ICR1_oligo1-F	GATTGGACCTAACAGTGATCCGCT
	ICR1_oligo1-R	AAACAGCGGATCACTGTTAGGTCC
SgRNA2 oligo targeted *ICR1*	ICR1_oligo2-F	GATTGACCGTAAATCTCCTCGAAG
	ICR1_oligo2-R	AAACCTTCGAGGAGATTTACGGTC
SgRNA3 oligo targeted *ICR1*	ICR1_oligo3-F	GATTGCTGGAAGCTCGAAGGTTTA
SgRNA3 oligo targeted *ICR1*	ICR1_oligo3-R	AAACTAAACCTTCGAGCTTCCAGC
SgRNA oligo targeted *ICR2*	ICR2_oligo-F	GATTGTCAACATGTCGCCTTATAT
	ICR2_oligo-R	AAACATATAAGGCGACATGTTGAC
SgRNA oligo targeted *ICR3*	ICR3_oligo-F	GATTGTGTGATAGGCCAGGATCAT
	ICR3_oligo-R	ACCCATGATCCTGGCCTATCACAC
SgRNA oligo targeted *ICR4*	ICR4_oligo-F	GATTGTATGAGGCCCACCACTCCT
	ICR4_oligo-R	AAACAGGAGTGGTGGGCCTCATAC
SgRNA oligo targeted ICR5	ICR5_oligo-F	GATTGTACATCTGTCTCGCTCTTG

	ICR5_oligo-R	AAACCAAGAGCGAGACAGATGTAC
His-ICR1	ICR1-F-ECoRI	CGGAATTCATGCCAAGAC CAAGAGTTTC
	ICR1-R-SalI	ACGCGTCGACCTTTTGCCCTTTCTTCCTCC
His-BASL	BASL_F_EcoRI	CGGAATTCATGGCTTCACAGTGGACAATA C
	BASL_R_XhoI	CCCTCGAGGAATCTACAACATTGGAACC
MBP-YDA	YDA_F_SacI	CGAGCTCATGCCTTGGTGGAGTAAATC
	YDA_R_HindIII	CCAAGCTTGGGTCCTCTGTTTGTTGATC
MBP-ICR1	ICR1-F-ECoRI	CGGAATTCATGCCAAGACCAAGAGTTTC
	ICR1-R-SalI	GCGTCGACTCACTTTTGCCCTTTCTTC
Real-time PCR for ICR1	qICR1-F	GATGTTTGGTGAGTTGTGGAGG
	qICR1-R	GAATGACACTCCACACAATCTG
Real-time PCR for YDA	qYDA-F	CTCGCATTCACCACACATTAG
	qYDA-R	GTAGTTTGTCTTTGGTGATGG
Real-time PCR for BASL	qBASL-F	ATGGCTTCACAGTGGACAATAC
	qBASL-R	CTCTCTGATCTCTTCTTCTTAG
Real-time PCR for ACTIN2	qACTIN2-F	TCTTCCGCTCTTTCTTTCCAAGC
	qACTIN2-R	ACCATTGTCACACACGATTGGTTG

T7 endonuclease I-based identification of CRISPR targeted mutagenesis

Genomic DNA was extracted from T1 transgenic plants by the CTAB methods (Rowland and Nguyen, 1993). The genomic regions surrounding the CRISPR target site for each gene were amplified by PCR. The PCR products were hybridized and annealed according to the manufacturer's instructions (NEB). Final products were digested with T7 endonuclease I (NEB) for mutation identification.

Quantification of stomatal phenotypes in *Arabidopsis*.

Five-dpg (day post germination) cotyledons were stained with PI (Invitrogen) and imaged by the EC Plan-Neofluar (20X/0.5) lenses on a Carl Zeiss AXIO SCOPE A1

fluorescence microscope equipped with a ProgRes MF CCD camera (Jenoptik). Images were taken from similar central .1mm^2 areas in the >20 adaxial cotyledons. In total, 1200 to 2000 cells were collected and categorized. As described in (Dong et al., 2009), the epidermal cells were scored for 4 groups: pavement cells, guard cells, clustered guard cells and small dividing cells. The stomata index represents the ratio of stomata number relative to the total cell number. Student *t* test was performed to show statistical significance.

Real-time PCR analysis

Total RNA was extracted from 4-day-old seedlings and reverse transcribed to cDNAs by SuperScript III First-Strand Synthesis System (Invitrogen) with oligo dT primers. *ICR1*, *BASL*, *YDA* and control *ACTIN2* were amplified from 10 ng cDNAs for 40 cycles using SYBR Green Master Mix (Applied Biosystems). Transcript expression levels were normalized to Actin2. Three biological replicates were performed, with three technical replicates per biological replicate.

Drug Treatment

Plants were grown on ½ MS media as described above. For treatment, seedlings were gently removed from plates and placed in tubes containing 1 μM or 20 μM oryzalin (made fresh from 1 mM DMSO stock) or 0.1% DMSO for the times indicated in the figure legends. Pilot experiments were performed using MT-binding protein MAP65-3-mRFP to determine the time required for effective treatment. Typically, after 20 μM

oryzalin for 20 min, small MT stubs remained. 20 μM oryzalin for 60 min completely remove these stubs.

Yeast Two-Hybrid Analysis

Matchmaker Gold Yeast Two-Hybrid System (Clontech) was used to construct ICR1 into pGBKT7 BD vector and BASL/YDA variants into pGADT7 AD vector. Bait and prey plasmids were co-transformed into yeast strain AH109, and no self-activation was detected for BD-ICR1 with the AD-empty. 1x, 0.1x, 0.01x dilution were used to determine the interaction strength.

Recombinant protein production and pull-down assay

Constructs were introduced into BL21 (DE3) competent cells. The recombinant His-tagged ICR1 and BASL were purified using Ni-NTA agarose (Qiagen) according to the manufacturer's protocol. The maltose-binding protein (MBP)-tagged ICR1 and YDA were purified using Amylose Resin (New England Biolabs) according to the manufacturer's protocol. For pull-down assays, 5 μg of purified HIS-tagged ICR1 and 40 μl of Amylose Resin, which pre-absorbed 2 μg of MBP-tagged YDA proteins, were incubated in 100 μl Binding Buffer (50 mM Tris-Cl, pH 7.5, 10 mM MgCl2, 150 mM NaCl and 1mM DTT) for 1 h at 4C°. After washing 5 times with 500 μl of Binding Buffer, 30 μl of 2X Sample Buffer was added and mixed thoroughly for 5 min heat at 95-100°C. Centrifuge for 5 min at 12,000g. The bound proteins on the Amylose Resin were separated by SDS-PAGE and visualized immunoblot with anti-HIS (Cell Signaling Tech) and MBP antibody (New England Biolabs).

Bioinformatics

An amino acid sequence alignment of *Arabidopsis ICR* genes was generated using the ClustalW2 algorithm (EMBL-EBI online tools). Maximum likelihood method was used to perform phylogenetic analysis.

All other methods were as described in previous chapters.

CONCLUSION AND PERSPECTIVES

Polarization occurs in essentially all cellular organisms and is required for fundamental processes in morphogenesis, cell division as well as cell differentiation (Freisinger et al., 2013; Yang and Lavagi, 2012). In higher plants, the key roles of cell polarization in stem cell ACD have recently emerged and are manifested by asymmetrically distributed proteins and signaling pathways. This Ph.D. thesis advanced our understanding on a few important aspects of these processes: 1) polarity partner/s of BASL and its/their contribution; 2) cellular trafficking for polarity maintenance; and 3) new regulators in the endocytic trafficking routes.

In Chapter 2, my work helped to establish that BASL physically interacts with the MPKKK YDA and discovered that YDA is polarized subcellularly to regulate stomatal ACD. Combined with the work from Dr. Ying Zhang, our data connected the regulation of BASL polarity and function to a conserved Mitogen-activated protein kinase (MAPK) pathway. As a new polarity component, YDA forms a positive-feedback loop with BASL and constitutes a polarity module at the cortex. Furthermore, the polarization of the BASL-MAPK signaling feedback module represents a new mechanism connecting cell polarity to fate differentiation during asymmetric stem cell division in plants. However, more unknown questions have been generated for future investigation. Since both BASL and YDA do not possess transmembrane domains, their PM association is expected to occur through interaction with other PM-embedded partners. The finding that YDA lost its polarization but still maintained PM localization without *BASL*, suggested a potential BASL-independent mechanism for YDA association on PM. In

addition, among the six phosphorylation sites of BASL, one site was not detected phosphorylated by MPK3/6 (Zhang et al., 2015), raising the possibility of regulation from other kinases beyond MAPKs. Identifications of new interactors of BASL and YDA are needed to understand the molecular mechanism of polarization.

In chapter 3, I investigated the potential involvement of BASL-YDA polarity complex in the endomembrane system. Cytological studies on BASL-YDA endocytic trafficking patterns implicated their dynamic association with endomembrane organelles. By using specific trafficking inhibitors, I specified that internalized BASL and YDA are transited to late endosome/MVB, and eventually targeted towards vacuole for degradation. This data for the first time demonstrated that PM-associated BASL-YDA polarity complex is modulated by the endomembrane system. However, differences in their responses or sensitivities to trafficking inhibitors indicated that BASL and YDA may also participate in unique although overlapping endocytic routes. BASL and YDA need to be endocytosed from PM, but the molecular mechanisms regulating this process remain unknown. Furthermore, BASL barely shows punctate endosome localization, possibly because of its high dynamics and masking from strong nuclear sub-portion. Instead of directly examining BASL transit patterns, genetic analysis and application of specific trafficking inhibitors would be helpful for further investigations.

In Chapter 4, I identified a protein of BASL-YDA polarity complex and provided insights for how this self-amplifying BASL-YDA signaling loop can be restricted and maintained at the subcellular level. I showed that degradation of BASL-YDA is facilitated by the ROP effector ICR1 protein. As a MT-associated protein, ICR1 exerts a

negative regulation on the cortical polarity complex, possibly through the cooperation of the late endosome maturation factor FAB1/PIKfyve. Furthermore, the microtubule association of ICR1 is required for its function, suggesting a novel connection of MTs with endomembrane trafficking in the plant system. However, beyond the scope of the work presented here, further elucidation is anticipated on how ICR1 regulates the MT cytoskeleton. Besides serving as a scaffold to recruit interactive partners to MT, ICR1 may also possess specific functions on MT organization, e.g. stabilization or depolymerization effects, as evidenced by its family member, ICR3.

REFERENCES

Abrash, E.B., Bergmann, D.C., 2009a. Asymmetric Cell Divisions: A View from Plant Development. Dev Cell 16, 783-796.

Abrash, E.B., Bergmann, D.C., 2009b. Asymmetric cell divisions: a view from plant development. Dev Cell 16, 783-796.

Adams, A.E., Johnson, D.I., Longnecker, R.M., Sloat, B.F., Pringle, J.R., 1990. CDC42 and CDC43, two additional genes involved in budding and the establishment of cell polarity in the yeast Saccharomyces cerevisiae. J Cell Biol 111, 131-142.

Al-Bassam, J., Chang, F., 2011. Regulation of microtubule dynamics by TOG-domain proteins XMAP215/Dis1 and CLASP. Trends in cell biology 21, 604-614.

Ambrose, C., Ruan, Y., Gardiner, J., Tamblyn, L.M., Catching, A., Kirik, V., Marc, J., Overall, R., Wasteneys, G.O., 2013. CLASP interacts with sorting nexin 1 to link microtubules and auxin transport via PIN2 recycling in Arabidopsis thaliana. Dev Cell 24, 649-659.

Barbosa, I.C., Zourelidou, M., Willige, B.C., Weller, B., Schwechheimer, C., 2014. D6 PROTEIN KINASE activates auxin transport-dependent growth and PIN-FORMED phosphorylation at the plasma membrane. Developmental cell 29, 674-685.

Bayer, M., Nawy, T., Giglione, C., Galli, M., Meinnel, T., Lukowitz, W., 2009. Paternal control of embryonic patterning in Arabidopsis thaliana. Science 323, 1485-1488.

Belanger, K.D., Quatrano, R.S., 2000. Polarity: the role of localized secretion. Current Opinion in Plant Biology 3, 67-72.

Berdnik, D., Torok, T., Gonzalez-Gaitan, M., Knoblich, J.A., 2002. The endocytic protein alpha-Adaptin is required for numb-mediated asymmetric cell division in Drosophila. Developmental cell 3, 221-231.

Bergmann, D.C., Lukowitz, W., Somerville, C.R., 2004. Stomatal development and pattern controlled by a MAPKK kinase. Science 304, 1494-1497.

Bergmann, D.C., Sack, F.D., 2007. Stomatal development. Annual review of plant biology 58, 163-181.

Bloch, D., Pleskot, R., Pejchar, P., Potocky, M., Trpkosova, P., Cwiklik, L., Vukasinovic, N., Sternberg, H., Yalovsky, S., Zarsky, V., 2016. Exocyst SEC3 and Phosphoinositides Define Sites of Exocytosis in Pollen Tube Initiation and Growth. Plant physiology 172, 980-1002.

Bozkurt, T.O., Belhaj, K., Dagdas, Y.F., Chaparro-Garcia, A., Wu, C.H., Cano, L.M., Kamoun, S., 2015. Rerouting of plant late endocytic trafficking toward a pathogen interface. Traffic (Copenhagen, Denmark) 16, 204-226.

Brandizzi, F., Wasteneys, G.O., 2013. Cytoskeleton-dependent endomembrane organization in plant cells: an emerging role for microtubules. Plant J 75, 339-349.

Brownlee, C., Bouget, F.Y., 1998. Polarity determination in Fucus: From zygote to multicellular embryo. Semin Cell Dev Biol 9, 179-185.

Butty, A.C., Perrinjaquet, N., Petit, A., Jaquenoud, M., Segall, J.E., Hofmann, K., Zwahlen, C., Peter, M., 2002. A positive feedback loop stabilizes the guanine-nucleotide exchange factor Cdc24 at sites of polarization. EMBO J 21, 1565-1576.

Cardenas, L., 2009. New findings in the mechanisms regulating polar growth in root hair cells. Plant Signal Behav 4, 4-8.

Cargnello, M., Roux, P.P., 2011. Activation and function of the MAPKs and their substrates, the MAPK-activated protein kinases. Microbiology and molecular biology reviews : MMBR 75, 50-83.

Carol, R.J., Dolan, L., 2006. The role of reactive oxygen species in cell growth: lessons from root hairs. J Exp Bot 57, 1829-1834.

Cartwright, H.N., Humphries, J.A., Smith, L.G., 2009. PAN1: A Receptor-Like Protein That Promotes Polarization of an Asymmetric Cell Division in Maize. Science 323, 649-651.

Chant, J., 1999. Cell polarity in yeast. Annual review of cell and developmental biology 15, 365-391.

Cole, R.A., Fowler, J.E., 2006. Polarized growth: maintaining focus on the tip. Curr Opin Plant Biol 9, 579-588.

Craddock, C., Lavagi, I., Yang, Z., 2012. New insights into Rho signaling from plant ROP/Rac GTPases. Trends in cell biology 22, 492-501.

Cui, Y., Li, X., Chen, Q., He, X., Yang, Q., Zhang, A., Yu, X., Chen, H., Liu, N., Xie, Q., Yang, W., Zuo, J., Palme, K., Li, W., 2010. BLOS1, a putative BLOC-1 subunit, interacts with SNX1 and modulates root growth in Arabidopsis. J Cell Sci 123, 3727-3733.

Dai, M., Zhang, C., Kania, U., Chen, F., Xue, Q., McCray, T., Li, G., Qin, G., Wakeley, M., Terzaghi, W., Wan, J., Zhao, Y., Xu, J., Friml, J., Deng, X.W., Wang, H., 2012. A PP6-type phosphatase holoenzyme directly regulates PIN phosphorylation and auxin efflux in Arabidopsis. Plant Cell 24, 2497-2514.

De Smet, I., Beeckman, T., 2011. Asymmetric cell division in land plants and algae: the driving force for differentiation. Nat Rev Mol Cell Bio 12, 177-188.

Dell'Angelica, E.C., 2004. The building BLOC(k)s of lysosomes and related organelles. Current opinion in cell biology 16, 458-464.

Dettmer, J., Hong-Hermesdorf, A., Stierhof, Y.D., Schumacher, K., 2006. Vacuolar H+-ATPase activity is required for endocytic and secretory trafficking in Arabidopsis. The Plant cell 18, 715-730.

Dhonukshe, P., Aniento, F., Hwang, I., Robinson, D.G., Mravec, J., Stierhof, Y.D., Friml, J., 2007. Clathrin-mediated constitutive endocytosis of PIN auxin efflux carriers in Arabidopsis. Curr Biol 17, 520-527.

Dong, J., Bergmann, D.C., 2010. Stomatal patterning and development. Curr Top Dev Biol 91, 267-297.

Dong, J., MacAlister, C.A., Bergmann, D.C., 2009. BASL controls asymmetric cell division in Arabidopsis. Cell 137, 1320-1330.

Drubin, D.G., Nelson, W.J., 1996. Origins of cell polarity. Cell 84, 335-344.

Elkin, S.R., Lakoduk, A.M., Schmid, S.L., 2016. Endocytic pathways and endosomal trafficking: a primer. Wien Med Wochenschr 166, 196-204.

Esch, R.K., Errede, B., 2002. Pheromone induction promotes Ste11 degradation through a MAPK feedback and ubiquitin-dependent mechanism. P Natl Acad Sci USA 99, 9160-9165.

Etienne-Manneville, S., 2004. Cdc42 - the centre of polarity. J Cell Sci 117, 1291-1300.

Evangelista, M., Pruyne, D., Amberg, D.C., Boone, C., Bretscher, A., 2002. Formins direct Arp2/3-independent actin filament assembly to polarize cell growth in yeast. Nat Cell Biol 4, 260-269.

Facette, M.R., Park, Y., Sutimantanapi, D., Luo, A.D., Cartwright, H.N., Yang, B., Bennett, E.J., Sylvester, A.W., Smith, L.G., 2015. The SCAR/WAVE complex polarizes PAN receptors and promotes division asymmetry in maize. Nat Plants 1.

Facette, M.R., Smith, L.G., 2012. Division polarity in developing stomata. Current opinion in plant biology 15, 585-592.

Faure, J.E., Rotman, N., Fortune, P., Dumas, C., 2002. Fertilization in Arabidopsis thaliana wild type: Developmental stages and time course. Plant J 30, 481-488.

Feraru, E., Friml, J., 2008. PIN polar targeting. Plant physiology 147, 1553-1559.

Freisinger, T., Klunder, B., Johnson, J., Muller, N., Pichler, G., Beck, G., Costanzo, M., Boone, C., Cerione, R.A., Frey, E., Wedlich-Soldner, R., 2013. Establishment of a robust single axis of cell polarity by coupling multiple positive feedback loops. Nature communications 4, 1807.

Friedman, J.R., Webster, B.M., Mastronarde, D.N., Verhey, K.J., Voeltz, G.K., 2010. ER sliding dynamics and ER-mitochondrial contacts occur on acetylated microtubules. J Cell Biol 190, 363-375.

Friml, J., 2003. Auxin transport - shaping the plant. Current opinion in plant biology 6, 7-12.

Friml, J., Yang, X., Michniewicz, M., Weijers, D., Quint, A., Tietz, O., Benjamins, R., Ouwerkerk, P.B., Ljung, K., Sandberg, G., Hooykaas, P.J., Palme, K., Offringa, R., 2004. A PINOID-dependent binary switch in apical-basal PIN polar targeting directs auxin efflux. Science 306, 862-865.

Fu, Y., Gu, Y., Zheng, Z., Wasteneys, G., Yang, Z., 2005. Arabidopsis interdigitating cell growth requires two antagonistic pathways with opposing action on cell morphogenesis. Cell 120, 687-700.

Fuller, M.T., Spradling, A.C., 2007. Male and female Drosophila germline stem cells: two versions of immortality. Science 316, 402-404.

Fushimi, K., Sasaki, S., Marumo, F., 1997. Phosphorylation of serine 256 is required for cAMP-dependent regulatory exocytosis of the aquaporin-2 water channel. J Biol Chem 272, 14800-14804.

Galway, M.E., Heckman, J.W., Jr., Schiefelbein, J.W., 1997. Growth and ultrastructure of Arabidopsis root hairs: the rhd3 mutation alters vacuole enlargement and tip growth. Planta 201, 209-218.

Geldner, N., 2004. The plant endosomal system - its structure and role in signal transduction and plant development. Planta 219, 547-560.

Geldner, N., Anders, N., Wolters, H., Keicher, J., Kornberger, W., Muller, P., Delbarre, A., Ueda, T., Nakano, A., Jurgens, G., 2003. The Arabidopsis GNOM ARF-GEF mediates endosomal recycling, auxin transport, and auxin-dependent plant growth. Cell 112, 219-230.

Geldner, N., Denervaud-Tendon, V., Hyman, D.L., Mayer, U., Stierhof, Y.D., Chory, J., 2009. Rapid, combinatorial analysis of membrane compartments in intact plants with a multicolor marker set. Plant J 59, 169-178.

Geldner, N., Hyman, D.L., Wang, X.L., Schumacher, K., Chory, J., 2007. Endosomal signaling of plant steroid receptor kinase BRI1. Gene Dev 21, 1598-1602.

Goldstein, B., Macara, I.G., 2007. The PAR proteins: fundamental players in animal cell polarization. Dev Cell 13, 609-622.

Good, M.C., Zalatan, J.G., Lim, W.A., 2011. Scaffold proteins: hubs for controlling the flow of cellular information. Science (New York, N.Y.) 332, 680-686.

Greenwood, S., Struhl, G., 1999. Progression of the morphogenetic furrow in the Drosophila eye: the roles of Hedgehog, Decapentaplegic and the Raf pathway. Development (Cambridge, England) 126, 5795-5808.

Grill, S.W., Howard, J., Schaffer, E., Stelzer, E.H., Hyman, A.A., 2003. The distribution of active force generators controls mitotic spindle position. Science 301, 518-521.

Group, M., 2002. Mitogen-activated protein kinase cascades in plants: a new nomenclature. Trends Plant Sci 7, 301-308.

Grunewald, W., Friml, J., 2010. The march of the PINs: developmental plasticity by dynamic polar targeting in plant cells. EMBO J 29, 2700-2714.

Gu, Y., Fu, Y., Dowd, P., Li, S., Vernoud, V., Gilroy, S., Yang, Z., 2005. A Rho family GTPase controls actin dynamics and tip growth via two counteracting downstream pathways in pollen tubes. J Cell Biol 169, 127-138.

Gu, Y., Wang, Z., Yang, Z., 2004. ROP/RAC GTPase: an old new master regulator for plant signaling. Current opinion in plant biology 7, 527-536.

Guan, Y., Guo, J., Li, H., Yang, Z., 2013. Signaling in pollen tube growth: crosstalk, feedback, and missing links. Mol Plant 6, 1053-1064.

Hara, K., Kajita, R., Torii, K.U., Bergmann, D.C., Kakimoto, T., 2007. The secretory peptide gene EPF1 enforces the stomatal one-cell-spacing rule. Genes Dev 21, 1720-1725.

Hazak, O., Bloch, D., Poraty, L., Sternberg, H., Zhang, J., Friml, J., Yalovsky, S., 2010. A rho scaffold integrates the secretory system with feedback mechanisms in regulation of auxin distribution. PLoS biology 8, e1000282.

Hazak, O., Obolski, U., Prat, T., Friml, J., Hadany, L., Yalovsky, S., 2014. Bimodal regulation of ICR1 levels generates self-organizing auxin distribution. P Natl Acad Sci USA 111, E5471-E5479.

Heisler, M.G., Ohno, C., Das, P., Sieber, P., Reddy, G.V., Long, J.A., Meyerowitz, E.M., 2005. Patterns of auxin transport and gene expression during primordium development revealed by live imaging of the Arabidopsis inflorescence meristem. Curr Biol 15, 1899-1911.

Helariutta, Y., Fukaki, H., Wysocka-Diller, J., Nakajima, K., Jung, J., Sena, G., Hauser, M.T., Benfey, P.N., 2000. The SHORT-ROOT gene controls radial patterning of the Arabidopsis root through radial signaling. Cell 101, 555-567.

Hepler, P.K., Vidali, L., Cheung, A.Y., 2001. Polarized cell growth in higher plants. Annu Rev Cell Dev Biol 17, 159-187.

Hirano, T., Matsuzawa, T., Takegawa, K., Sato, M.H., 2011a. Loss-of-Function and Gain-of-Function Mutations in FAB1A/B Impair Endomembrane Homeostasis, Conferring Pleiotropic Developmental Abnormalities in Arabidopsis. Plant Physiol 155, 797-807.

Hirano, T., Matsuzawa, T., Takegawa, K., Sato, M.H., 2011b. Loss-of-function and gain-of-function mutations in FAB1A/B impair endomembrane homeostasis, conferring pleiotropic developmental abnormalities in Arabidopsis. Plant Physiol 155, 797-807.

Hirano, T., Munnik, T., Sato, M.H., 2015a. Phosphatidylinositol 3-Phosphate 5-Kinase, FAB1/PIKfyve Kinase Mediates Endosome Maturation to Establish Endosome-Cortical Microtubule Interaction in Arabidopsis. Plant Physiol 169, 1961-1974.

Hirano, T., Munnik, T., Sato, M.H., 2015b. Phosphatidylinositol 3-Phosphate 5-Kinase, FAB1/PIKfyve Kinase Mediates Endosome Maturation to Establish Endosome-Cortical Microtubule Interaction in Arabidopsis. Plant physiology 169, 1961-1974.

Hodge, R.G., Ridley, A.J., 2016. Regulating Rho GTPases and their regulators. Nature reviews. Molecular cell biology 17, 496-510.

Humphries, J.A., Vejlupkova, Z., Luo, A., Meeley, R.B., Sylvester, A.W., Fowler, J.E., Smith, L.G., 2011. ROP GTPases act with the receptor-like protein PAN1 to polarize asymmetric cell division in maize. Plant Cell 23, 2273-2284.

Hunt, L., Gray, J.E., 2009. The signaling peptide EPF2 controls asymmetric cell divisions during stomatal development. Curr Biol 19, 864-869.

Inaba, M., Yamashita, Y.M., 2012. Asymmetric stem cell division: precision for robustness. Cell stem cell 11, 461-469.

Jaillais, Y., Fobis-Loisy, I., Miege, C., Rollin, C., Gaude, T., 2006. AtSNX1 defines an endosome for auxin-carrier trafficking in Arabidopsis. Nature 443, 106-109.

Jean, S., Kiger, A.A., 2012. Coordination between RAB GTPase and phosphoinositide regulation and functions. Nature reviews. Molecular cell biology 13, 463-470.

Jewaria, P.K., Hara, T., Tanaka, H., Kondo, T., Betsuyaku, S., Sawa, S., Sakagami, Y., Aimoto, S., Kakimoto, T., 2013. Differential effects of the peptides Stomagen, EPF1 and EPF2 on activation of MAP kinase MPK6 and the SPCH protein level. Plant Cell Physiol 54, 1253-1262.

Johnson, J.M., Jin, M., Lew, D.J., 2011. Symmetry breaking and the establishment of cell polarity in budding yeast. Current opinion in genetics & development 21, 740-746.

Kaksonen, M., Toret, C.P., Drubin, D.G., 2006. Harnessing actin dynamics for clathrin-mediated endocytosis. Nature reviews. Molecular cell biology 7, 404-414.

Kanaoka, M.M., Pillitteri, L.J., Fujii, H., Yoshida, Y., Bogenschutz, N.L., Takabayashi, J., Zhu, J.K., Torii, K.U., 2008. SCREAM/ICE1 and SCREAM2 specify three cell-state transitional steps leading to arabidopsis stomatal differentiation. Plant Cell 20, 1775-1785.

Katsura, T., Gustafson, C.E., Ausiello, D.A., Brown, D., 1997. Protein kinase A phosphorylation is involved in regulated exocytosis of aquaporin-2 in transfected LLC-PK1 cells. Am J Physiol-Renal 272, F816-F822.

Kirchhausen, T., Owen, D., Harrison, S.C., 2014. Molecular structure, function, and dynamics of clathrin-mediated membrane traffic. Cold Spring Harb Perspect Biol 6, a016725.

Kitakura, S., Vanneste, S., Robert, S., Lofke, C., Teichmann, T., Tanaka, H., Friml, J., 2011. Clathrin mediates endocytosis and polar distribution of PIN auxin transporters in Arabidopsis. Plant Cell 23, 1920-1931.

Kiyomitsu, T., Cheeseman, I.M., 2012. Chromosome- and spindle-pole-derived signals generate an intrinsic code for spindle position and orientation. Nat Cell Biol 14, 311-317.

Klein, T.J., Mlodzik, M., 2005. Planar cell polarization: an emerging model points in the right direction. Annu Rev Cell Dev Biol 21, 155-176.

Kleine-Vehn, J., Dhonukshe, P., Sauer, M., Brewer, P.B., Wisniewska, J., Paciorek, T., Benkova, E., Friml, J., 2008a. ARF GEF-dependent transcytosis and polar delivery of PIN auxin carriers in Arabidopsis. Curr Biol 18, 526-531.

Kleine-Vehn, J., Leitner, J., Zwiewka, M., Sauer, M., Abas, L., Luschnig, C., Friml, J., 2008b. Differential degradation of PIN2 auxin efflux carrier by retromer-dependent vacuolar targeting. Proc Natl Acad Sci U S A 105, 17812-17817.

Knoblich, J.A., 2008. Mechanisms of asymmetric stem cell division. Cell 132, 583-597.

Knoblich, J.A., 2010. Asymmetric cell division: recent developments and their implications for tumour biology. Nat Rev Mol Cell Bio 11, 849-860.

Knoblich, J.A., Jan, L.Y., Jan, Y.N., 1995. Asymmetric segregation of Numb and Prospero during cell division. Nature 377, 624-627.

Komis, G., Illes, P., Beck, M., Samaj, J., 2011. Microtubules and mitogen-activated protein kinase signalling. Current opinion in plant biology 14, 650-657.

Kozlowski, C., Srayko, M., Nedelec, F., 2007. Cortical microtubule contacts position the spindle in C. elegans embryos. Cell 129, 499-510.

Kozubowski, L., Saito, K., Johnson, J.M., Howell, A.S., Zyla, T.R., Lew, D.J., 2008. Symmetry-breaking polarization driven by a Cdc42p GEF-PAK complex. Current biology : CB 18, 1719-1726.

Kubo, M., Udagawa, M., Nishikubo, N., Horiguchi, G., Yamaguchi, M., Ito, J., Mimura, T., Fukuda, H., Demura, T., 2005. Transcription switches for protoxylem and metaxylem vessel formation. Genes Dev 19, 1855-1860.

Lam, S.K., Cai, Y., Tse, Y.C., Wang, J., Law, A.H., Pimpl, P., Chan, H.Y., Xia, J., Jiang, L., 2009. BFA-induced compartments from the Golgi apparatus and trans-Golgi network/early endosome are distinct in plant cells. The Plant journal : for cell and molecular biology 60, 865-881.

Lampard, G.R., Lukowitz, W., Ellis, B.E., Bergmann, D.C., 2009. Novel and expanded roles for MAPK signaling in Arabidopsis stomatal cell fate revealed by cell type-specific manipulations. Plant Cell 21, 3506-3517.

Lampard, G.R., MacAlister, C.A., Bergmann, D.C., 2008. Arabidopsis Stomatal Initiation Is Controlled by MAPK-Mediated Regulation of the bHLH SPEECHLESS. Science 322, 1113-1116.

Laskowski, M., Grieneisen, V.A., Hofhuis, H., Hove, C.A., Hogeweg, P., Maree, A.F., Scheres, B., 2008. Root system architecture from coupling cell shape to auxin transport. PLoS Biol 6, e307.

Lau, O.S., Bergmann, D.C., 2012. Stomatal development: a plant's perspective on cell polarity, cell fate transitions and intercellular communication. Development (Cambridge, England) 139, 3683-3692.

Lau, O.S., Davies, K.A., Chang, J., Adrian, J., Rowe, M.H., Ballenger, C.E., Bergmann, D.C., 2014a. Direct roles of SPEECHLESS in the specification of stomatal self-renewing cells. Science 345, 1605-1609.

Lau, O.S., Davies, K.A., Chang, J., Adrian, J., Rowe, M.H., Ballenger, C.E., Bergmann, D.C., 2014b. Direct roles of SPEECHLESS in the specification of stomatal self-renewing cells. Science 345, 1605-1609.

Lavy, M., Bloch, D., Hazak, O., Gutman, I., Poraty, L., Sorek, N., Sternberg, H., Yalovsky, S., 2007. A Novel ROP/RAC effector links cell polarity, root-meristem maintenance, and vesicle trafficking. Curr Biol 17, 947-952.

Lee, G.J., Sohn, E.J., Lee, M.H., Hwang, I., 2004. The Arabidopsis rab5 homologs rha1 and ara7 localize to the prevacuolar compartment. Plant & cell physiology 45, 1211-1220.

Lee, J.S., Hnilova, M., Maes, M., Lin, Y.C., Putarjunan, A., Han, S.K., Avila, J., Torii, K.U., 2015. Competitive binding of antagonistic peptides fine-tunes stomatal patterning. Nature 522, 439-443.

Lee, J.S., Kuroha, T., Hnilova, M., Khatayevich, D., Kanaoka, M.M., McAbee, J.M., Sarikaya, M., Tamerler, C., Torii, K.U., 2012. Direct interaction of ligand-receptor pairs specifying stomatal patterning. Gene Dev 26, 126-136.

Leitner, J., Petrasek, J., Tomanov, K., Retzer, K., Parezova, M., Korbei, B., Bachmair, A., Zazimalova, E., Luschnig, C., 2012. Lysine63-linked ubiquitylation of PIN2 auxin carrier protein governs hormonally controlled adaptation of Arabidopsis root growth. Proceedings of the National Academy of Sciences of the United States of America 109, 8322-8327.

Li, R., Rodriguez-Furlan, C., Wang, J., van de Ven, W., Gao, T., Raikhel, N.V., Hicks, G.R., 2017. Different Endomembrane Trafficking Pathways Establish Apical and Basal Polarities. Plant Cell 29, 90-108.

Li, S., Gu, Y., Yan, A., Lord, E., Yang, Z.B., 2008a. RIP1 (ROP Interactive Partner 1)/ICR1 marks pollen germination sites and may act in the ROP1 pathway in the control of polarized pollen growth. Molecular plant 1, 1021-1035.

Li, S.D., Gu, Y., Yan, A., Lord, E., Yang, Z.B., 2008b. RIP1 (ROP Interactive Partner 1)/ICR1 Marks Pollen Germination Sites and May Act in the ROP1 Pathway in the Control of Polarized Pollen Growth. Mol Plant 1, 1021-1035.

Lin, D., Nagawa, S., Chen, J., Cao, L., Chen, X., Xu, T., Li, H., Dhonukshe, P., Yamamuro, C., Friml, J., Scheres, B., Fu, Y., Yang, Z., 2012. A ROP GTPase-dependent auxin signaling pathway regulates the subcellular distribution of PIN2 in Arabidopsis roots. Curr Biol 22, 1319-1325.

Lin, D.S., Ren, H.B., Fu, Y., 2015. ROP GTPase-mediated auxin signaling regulates pavement cell interdigitation in Arabidopsis thaliana. Journal of Integrative Plant Biology 57, 31-39.

Lu, M.S., Johnston, C.A., 2013. Molecular pathways regulating mitotic spindle orientation in animal cells. Development 140, 1843-1856.

Lukowitz, W., Roeder, A., Parmenter, D., Somerville, C., 2004. A MAPKK kinase gene regulates extra-embryonic cell fate in Arabidopsis. Cell 116, 109-119.

Luo, Y., Scholl, S., Doering, A., Zhang, Y., Irani, N.G., Di Rubbo, S., Neumetzler, L., Krishnamoorthy, P., Van Houtte, I., Mylle, E., Bischoff, V., Vernhettes, S., Winne, J., Friml, J., Stierhof, Y.D., Schumacher, K., Persson, S., Russinova, E., 2015. V-ATPase activity in the TGN/EE is required for exocytosis and recycling in Arabidopsis. Nat Plants 1, 15094.

MacAlister, C.A., Ohashi-Ito, K., Bergmann, D.C., 2007a. Transcription factor control of asymmetric cell divisions that establish the stomatal lineage. Nature 445, 537-540.

MacAlister, C.A., Ohashi-Ito, K., Bergmann, D.C., 2007b. Transcription factor control of asymmetric cell divisions that establish the stomatal lineage. Nature 445, 537-540.

Mao, Y., Zhang, H., Xu, N., Zhang, B., Gou, F., Zhu, J.K., 2013. Application of the CRISPR-Cas system for efficient genome engineering in plants. Mol Plant 6, 2008-2011.

Marco, E., Wedlich-Soldner, R., Li, R., Altschuler, S.J., Wu, L.F., 2007. Endocytosis optimizes the dynamic localization of membrane proteins that regulate cortical polarity. Cell 129, 411-422.

Matsuoka, K., Higuchi, T., Maeshima, M., Nakamura, K., 1997. A Vacuolar-Type H+-ATPase in a Nonvacuolar Organelle Is Required for the Sorting of Soluble Vacuolar Protein Precursors in Tobacco Cells. The Plant cell 9, 533-546.

Mayor, S., Parton, R.G., Donaldson, J.G., 2014. Clathrin-Independent Pathways of Endocytosis. Csh Perspect Biol 6.

McCaffrey, L.M., Macara, I.G., 2012. Signaling pathways in cell polarity. Cold Spring Harb Perspect Biol 4.

Mellman, I., Nelson, W.J., 2008. Coordinated protein sorting, targeting and distribution in polarized cells. Nat Rev Mol Cell Biol 9, 833-845.

Meng, X., Wang, H., He, Y., Liu, Y., Walker, J.C., Torii, K.U., Zhang, S., 2012. A MAPK cascade downstream of ERECTA receptor-like protein kinase regulates Arabidopsis inflorescence architecture by promoting localized cell proliferation. The Plant cell 24, 4948-4960.

Michniewicz, M., Zago, M.K., Abas, L., Weijers, D., Schweighofer, A., Meskiene, I., Heisler, M.G., Ohno, C., Zhang, J., Huang, F., Schwab, R., Weigel, D., Meyerowitz, E.M., Luschnig, C., Offringa, R., Friml, J., 2007. Antagonistic regulation of PIN phosphorylation by PP2A and PINOID directs auxin flux. Cell 130, 1044-1056.

Mineyuki, Y., 1999. The Preprophase Band of Microtubules: Its Function as a Cytokinetic Apparatus in Higher Plants, in: Kwang, W.J. (Ed.), International Review of Cytology. Academic Press, pp. 1-49.

Molendijk, A.J., Bischoff, F., Rajendrakumar, C.S., Friml, J., Braun, M., Gilroy, S., Palme, K., 2001. Arabidopsis thaliana Rop GTPases are localized to tips of root hairs and control polar growth. EMBO J 20, 2779-2788.

Morin, X., Bellaiche, Y., 2011. Mitotic Spindle Orientation in Asymmetric and Symmetric Cell Divisions during Animal Development. Developmental Cell 21, 102-119.

Morita, M.T., Shimada, T., 2014. The Plant Endomembrane System-A Complex Network Supporting Plant Development and Physiology. Plant Cell Physiol 55, 667-671.

Moseley, J.B., Goode, B.L., 2006. The yeast actin cytoskeleton: from cellular function to biochemical mechanism. Microbiology and molecular biology reviews : MMBR 70, 605-645.

Mucha, E., Hoefle, C., Huckelhoven, R., Berken, A., 2010. RIP3 and AtKinesin-13A - a novel interaction linking Rho proteins of plants to microtubules. European journal of cell biology 89, 906-916.

Munoz-Nortes, T., Wilson-Sanchez, D., Candela, H., Micol, J.L., 2014. Symmetry, asymmetry, and the cell cycle in plants: known knowns and some known unknowns. J Exp Bot 65, 2645-2655.

Murphy, L.O., Smith, S., Chen, R.H., Fingar, D.C., Blenis, J., 2002. Molecular interpretation of ERK signal duration by immediate early gene products. Nature cell biology 4, 556-564.

Nadeau, J.A., Sack, F.D., 2002a. Control of stomatal distribution on the Arabidopsis leaf surface. Science 296, 1697-1700.

Nadeau, J.A., Sack, F.D., 2002b. Control of stomatal distribution on the Arabidopsis leaf surface. Science 296, 1697-1700.

Nakagami, H., Kiegerl, S., Hirt, H., 2004. OMTK1, a novel MAPKKK, channels oxidative stress signaling through direct MAPK interaction. The Journal of biological chemistry 279, 26959-26966.

Nakagami, H., Pitzschke, A., Hirt, H., 2005. Emerging MAP kinase pathways in plant stress signalling. Trends Plant Sci 10, 339-346.

Nakagawa, T., Nakamura, S., Tanaka, K., Kawamukai, M., Suzuki, T., Nakamura, K., Kimura, T., Ishiguro, S., 2008. Development of R4 gateway binary vectors (R4pGWB) enabling high-throughput promoter swapping for plant research. Biosci Biotechnol Biochem 72, 624-629.

Nakajima, K., Sena, G., Nawy, T., Benfey, P.N., 2001. Intercellular movement of the putative transcription factor SHR in root patterning. Nature 413, 307-311.

Nance, J., Zallen, J.A., 2011. Elaborating polarity: PAR proteins and the cytoskeleton. Development (Cambridge, England) 138, 799-809.

Neumuller, R.A., Knoblich, J.A., 2009. Dividing cellular asymmetry: asymmetric cell division and its implications for stem cells and cancer. Gene Dev 23, 2675-2699.

Oda, Y., Fukuda, H., 2013. Rho of Plant GTPase Signaling Regulates the Behavior of Arabidopsis Kinesin-13A to Establish Secondary Cell Wall Patterns. Plant Cell 25, 4439-4450.

Oda, Y., Iida, Y., Kondo, Y., Fukuda, H., 2010. Wood Cell-Wall Structure Requires Local 2D-Microtubule Disassembly by a Novel Plasma Membrane-Anchored Protein. Current Biology 20, 1197-1202.

Offringa, R., Huang, F., 2013. Phosphorylation-dependent trafficking of plasma membrane proteins in animal and plant cells. J Integr Plant Biol 55, 789-808.

Ohashi-Ito, K., Bergmann, D.C., 2006. Arabidopsis FAMA controls the final proliferation/differentiation switch during stomatal development. Plant Cell 18, 2493-2505.

Park, H.O., Bi, E., 2007. Central roles of small GTPases in the development of cell polarity in yeast and beyond. Microbiology and molecular biology reviews : MMBR 71, 48-96.

Peer, W.A., 2011. Plasma Membrane Protein Trafficking. Plant Cell Monogr 19, 31-56.

Pillitteri, L.J., Dong, J., 2013. Stomatal development in Arabidopsis. Arabidopsis Book 11, e0162.

Pillitteri, L.J., Guo, X., Dong, J., 2016. Asymmetric cell division in plants: mechanisms of symmetry breaking and cell fate determination. Cell Mol Life Sci 73, 4213-4229.

Pillitteri, L.J., Peterson, K.M., Horst, R.J., Torii, K.U., 2011. Molecular Profiling of Stomatal Meristemoids Reveals New Component of Asymmetric Cell Division and Commonalities among Stem Cell Populations in Arabidopsis. Plant Cell 23, 3260-3275.

Pillitteri, L.J., Sloan, D.B., Bogenschutz, N.L., Torii, K.U., 2007. Termination of asymmetric cell division and differentiation of stomata. Nature 445, 501-505.

Prehoda, K.E., 2009. Polarization of Drosophila neuroblasts during asymmetric division. Cold Spring Harbor perspectives in biology 1, a001388.

Pruyne, D., Legesse-Miller, A., Gao, L., Dong, Y., Bretscher, A., 2004. Mechanisms of polarized growth and organelle segregation in yeast. Annu Rev Cell Dev Biol 20, 559-591.

Qin, Y., Dong, J., 2015. Focusing on the Focus: What Else beyond the Master Switches for Polar Cell Growth? Mol Plant 8, 582-594.

Rohatgi, R., Ma, L., Miki, H., Lopez, M., Kirchhausen, T., Takenawa, T., Kirschner, M.W., 1999. The Interaction between N-WASP and the Arp2/3 Complex Links Cdc42-Dependent Signals to Actin Assembly. Cell 97, 221-231.

Rowland, L.J., Nguyen, B., 1993. Use of Polyethylene-Glycol for Purification of DNA from Leaf Tissue of Woody-Plants. Biotechniques 14, 734-&.

Samaj, J., Baluska, F., Voigt, B., Schlicht, M., Volkmann, D., Menzel, D., 2004. Endocytosis, actin cytoskeleton, and signaling. Plant physiology 135, 1150-1161.

Schaefer, E., Belcram, K., Uyttewaal, M., Duroc, Y., Goussot, M., Legland, D., Laruelle, E., de Tauzia-Moreau, M.L., Pastuglia, M., Bouchez, D., 2017. The preprophase band of microtubules controls the robustness of division orientation in plants. Science 356, 186-189.

Schlereth, A., Moller, B., Liu, W., Kientz, M., Flipse, J., Rademacher, E.H., Schmid, M., Jurgens, G., Weijers, D., 2010. MONOPTEROS controls embryonic root initiation by regulating a mobile transcription factor. Nature 464, 913-916.

Sette, C., Inouye, C.J., Stroschein, S.L., Iaquinta, P.J., Thorner, J., 2000. Mutational analysis suggests that activation of the yeast pheromone response mitogen-activated protein kinase pathway involves conformational changes in the Ste5 scaffold protein. Mol Biol Cell 11, 4033-4049.

Settleman, J., 2005. Intercalating Arabidopsis leaf cells: a jigsaw puzzle of lobes, necks, ROPs, and RICs. Cell 120, 570-572.

Shpak, E.D., McAbee, J.M., Pillitteri, L.J., Torii, K.U., 2005a. Stomatal patterning and differentiation by synergistic interactions of receptor kinases. Science (New York, N.Y.) 309, 290-293.

Shpak, E.D., McAbee, J.M., Pillitteri, L.J., Torii, K.U., 2005b. Stomatal patterning and differentiation by synergistic interactions of receptor kinases. Science 309, 290-293.

Siligato, R., Wang, X., Yadav, S.R., Lehesranta, S., Ma, G.J., Ursache, R., Sevilem, I., Zhang, J., Gorte, M., Prasad, K., Wrzaczek, M., Heidstra, R., Murphy, A., Scheres, B., Mahonen, A.P., 2016. MultiSite Gateway-Compatible Cell Type-Specific Gene-Inducible System for Plants. Plant Physiol 170, 627-641.

Siller, K.H., Cabernard, C., Doe, C.Q., 2006. The NuMA-related Mud protein binds Pins and regulates spindle orientation in Drosophila neuroblasts. Nat Cell Biol 8, 594-600.

Slaughter, B.D., Smith, S.E., Li, R., 2009a. Symmetry breaking in the life cycle of the budding yeast. Cold Spring Harbor perspectives in biology 1, a003384.

Slaughter, B.D., Smith, S.E., Li, R., 2009b. Symmetry Breaking in the Life Cycle of the Budding Yeast. Csh Perspect Biol 1.

Smekalova, V., Luptovciak, I., Komis, G., Samajova, O., Ovecka, M., Doskocilova, A., Takac, T., Vadovic, P., Novak, O., Pechan, T., Ziemann, A., Kosutova, P., Samaj, J., 2014. Involvement of YODA and mitogen activated protein kinase 6 in Arabidopsis post-embryogenic root development through auxin up-regulation and cell division plane orientation. The New phytologist 203, 1175-1193.

Smith, L.G., 2003. Cytoskeletal control of plant cell shape: getting the fine points. Curr Opin Plant Biol 6, 63-73.

Smith, S.E., Rubinstein, B., Mendes Pinto, I., Slaughter, B.D., Unruh, J.R., Li, R., 2013. Independence of symmetry breaking on Bem1-mediated autocatalytic activation of Cdc42. J Cell Biol 202, 1091-1106.

Sonoda, J., Wharton, R.P., 2001. Drosophila Brain Tumor is a translational repressor. Genes Dev 15, 762-773.

Spana, E.P., Doe, C.Q., 1995. The prospero transcription factor is asymmetrically localized to the cell cortex during neuroblast mitosis in Drosophila. Development (Cambridge, England) 121, 3187-3195.

Steiner, A., Rybak, K., Altmann, M., McFarlane, H.E., Klaeger, S., Nguyen, N., Facher, E., Ivakov, A., Wanner, G., Kuster, B., Persson, S., Braun, P., Hauser, M.T., Assaad, F.F., 2016. Cell cycle-regulated PLEIADE/AtMAP65-3 links membrane and microtubule dynamics during plant cytokinesis. The Plant journal : for cell and molecular biology 88, 531-541.

Suarez-Rodriguez, M.C., Adams-Phillips, L., Liu, Y., Wang, H., Su, S.H., Jester, P.J., Zhang, S., Bent, A.F., Krysan, P.J., 2007. MEKK1 is required for flg22-induced MPK4 activation in Arabidopsis plants. Plant physiology 143, 661-669.

Takano, J., Tanaka, M., Toyoda, A., Miwa, K., Kasai, K., Fuji, K., Onouchi, H., Naito, S., Fujiwara, T., 2010. Polar localization and degradation of Arabidopsis boron transporters through distinct trafficking pathways. Proceedings of the National Academy of Sciences of the United States of America 107, 5220-5225.

Takei, K., Haucke, V., 2001. Clathrin-mediated endocytosis: membrane factors pull the trigger. Trends Cell Biol 11, 385-391.

Tamura, K., Shimada, T., Ono, E., Tanaka, Y., Nagatani, A., Higashi, S.I., Watanabe, M., Nishimura, M., Hara-Nishimura, I., 2003. Why green fluorescent fusion proteins have not been observed in the vacuoles of higher plants. The Plant journal : for cell and molecular biology 35, 545-555.

Tena, G., 2016. Stomatal development: Grasses vs Arabidopsis. Nat Plants 2, 16124.

Thompson, B.J., 2013. Cell polarity: models and mechanisms from yeast, worms and flies. Development (Cambridge, England) 140, 13-21.

Torii, K.U., 2012. Mix-and-match: ligand-receptor pairs in stomatal development and beyond. Trends in plant science 17, 711-719.

Torii, K.U., Mitsukawa, N., Oosumi, T., Matsuura, Y., Yokoyama, R., Whittier, R.F., Komeda, Y., 1996. The Arabidopsis ERECTA gene encodes a putative receptor protein kinase with extracellular leucine-rich repeats. Plant Cell 8, 735-746.

Traub, L.M., Bonifacino, J.S., 2013. Cargo recognition in clathrin-mediated endocytosis. Cold Spring Harb Perspect Biol 5, a016790.

van Drogen, F., O'Rourke, S.M., Stucke, V.M., Jaquenoud, M., Neiman, A.M., Peter, M., 2000. Phosphorylation of the MEKK Ste11p by the PAK-like kinase Ste20p is required for MAP kinase signaling in vivo. Current Biology 10, 630-639.

Vaten, A., Bergmann, D.C., 2013. Correction: Mechanisms of stomatal development: an evolutionary view. Evodevo 4, 11.

Vetter, I.R., Wittinghofer, A., 2001. The guanine nucleotide-binding switch in three dimensions. Science 294, 1299-1304.

Voinnet, O., Rivas, S., Mestre, P., Baulcombe, D., 2003. An enhanced transient expression system in plants based on suppression of gene silencing by the p19 protein of tomato bushy stunt virus. Plant J 33, 949-956.

von Dassow, G., 2009. Concurrent cues for cytokinetic furrow induction in animal cells. Trends in cell biology 19, 165-173.

Wang, H., Ngwenyama, N., Liu, Y., Walker, J.C., Zhang, S., 2007. Stomatal development and patterning are regulated by environmentally responsive mitogen-activated protein kinases in Arabidopsis. Plant Cell 19, 63-73.

Wang, J., Cai, Y., Miao, Y., Lam, S.K., Jiang, L., 2009. Wortmannin induces homotypic fusion of plant prevacuolar compartments. Journal of experimental botany 60, 3075-3083.

Wang, P.W., Hussey, P.J., 2015. Interactions between plant endomembrane systems and the actin cytoskeleton. Front Plant Sci 6.

Ward, T.H., Brandizzi, F., 2004. Dynamics of proteins in Golgi membranes: comparisons between mammalian and plant cells highlighted by photobleaching techniques. Cell Mol Life Sci 61, 172-185.

Wedlich-Soldner, R., Altschuler, S., Wu, L., Li, R., 2003. Spontaneous cell polarization through actomyosin-based delivery of the Cdc42 GTPase. Science 299, 1231-1235.

Wedlich-Soldner, R., Wai, S.C., Schmidt, T., Li, R., 2004. Robust cell polarity is a dynamic state established by coupling transport and GTPase signaling. J Cell Biol 166, 889-900.

Willemsen, V., Friml, J., Grebe, M., van den Toorn, A., Palme, K., Scheres, B., 2003. Cell polarity and PIN protein positioning in Arabidopsis require STEROL METHYLTRANSFERASE1 function. Plant Cell 15, 612-625.

Williams, S.E., Fuchs, E., 2013. Oriented divisions, fate decisions. Current opinion in cell biology 25, 749-758.

Wisniewska, J., Xu, J., Seifertova, D., Brewer, P.B., Ruzicka, K., Blilou, I., Rouquie, D., Benkova, E., Scheres, B., Friml, J., 2006. Polar PIN localization directs auxin flow in plants. Science 312, 883.

Woods, B., Kuo, C.C., Wu, C.F., Zyla, T.R., Lew, D.J., 2015. Polarity establishment requires localized activation of Cdc42. J Cell Biol 211, 19-26.

Wu, C., Jansen, G., Zhang, J., Thomas, D.Y., Whiteway, M., 2006. Adaptor protein Ste50p links the Ste11p MEKK to the HOG pathway through plasma membrane association. Genes & development 20, 734-746.

Xu, J., Scheres, B., 2005a. Cell polarity: ROPing the ends together. Current Opinion in Plant Biology 8, 613-618.

Xu, J., Scheres, B., 2005b. Dissection of Arabidopsis ADP-RIBOSYLATION FACTOR 1 function in epidermal cell polarity. Plant Cell 17, 525-536.

Xu, T., Wen, M., Nagawa, S., Fu, Y., Chen, J.G., Wu, M.J., Perrot-Rechenmann, C., Friml, J., Jones, A.M., Yang, Z., 2010. Cell surface- and rho GTPase-based auxin signaling controls cellular interdigitation in Arabidopsis. Cell 143, 99-110.

Yang, Z., 2008. Cell polarity signaling in Arabidopsis. Annu Rev Cell Dev Biol 24, 551-575.

Yang, Z., Lavagi, I., 2012. Spatial control of plasma membrane domains: ROP GTPase-based symmetry breaking. Current opinion in plant biology 15, 601-607.

Yuan, L., Gu, R., Xuan, Y., Smith-Valle, E., Loque, D., Frommer, W.B., von Wiren, N., 2013. Allosteric regulation of transport activity by heterotrimerization of Arabidopsis ammonium transporter complexes in vivo. Plant Cell 25, 974-984.

Zhang, X., Facette, M., Humphries, J.A., Shen, Z., Park, Y., Sutimantanapi, D., Sylvester, A.W., Briggs, S.P., Smith, L.G., 2012. Identification of PAN2 by quantitative proteomics as a leucine-rich repeat-receptor-like kinase acting upstream of PAN1 to polarize cell division in maize. Plant Cell 24, 4577-4589.

Zhang, Y., Bergmann, D.C., Dong, J., 2016a. Fine-scale dissection of the subdomains of polarity protein BASL in stomatal asymmetric cell division. J Exp Bot 67, 5093-5103.

Zhang, Y., Guo, X., Dong, J., 2016b. Phosphorylation of the Polarity Protein BASL Differentiates Asymmetric Cell Fate through MAPKs and SPCH. Curr Biol 26, 2957-2965.

Zhang, Y., McCormick, S., 2007. A distinct mechanism regulating a pollen-specific guanine nucleotide exchange factor for the small GTPase Rop in Arabidopsis thaliana. Proc Natl Acad Sci U S A 104, 18830-18835.

Zhang, Y., Wang, P., Shao, W., Zhu, J.K., Dong, J., 2015. The BASL polarity protein controls a MAPK signaling feedback loop in asymmetric cell division. Developmental cell 33, 136-149.